BeFo
STIFTELSEN BERGTEKNISK FORSKNING
ROCK ENGINEERING RESEARCH FOUNDATION

DYNAMIC MODELLING OF ROCK BOLTS AT KIIRUNAVAARA MINE

Pin Zhou
Mohsen Bazargan
Flavio Lanaro
Shahin Shirzadegan
Nooraddin Nikadat
Senzia Warema
Changping Yi
Erling Nordlund

BeFo Report 244

STIFTELSEN BERGTEKNISK FORSKNING
ROCK ENGINEERING RESEARCH FOUNDATION

DYNAMIC MODELLING OF ROCK BOLTS AT KIIRUNAVAARA MINE

Dynamisk modellering av bultar i Kiirunavaara gruva

Pin Zhou

Mohsen Bazargan

Flavio Lanaro

Shahin Shirzadegan

Nooraddin Nikadat

Senzia Warema

Changping Yi

Erling Nordlund

BeFo Report 244
Stockholm 2024
ISSN 1104-1773
ISRN BEFO-R-244-SE

PREFACE

Dynamic loading of rock bolts is a complex topic that requires a thorough understanding of rock mechanics, bolt type and materials, static and dynamic loading processes. This report addresses this problem by using a combination of data collection in a controlled environment, the Kiirunavaara Mine, and numerical modelling of complex, multi-opening excavations in order develop a method for comparing and improving design of support systems.

The members of the reference group were Axel Bolin, Eva Hakami, Fredrik Johansson, Henrik Ittner, Patrik Vidstrand, Savka Dineva, Pin Zhang and Linda Jonsson. The research project was funded by BeFo and Rejlers Sverige AB.

Stockholm

Patrik Vidstrand

FÖRORD

Dynamisk belastning av bergbultar är ett komplext ämne som kräver en grundlig förståelse av bergmekanik, bulttyp och material, samt av statiska- och dynamiska belastningsprocesser. Denna rapport tar upp detta problem genom att använda en kombination av datainsamling i en kontrollerad miljö, Kiirunavaaragruvan, och numerisk modellering av komplexa tunnelgeometrier med flera öppningar för att utveckla en metod för att jämföra och förbättra design av förstärkningssystem.

Medlemmarna i referensgruppen var Axel Bolin, Eva Hakami, Fredrik Johansson, Henrik Ittner, Patrik Vidstrand, Savka Dineva, Pin Zhang och Linda Jonsson. Forskningsprojektet finansierades av BeFo och Rejlers Sverige AB.

Stockholm

Patrik Vidstrand

SUMMARY

Seven large scale dynamic tests of rock support were conducted at LKAB's Kiirunavaara Mine in order to develop a methodology for the design of dynamic load resistant rock supports. The tests were performed to increase the understanding of the response of rock support installed on the walls and roof in a tunnel and subjected to strong dynamic loading. The tests were originally numerically simulated by using two numerical tools, LS-DYNA and UDEC, in a former PhD Project at Luleå University of Technology, LTU (Shirzadegan, 2020), to investigate the performance of the test set up, the response of supported and unsupported excavations during the field tests as well as the complex interaction of stress waves and rock support. The comparison of the numerical results and the results obtained from field tests showed that the combination of LS-DYNA and UDEC could satisfactorily simulate the field tests. This work is the continuation of the LTU project with LS-DYNA and UDEC.

Since the analyses were previously conducted with 2D models, while in reality the structural geology, ground motion measurements, fracture investigations and support motion, as well as the deformation measurements, occur in a 3D space, in the present project three-dimensional analysis are carried out using 3DEC that can assist in studying the interaction of the dynamic load with rock joints, rock blocks, tunnel wall and installed rock support. In this project the analyses are carried out in two stages: (i) the explosion stage is modelled in 3D with the finite element code LS-DYNA and (ii) the wave propagation stage is modelled in 3D with the program 3DEC, where the results from LS-DYNA are used as input.

The numerical simulations in this project can be used to analyse the behaviour of rock masses and rock support systems under dynamic loading conditions. These simulations provide valuable information about the response of the rock mass to dynamic loading and can be used to optimize the design of rock support systems. The numerical results evaluate different rock support performance (Swellex Mn24 bolt and D-bolt) under dynamic loading conditions.

3DEC modelling in the present study shows that: a) numerically calculated velocity patterns match well those observed in the field for Test No. 6, b) larger displacements occurred for certain rock blocks in the unsupported crosscut and, c) the patterns of the most displaced rock blocks in the model very much resemble the positions where fallouts were observed in the field close to the footwall drift in the unsupported crosscut.

Keywords: LS-DYNA, 3DEC, dynamic conditions, dynamic bolt.

SAMMANFATTNING

Sju storskaliga dynamiska tester av bergbultar har genomförts vid LKAB:s Kiirunavaaragruva för att utveckla en metodik för design och optimering av dynamiska bultar. Testerna utfördes för att öka förståelsen för responsen från bergförstärkningen installerad i väggar och tak i en tunnel och utsatta för stor dynamisk belastning. Testerna simulerades genom att använda två numeriska verktyg, LS-DYNA och UDEC, för att undersöka testuppsättningens prestanda, responsen från oförstärkta och förstärkta tunnlar under fältförsöken samt den komplexa interaktionen mellan spänningsvågor och berget. Jämförelsen av de numeriska resultaten och resultaten med fälttester visade att kombinationen av LS-DYNA och UDEC på ett tillfredsställande sätt kunde simulera fältförsöken. Detta arbete är en fortsättning på ett tidigare doktorandprojekt vid LTU (Shirzadegan, 2020).

Eftersom analyserna tidigare utfördes med 2D-modeller, medan strukturgeologin, deformationsmätningarna markrörelsemätningar, sprickundersökningar och rörelser i förstärkningen, sker i ett 3D-rum, presenterar vi i detta projekt en tredimensionell analys med 3DEC för att hjälpa till att studera samspelet mellan de dynamiska lasterna och bergsprickor, bergblock, tunnelvägg och tak och installerad bergsförstärkning. I detta projekt presenteras analyserna i två steg: (i) explosionssteget modellerat i 3D med den finita elementkoden LS-DYNA och (ii) vågutbredningssteget modellerat i 3D med 3DEC, där resultaten från LS-DYNA används som input.

De numeriska simuleringarna i detta projekt kan användas för att analysera beteendet hos bergmassor och bergförstärkningen under dynamiska belastningsförhållanden. Dessa 3D-simuleringar kan ge värdefull information om bergmassans svar på dynamisk belastning samt användas för att optimera designen av bergförstärkningen. Dessa numeriska resultat syftar till att utvärdera olika bergbultars prestanda (Swellex Mn24 bolt och D-bult) under dynamiska belastningsförhållanden. Vidare blir det möjligt att genomföra storskaliga syntetiska tester av bergförstärkningen för Kiirunavaaragruva. När man erhållit en kalibrerad numerisk modell i 3DEC kommer det vara möjligt att testa prestandan hos olika bultsystem med samma randvillkor i framtida studier.

3DEC-modelleringen i den aktuella studien visar att: a) numeriskt beräknade hastighetsmönster överensstämmer väl med dem som observerats i fältet för Test nr 6, b) större förskjutningar inträffade för vissa bergblock i den oförstärkta tvärtunneln, och c) mönstren för de mest förskjutna bergblocken i modellen liknar mycket väl de positioner där utfall observerades i fältet nära fotväggstunneln i den oförstärkta tvärtunneln.

Nyckelord: LS-DYNA, 3DEC, dynamiska förhållanden, dynamisk bult.

CONTENTS

1. INTRODUCTION

Seven large scale dynamic tests of rock support were conducted at LKAB's Kiirunavaara mine in order to develop a methodology for the design of dynamic load resistant rock supports. The tests were performed to increase the understanding of the response of rock support installed on the walls and roof of a tunnel subjected to strong dynamic loading. The tests were previously numerically simulated by using two numerical codes, LS-DYNA and UDEC, to investigate the performance of the test set up, the response of supported and unsupported excavations during the field tests as well as the complex interaction of stress waves and rock support. This was reported in a doctoral thesis "Development of a Methodology for Dynamic Testing of Rock Support" at LTU (Shirzadegan, 2020).

The conventional approach for design of rock support comprises: (i) the identification of potential failure modes and (ii) a comparison of the available capacity with the driving force/demand (including dynamic components). The factor of safety or the probability of failure calculated for the potential failure modes can then be used to estimate the demand on the rock support. This approach, is however, not suitable for the design of rock support systems subjected to seismic loading conditions, since neither the demand on the support system nor the capacity of the support system can be satisfactorily defined in dynamic conditions by only one factor of safety (Stacey, 2012).

The performance of ground support systems subjected to seismically induced loading has therefore, due to its complexity, been until now determined by controlled on-site tests. Several researchers have carried out field tests in different mines worldwide aiming to improve the understanding and quantify the dynamic performance of support systems (Ortlepp, 1969; 1992; Tannant et al., 1994; Tannant et al., 1995; Ansell, 1999) (Hagan et al., 2001; Espley et al., 2002; Archibald et al., 2003; Ansell, 2004; Heal et al., 2005; Andrieux et al., 2005; Heal & Potvin, 2007; Potvin et al., 2010). Different test designs were used by different researchers and have led to various levels of success in evaluating the performance of the installed rock support.

With this in regard, seven large scale dynamic tests of rock support were conducted at a number of crosscuts in the northern part of the LKAB's Kiirunavaara mine. Results from the tests are presented in Shirzadegan et al. (2016a) and (2016b). During the procedure of testing (Tests No. 1 to 5), it was realized that one of the challenges was to design the tests in a way that, the effect of the blasting gases on the crosscut walls was negligible, and that the damage on the wall surfaces should be caused by the mechanical waves generated by the blast. The compressive radial stress at the wave front should be reflected at the surface of the wall and result in a tensile stress which might exceed the tensile strength of the rock mass or/and intact rock.

For this purpose, 2D numerical analyses with UDEC were conducted to study the effect of the thickness of the burden between the blasthole and the tunnel on the test results. Analyses comprised a first part, the detonation phase, which was simulated using LS-

DYNA. The result from LS-DYNA was used in the second part as an internal boundary condition generating the dynamic load after the detonation phase in two dimensional models in UDEC. The numerical analyses provided results in terms of ground motion and level of damage on the surface of the crosscut wall in Tests No. 1 to 5. Similar numerical studies with UDEC, in combination with finite element code that simulates blasting, were also previously performed by other authors (Chen & Zhao, 1998; Chen et al., 2000; Wang et al., 2009; Zhang et al., 2013; Deng et al., 2015).

Based on the results of Tests No. 1 to 5, an analogical method was employed to improve the design of further one more field test, Test No. 6. The optimized test design for Test No. 6 was deduced mainly from the prediction of ground motion and level of damage on the surface measured at the crosscut wall as presented in Figure 1-1.

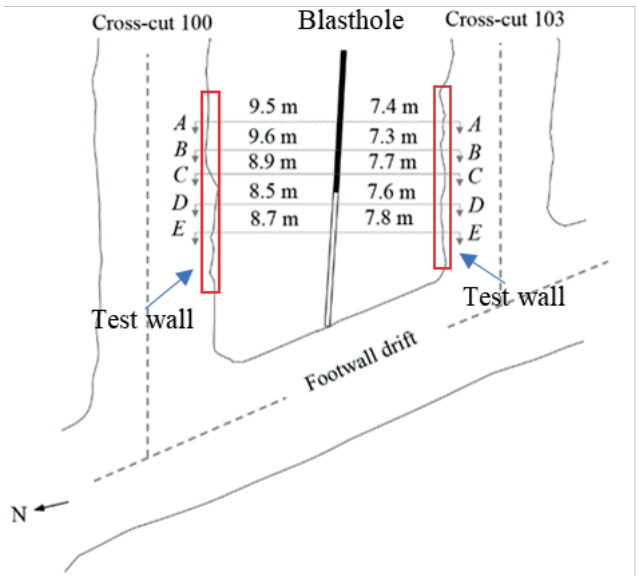

Figure 1-1. Schematic layout of the test site for studying the performance of dynamic rock support for Test No. 6 at Kiirunavaara mine.

Numerical back analysis of this Test No. 6 was then performed using a combination of UDEC and LS-DYNA. In those analyses, the installed rock bolt Swellex Mn24, reinforced shotcrete, and the dominant joint sets mapped around the crosscuts (Andersson, 2010; Andersson, 2011) were integrated into the UDEC models. The bolt properties were decided according to the studies on Swellex Mn24 (Li & Håkansson, 1999), supported by (Shirzadegan, 2020), and discussions with the bolt producer's representatives of Epiroc. The properties for reinforced shotcrete were selected based on the data from a series of laboratory tests by (Malmgren, 2007; Saiang et al., 2005). The

results from the numerical analysis (using UDEC and LS-DYNA) of the tests and their comparisons to the field data in two-dimensions (Shirzadegan, 2020).

The valuable experience obtained from the initial field tests at Kiirunavaara mine combined with the later analyses with UDEC, and the agreement obtained between field test and UDEC results suggested that numerical analysis can be used as an important tool for the design of large-scale tests on dynamic rock support. This would lead to greatly reduced time and costs while searching for improved design of the field tests, and consequently the optimised rock support in dynamically prone areas of the mine due to rock burst and/or seismic activity.

Since in that previous project, only 2D analyses were conducted and only one type of rock bolt support was numerically analysed, the present study carries out analyses in three dimensions using the software 3DEC and models different types of commercial dynamic rock bolts that can potentially be installed in burst prone and seismically active areas of a mine. Performing analysis in 3D provides the opportunity to model and study the interaction of the rock blocks, joints and rock support in the Test No. 6 in a more realistic way. Furthermore, since the ground motion gauges/sensors in the field tests were distributed all over the test wall, and parallel to the blasthole, the effect of dynamic load on the rock mass and on the surface of the tunnel wall at different positions can be studied more in detail as a three-dimensional problem.

Objectives

In order to study Test No. 6, where blastholes are placed in the pillar between two tunnels, in more details, 3D numerical analyses are conducted in the present study. The main objectives of the numerical modelling are to:

- identify the development of failure mechanism in the whole rock mass between the blasthole and the tested crosscuts, the depth of damage along the wall of the crosscut with respect to the location of the blasthole from the charge in the blasthole;
- study the ground motion generated at the surface of the tested crosscut wall to validate the numerical results by comparing the velocities obtained from first integration of accelerometer records during the field tests;
- study the performance of different types of dynamic rock support in the developed 3D model;
- compare the results from 3DEC (3D) and UDEC (2D) with those from the field tests, to assess the additional capability of the 3D compared to 2D models to simulate the test.

Limitations

This project does not cover:

- Validation of new field measurements against new rock support types;

- Design of other support systems other than substituting rock bolt properties in the models with other bolt properties.

Meanwhile, the parameters used as inputs for the modelled bolts are calibrated in order to become compatible with those defined for the bolt elements according to the 3DEC manual. The specific features along the bolt element length can have influence on the reinforcement performance, especially where the segments intersect rock joints in the model. The intersections between bolts and rock joints in 3DEC models are simplified by applying a specific segment element in that position, according to the 3DEC manual regardless of the bolt features along the real bolt length.

Organisation of the report

In Chapter 1 an introduction of this work is elaborated. Chapter 2 summarises the background by reviewing related field and numerical methodologies to this project. Chapter 3 presents the methodology adopted in this project. The geological interpretations and how these geologic features are conceptualized are described in Chapter 4. The numerical modelling of blasting by LS-DYNA and 3DEC to mimic the field test is clarified respectively in Chapter 5 and Chapter 6, respectively, followed by the modelling results in 3DEC in Chapter 7. Discussion of the results, conclusions of this research project and recommendation on further studies are highlighted in Chapter 8, 9 and 10, respectively.

2. BACKGROUND

Seismic events due to deep mining are a result of mining-induced stress changes caused by ore extraction and tunnelling. These events are random and, the exact time and locations of the occurrences are unpredictable and uncontrollable, which poses challenges to field tests of rock reinforcement system. Through field blasting tests by creating seismic-like forces, instrumentation and monitoring can be planned, data can be collected and used to determine whether the reinforcement system is capable of withstanding the dynamic loads generated by blasts. Replications of field tests can be realized by generating similar dynamic stress conditions to those experienced during seismic events. Meanwhile numerical tools showcase in many aspects the advantages over field tests on blasting. Hence, this chapter seeks to compile a brief literature review in the following parts:

- Rock bolting in mining industry;
- Numerical modelling of jointed rock masses;
- Numerical modelling of blasting damage;
- Numerical modelling of large-scale field tests on blasting.

Rock and soil mechanics are the branch of geological engineering that deals with the physical properties of rock and soil under load. It is fundamental to help with understanding tunnel stability, as the strength and behaviour of the surrounding soil and rock mass play a critical role in determining the stability of the tunnel.

Ground support systems are employed to reinforce the surrounding soil and rock mass and maintain the stability of tunnels and slopes. Different types of ground support systems have been developed such as mesh reinforcement, rock bolts, and shotcrete. For rock tunnels, the choice of ground support system depends mainly on the potential failure mode and on the desired safety level of reinforcement system and surrounding rock masses. Typical rock bolts used in practice include both conventional rock bolts (mechanical bolts, fully grouted bolts, self-drilling bolts, frictional bolts, combined rock bolts, and cable bolts) and energy-absorbing rock bolts/dynamic bolts (Li, 2017).

Different dynamic bolt has its own unique design, and their application depends on the specific requirements of the project, including the rock formation, the loading conditions, and the specific design requirements. The various dynamic rock bolt types have been studied for nearly 40 years (Sui et al., 2022). The simplest prototype of dynamic rock bolts was produced in the 1980s and consisted of a threaded rebar rock bolt with a partial casing. The purpose of the casing is to prevent the threaded reinforcement from bonding to the grout. The two main disadvantages of this type of rock bolt are the increased diameter of the borehole and the difficulty in resisting corrosion of the rock bolt. The anchor is not an energy absorbing anchor, hence not a real dynamic bolt in the true sense of the word. In 1995, Mccreath & Kaiser (1995) proposed the design principle of energy-absorbing rock bolts, pointing out that rock bolts should be capable of resisting large elongation (at least 200 to 300 mm) and have slip characteristics similar to the

deformation of the surrounding rock. These are mainly used in underground engineering rock support systems affected by instantaneous loads, such as rockburst and engineering blasts (Ansell, 2005). In the early 1990s, Ortlepp also proposed the concept of an energy-absorbing support system, which included rock bolts (Ortlepp, 1992; Ortlepp, 1994; Ortlepp & Stacey, 1998). In 1990, Jager developed the first real set of dynamic rock bolts, the cone rock bolts (Jager, 1992). This anchored bolt consists mainly of a smooth metal rod and a cone anchor. The outer surface of the smooth metal rod body is coated with a thin layer of lubricating material, such as wax, to slip in the grout body when the anchor is subjected to tension loading. Early cone rock bolts could only be anchored with cement mortar until the late 1990s when resin-anchored cone rock bolts (Modified Conebolt) were created (Li & Marklund, 2004). The modified cone anchor has an additional blade at the end of the taper to agitate the resin charge roll when installing the bolt. Through field applications, it has been found that if there are fracture surfaces or loose bits of rock behind the tray, the resin anchor may fail, thus rendering the anchor reinforcement function completely useless (Simser, 2002; Simser et al., 2006).

In order to reduce the effects of rock mass features on the deformation of rock bolts, bolts should be equipped with appropriately selected elements designed to make them more yieldable and limit the effects of load. For typically stratified rock tunnel roofs, yielding devices can be used directly with rock bolt support, which can significantly improve the work safety factor (Skrzypkowski et al., 2020a; Skrzypkowski et al., 2020b).

In recent years, the demand for dynamic rock bolts has been expanding globally as the concept of dynamic rock bolts and dynamic support has become better understood (Sui et al., 2022), and various types of dynamic rock bolts have appeared on the market, such as Garford rock bolts (Hyett et al., 1996; Varden et al., 2008; Varden R. P., 2009), D-type rock bolts (Li, 2010; Li., 2011; Li, 2012; Li et al., 2014; Yu & Li, 2015), Roofex rock bolts (Charette & Plouffe, 2007; Harvey & Ozbay, 2009; Ozbay & Neugebauer, 2009; An et al., 2013; Chen et al., 2014) and constant resistance/large deformation rock bolts (He. & Feng, 2010; He et al., 2013; He et al., 2014b; He o.a., 2014c; He et al., 2014d).

2.1 Bolt types analyzed

Two dynamic rock bolt types used in Kiirunavaara Mine are chosen for analysis in this project and short descriptions are summarized below:

- **Swellex Mn24 bolt:** This bolt is designed with a welded steel tube folded on itself and sealed at one extremity. The other extremity is set with a special head bushing used for inflation and retaining of the face plates typically used in rock bolting. The expansion of the bolt, inside the drilled borehole, creates a friction and interlocking anchor, which provides instant reinforcement and support of the rock (Figure 2-1).

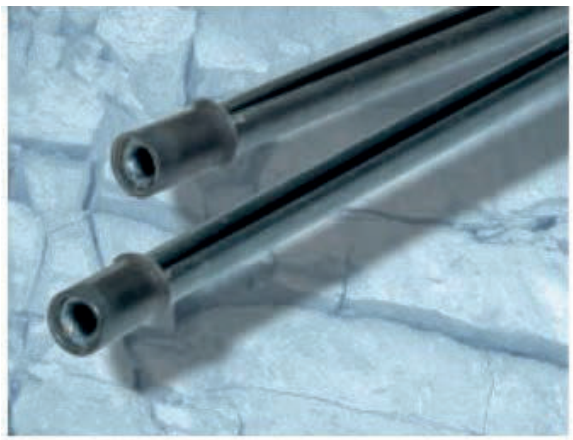

Figure 2-1. Swellex Mn24 bolt (Atlas Copco, 2023).

- **D-bolt:** This bolt is designed to absorb kinetic energy and built up of short sections with anchors in between. Every section can yield independently, if one section breaks the remaining sections can still take up forces (Li et al., 2014), see Figure 2-2.

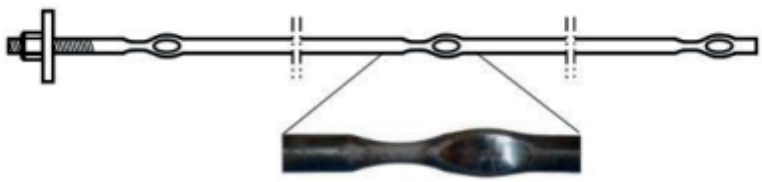

Figure 2-2. The layout of D-bolt (Li et al., 2014).

2.2 Numerical modelling of blasting damage

The Drill and Blast Method (DBM) remains the preferred rock mass excavation method worldwide in engineering practice such as underground caverning, mining, quarrying, tunnelling, and dam construction (Wang et al., 2018b). Various work has been done both in field and laboratory to improve understanding of the factors that contribute to rock damage due to blasting and to formulate guideline to blast-induced damage evaluation during rock tunnelling. To improve the replicability and the quality of blasting results. SveBeFo (Swedish Rock Engineering Research) and Swebrec (Swedish Blasting Research Centre) carried out extensive field investigations to measure and predict the extent of blast-induced cracks between 1991 and 2003. The main objective was to obtain a basis for improved contour blasting of tunnels. Ouchterlony (1997) proposed an equation for estimating radial crack length, later this equation was expanded by correction

factors (Ouchterlony et al., 2002). Saw cuts were extracted and crack mapping performed, both in the field and in the laboratory (Saiang, 2008; Olsson et al., 2009). Eldert (2018) employed Measurement While Drilling (MWD) technology to predict rock mass quality, quantify the extent of blast damage, and forecast the required rock support, furthermore the benefits and limitations of different methods for evaluating blast damage in tunnel were summarized.

Despite the advantages of DBM including wide acceptability and broad applicability, investigating blast-induced damage in the field or laboratory can be costly and time-consuming, and often restricted by other activities. Numerical modelling as a useful tool is becoming popular to predict blast-induced damage and fracturing of rocks. Validated and sound numerical results can provide insights into the experimental findings.

Many scholars have used continuum numerical modelling (Ma & An, 2008; Banadaki & Mohanty, 2012; Torbica & Lapčević, 2015), discontinuum (Park & Jeon, 2005; Yoon & Jeon, 2009; Ning et al., 2011; Onederra et al., 2012; Alibadian et al., 2014; Fakhimi & Lanari, 2014) and hybrid continuum-discontinuum numerical modelling tools (Mitelman & Elmo, 2014; An et al., 2020; Han et al., 2020) to simulate the blasting process. Ma & An (2008) implemented the Johnson-Holmquist (J-H) material constitutive model incorporated in LS-DYNA code and simulated the blast-induced rock fracture in a 2D model. The blasting input load is a pressure-time curve. They investigated the effects of loading rate on the fracture patterns, see Figure 2-3.

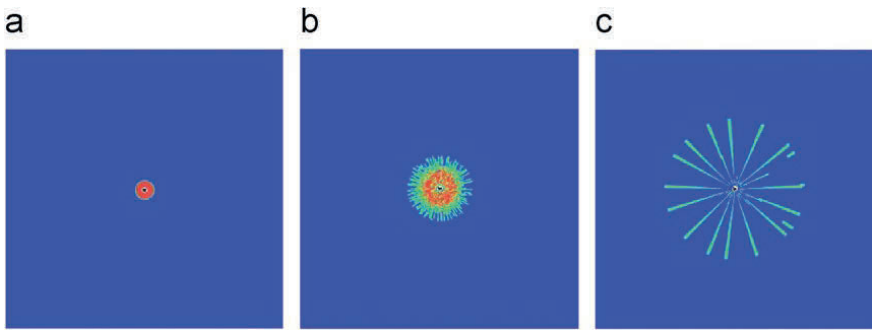

Figure 2-3. Fracture patterns for different stress loading rates in a borehole simulated by LS-DYNA: (a) 20 MPa/us, (b) 10 MPa/us, and (c) 1.0 MPa/us (Ma & An, 2008).

Banadaki & Mohanty (2012) carried out precise laboratory-scale single-hole blast experiments in cylindrical samples of a well-characterized granitic rock to study stress wave induced fracture patterns. The Johnson-Holmquist model in the ANSYS AUTODYN software was employed to model the rock behaviour in the small-scale tests. The numerical results and the experimental results for the same sample set-up are shown in Figure 2-4.

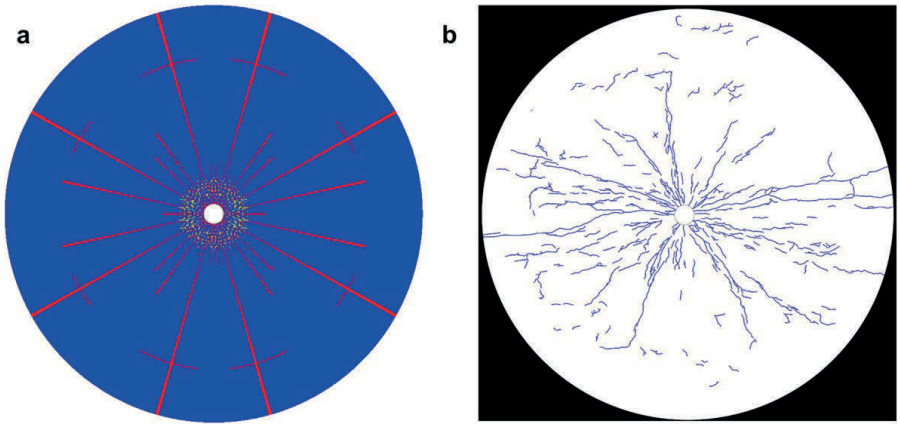

Figure 2-4. Comparison of the simulation results with ANSYS (a) and cracks developed at the gauge level (b) for a cylindrical sample of granitic rock (Banadaki & Mohanty, 2012)

Wang et al. (2018a) numerically investigated the rock blasting damage based on laboratory scale experiments. A numerical simulation method applying the damage model Johnson–Holmquist II (JH-2) combined with the arbitrary Lagrangian-Eulerian (ALE) method was employed in the work. The process of dynamic breakage and damage evolution of Barre granite is reproduced using LS-DYNA, based on the prototype experiments in the laboratory. The results show that both the crack patterns and measured pressures align with the results from the laboratory scale experiments. Blast-induced cracks based on numerical modelling are show in Figure 2-5.

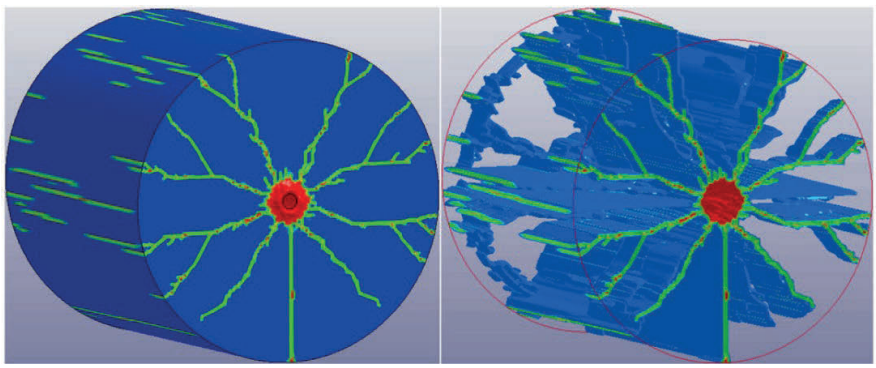

Figure 2-5. 3D blasting crack pattern in rock simulated with the Johnson–Holmquist II (JH-2) damage model with LS-DYNA (Wang et al., 2018a).

It is essential to address that in the case above, the rock mass was considered constitutively as a continuum material, even exhibiting breakage in crack-like patterns.

However, the rock masses that are exposed to blasting may contain naturally pre-existing fractures.

The distinct element method (DEM) is commonly used for stability assessment, and failure and deformation analysis of discontinuous media. In discontinuous models, the rock mass is represented by an assembly of bonded elements (e.g. particles and springs) and fractures as separation of the particles. Failure or dislocation is initiated when the stress between two elements exceeds a critical value of the spring. Within this framework, crack behaviour such as failure mode, location, density, and extension can be explicitly tracked when simulating rock blasting. Lak et al. (2019) developed a Discrete Fracture Network (DFN) model and introduced it in a DEM model to investigate the blast-induced fracture creation and, evolution in a jointed rock mass. The fracture propagations in a radial section of a blast hole in rock at different times is shown in Figure 2-6.

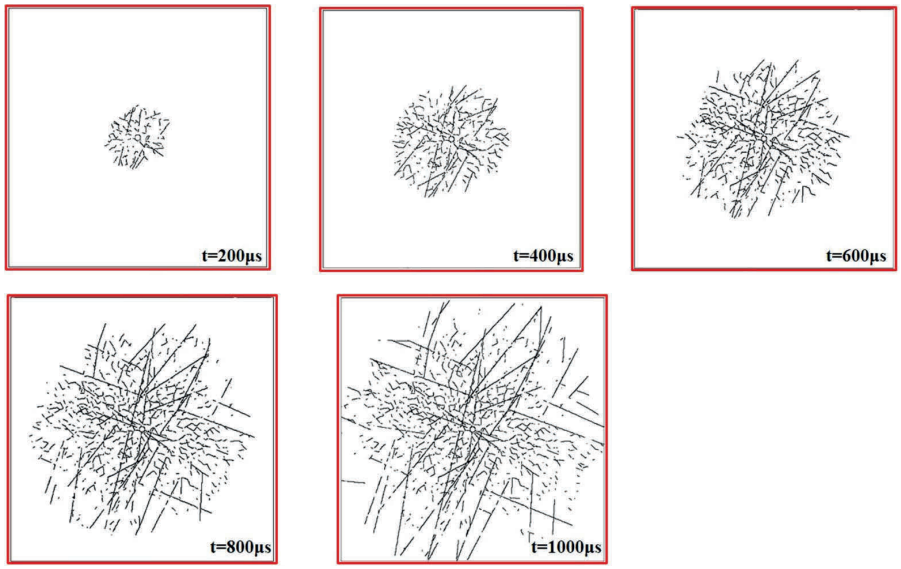

Figure 2-6. Fracture propagations in a radial section of a blast hole in rock at different times simulated with a DEM code (Lak et al., 2019).

Hybrid finite-discrete element (FEM-DEM) codes integrate the features of both finite and discrete element methods, enabling the inclusion of fracture-mechanics principles. Through this integration, these codes facilitate a simulation of brittle fracturing alongside failure kinematics. Mitelman & Elmo (2014) adopted fracture mechanics-based FEM-DEM using the proprietary code ELFEN to investigate blast-induced cracking and spalling of the rock material. Blast load generated by the explosive detonation is initially estimated using the ANSYS AUTODYN software. Example of rock fracturing due to an explosive charge is shown in Figure 2-7.

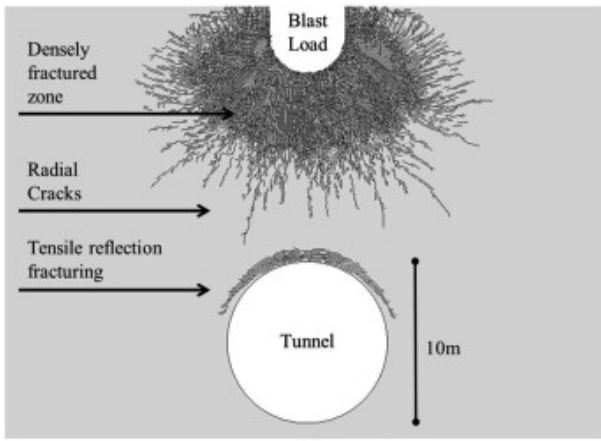

Figure 2-7. Rock fracturing due to an explosive charge with ANSYS AUTODYN (Mitelman & Elmo, 2014).

2.3 Numerical modelling of jointed rock masses

Intact rock is usually divided into smaller blocks by discontinuities (e.g. fractures and joints); in this report, the term "joint" is preferred but in general the term "joint", "fracture" and "discontinuity" refer to the description of the same type of objects. Both systematic and non-systematic fractures and joints create discontinuities that must be considered in Rock Mechanics (Priest, 1993). Due to the existence of joints that can vary in orientations and sizes, rock mass can exhibit non-uniform behaviours compared with man-made materials. Harrison & Hudson (2000) stated that "rock mass is largely discontinuous, anisotropic, inhomogeneous and non-elastic". Hence, an appropriate method that can capture the relevant behaviours of rock mass and the performance of support structures is critical in rock engineering and design (Palmström & Stille, 2007). Among the three main design tools, other than empirical and analytical methods, numerical analyses have been quite commonly adopted for its advantages in handling geologic complexity and modelling replication compared with laboratory and/or field tests (Figure 2-8).

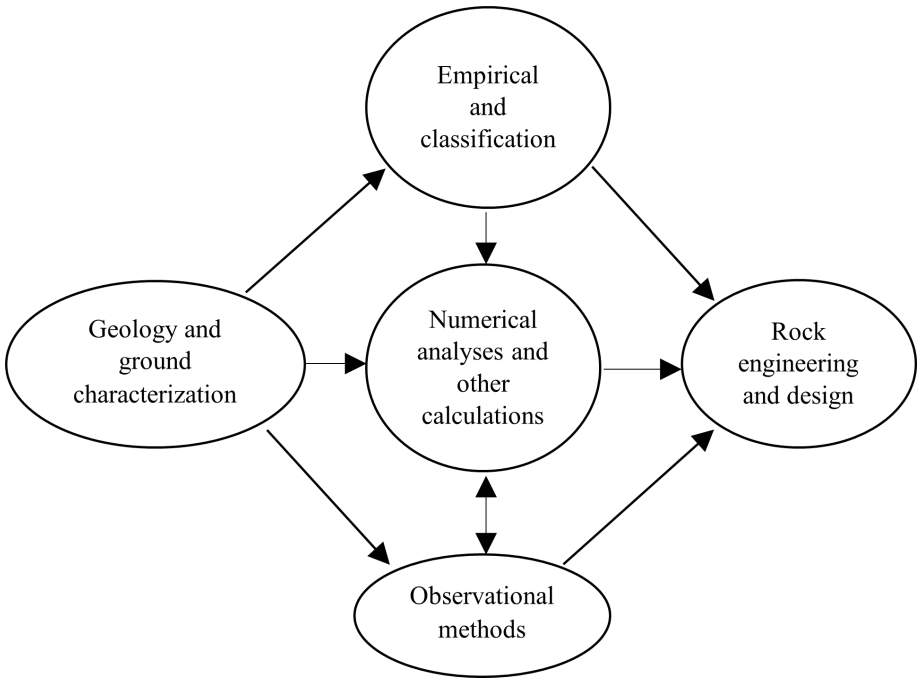

Figure 2-8. Main tools in the process of rock design (Palmström & Stille, 2007).

A literature review was carried out by Jing (2003) regarding numerical rock modelling for rock mechanics and rock engineering, where the most applied numerical methods were categorized in:

Continuum methods:

- Finite Difference Method (FDM),
- Finite Element Method (FEM), and
- Boundary Element Method (BEM).

Discontinuum methods:

- Discrete Element Method (DEM),
- Discrete Fracture Network (DFN) methods.

Hybrid continuum/discontinuum methods:

- Hybrid FEM/BEM,
- Hybrid DEM/BEM,
- Hybrid FEM/DEM, and
- Other hybrid models.

The use of equivalent continuum methods to simulate rock mass response to excavation (Barla & Barla, 2000) has gained wide acceptance with upscaled rock mass properties from intact rock by means of empirical equations (Hoek & Brown, 1997). The most representative explicit DEM methods (Jing, 2003) is the Distinct Element method created by Cundall (1980) with the computer codes UDEC and 3DEC, used in the present study.

2.3.1 UDEC

The Universal Distinct Element Code (UDEC) is a two-dimensional numerical software based on the distinct element method for discontinuum modelling. UDEC was originally developed to perform stability analysis of jointed rock slopes and has been applied most often in studies related to mining engineering both statically and dynamically (ITASCA Consulting Group, 2023).

Blasting effects on the installed dynamic rock bolts have been numerically modelled by applying dynamic velocity at model boundaries, the numerical results were compared with field test results in underground mine in order to determine the potentials of such modelling technique for evaluation of dynamic rock bolt performance in previous study (Shirzadegan, 2020).

2.3.2 3DEC

3DEC is a three-dimensional numerical software based on the distinct element method for discontinuum modelling (ITASCA Consulting Group, 2023). This program is basically the three-dimensional version of the UDEC code. 3DEC is a powerful tool for simulating the behaviour of complex geotechnical and rock mechanics systems, including underground structures, tunnel stability, seismic studies, slopes stability and landslides.

3DEC is used to simulate the behaviour of complex geotechnical and rock mechanics systems. The Distinct Element Method (DEM) can model the behaviour of discrete, rigid bodies in a granular material and allows for realistic simulation of interactions between discrete elements, such as frictional contact, sliding, and rolling. The software can be used to perform geotechnical and rock mechanics analysis, including slope stability analysis, stress-strain analysis, and, among other things, dynamic analysis.

3DEC also includes some advanced modelling features, such as the ability to model anisotropic material behaviour, to model dynamic loading conditions, and to model complex geometries and boundary conditions. 3DEC can be distinguished from 3D FEM codes for the following aspects (ITASCA Consulting Group, 2023):

- The rock mass is modelled as a 3D assemblage of rigid or deformable blocks.
- Discontinuities are regarded as distinct boundary interactions between these blocks; joint behaviour is prescribed for these interactions.
- Continuous material and discontinuous joint patterns can coexist in the same model; joints can be generated on a statistical basis.

- 3DEC employs an explicit in-time solution algorithm that accommodates both large displacement, rotation, and permits time-domain calculations.

2.3.3 Hybrid methods

It is noteworthy that the application of the most suitable numerical method to a particular rock Engineering problem, is not only a concern about to what degree the rock mass is jointed. Other factors such as the scale of the rock mass volume of interest, the purpose of the analysis with respect to failure modes, the availability of input data and the accuracy of the parameters shall be taken into account. Therefore, hybrid-methods becomes useful in some cases. An example of such hybrid methods is illustrated in Figure 2-9, where the constitutive models for intact rock and rock joint, as well as for equivalent continuum rock, are combined in the same analysis (Jing, 2003).

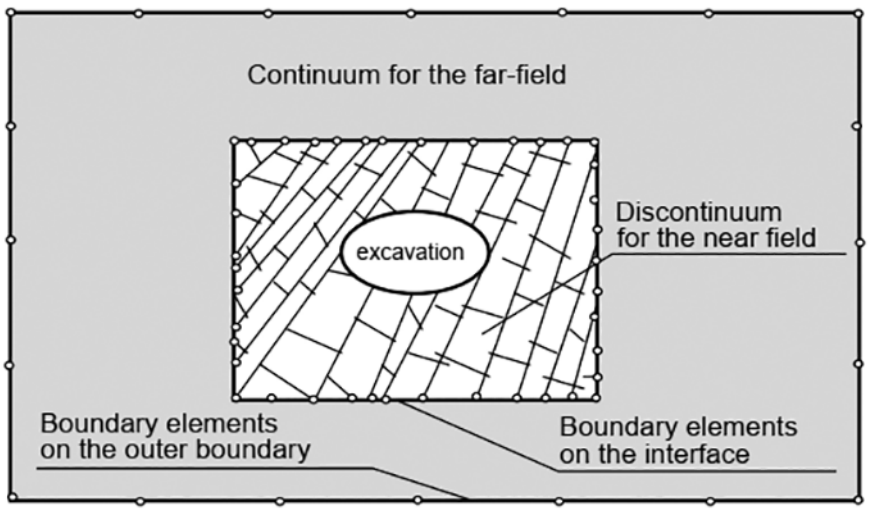

Figure 2-9. Concept of hybrid BEM/FEM/DEM methods for jointed rock mass (Jing, 2003).

2.4 Numerical modelling of large-scale field tests on blasting

To date, relatively limited work has been performed that incorporates numerical simulation of both blasting and further rock reinforcement reaction considering the influence of existing joints by means of DEM programs.

The work by Shirzadegan (2020) is intended to numerically mimic the interactions between jointed rock mass and reinforcement system under blasting conditions by means of the 2D program UDEC and LS-DYNA. Due to the geological uncertainties for example in the characterized joint set spacing of the studied areas, a sensitivity analysis was

conducted to identify which scenario was more likely to capture the behaviour of the rock mass in comparison with the field test results.

3. METHODOLOGY IN THE PRESENT STUDY

The numerical work in the current study comprises primarily two parts: LS-DYNA modelling and 3DEC modelling. The former simulates wave propagation resulting from the designed blast along the boreholes that were drilled across the crosscuts; the latter makes use of the outcomes from the former to establish blast boundary conditions for further analysis of the response of dynamic bolts to dynamic loadings applied to the rock mass. The procedural workflow for this study is delineated in the flowchart below (Figure 3-1).

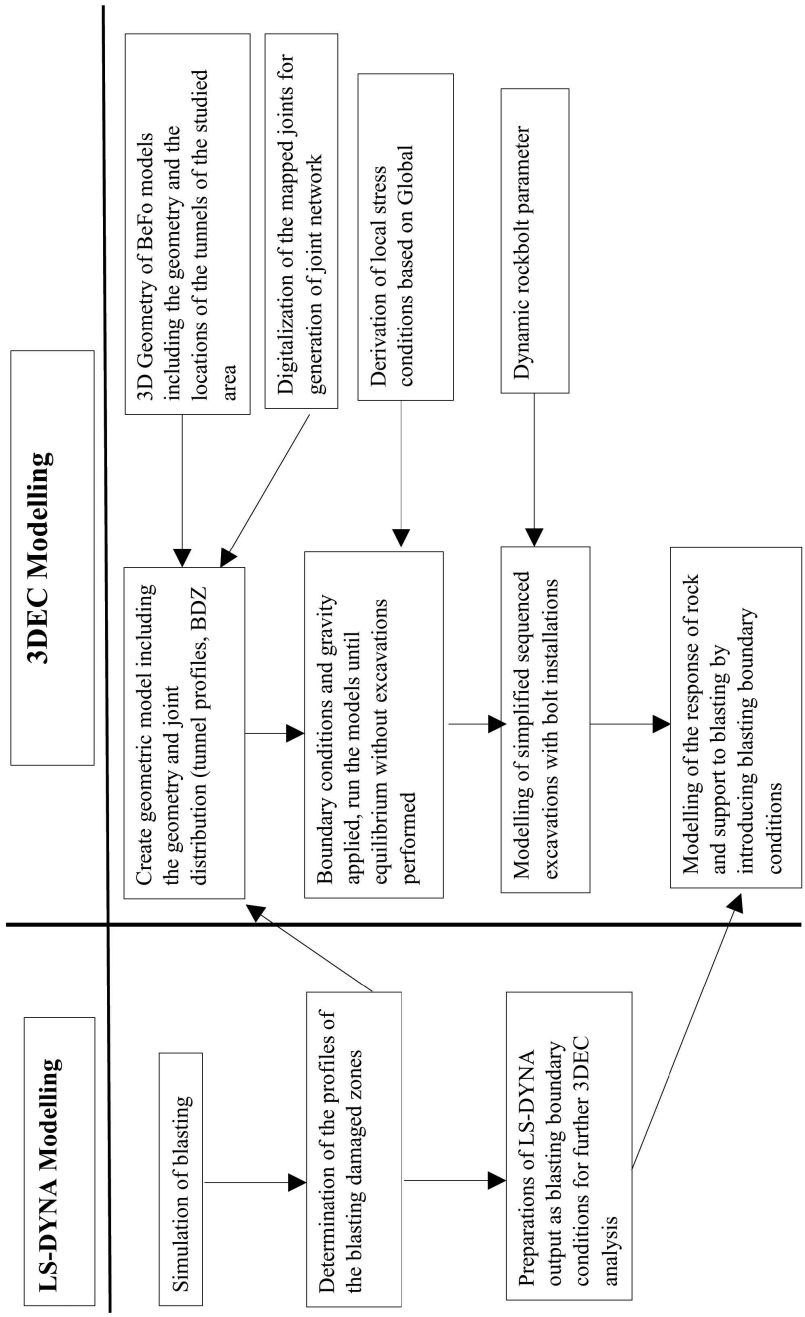

Figure 3-1. Flowchart of the working procedure for the present study.

4. GEOMETRY AND GEOLOGY OF TEST NO. 6 AT KIIRUNAVAARA MINE

4.1 Site description and geology

The in-situ blasting Test No. 6 was implemented to evaluate the performance of dynamic rock bolts in Kiirunavaara Mine, an iron mine located at Norrbotten in northern Sweden (Figure 4-1a). The mine has been in operation producing iron ore for longer than 100 years. The mined ore, after being processed to pellets, is then transported to Luleå in Sweden or, to Narvik Port in Norway. The orebody is about 80 m wide and 4 km long. The mining development depth today is at around 1.3 km.

The mine produces iron ore, which primarily consists of more than 60% magnetite-apatite and approximately 1% phosphorus. The orebody is formed within syenite and quartz porphyry bedrocks, striking approximately North-South and dipping 50 degrees (Figure 4-1b). Due to the shape of the ore body (Malmgren, 2005) a large sub-level caving method is employed, allowing the ore and the overlaying rock to cave and fall by gravity. Subsequently, the ore is mucked and loaded into a crushing unit. While this mining method is considered cost-effective, it also induces high stress redistribution around the rock, resulting in several seismic events in the mine, some of which resulting in rock bursts.

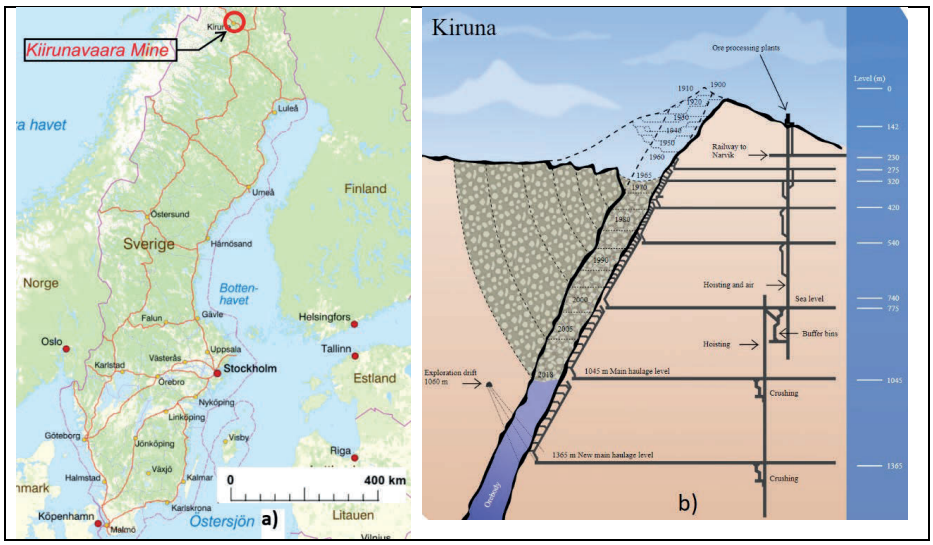

Figure 4-1. a) Location of the Kiirunavaara Mine in Northern Sweden run by LKAB; b) the orebody and mine layout.

During mining process and production stages, part of the rock is removed and creates discontinuities and voids that changes the stress field. Stresses will make their way around and deeper than the excavated zone. This process also affects the groundwater

circulations. Water flows through higher permeability rocks, and fluid circulation is affected by rock fracturing and stress concentrations. When the rock strength is exceeded due to the changes in rock stresses and water pressure, irreversible rock breakage is initiated, forming and propagating cracks even in some cases causing seismic events.

The field tests of blast damage of rock support were conducted at Crosscuts 100 and 103, Block 9, at level 741 m in the Sjömalmen orebody. In the middle of the pillar between Crosscut 100 and Crosscut 103, two blast holes were drilled and charged with explosive NSP711. The blast holes were charged halfway to reduce the effect of gas pressure on stemming materials used in the blast hole. The burden (e.g. distance between the borehole to the tunnel wall) to Crosscuts 100 and 103 is approximately 8.9 m and 7.7 m, respectively (Figure 4-2).

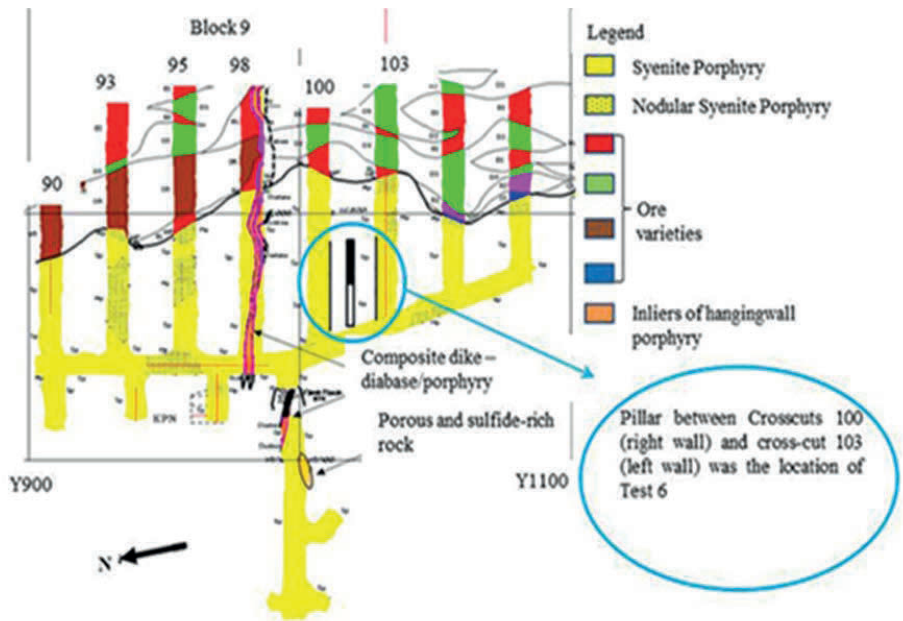

Figure 4-2. Layout of the site area (Andersson, 2010)

The rock mass at Block 9 and Block 12 have been mapped and documented by means of the rock quality system GSI (Hoek, 1994; Hoek et al., 1995) and GSI-index were estimated to be in the range 45 to 50 (Andersson, 2010). Figure 4-3 illustrates the mapped joints at Block 9 including Crosscuts 100 and 103 where the field tests had been performed. The mapped joints at Block 9 and Block 12 were categorized into three major joint sets as shown by the rose diagram technique (Figure 4-4).

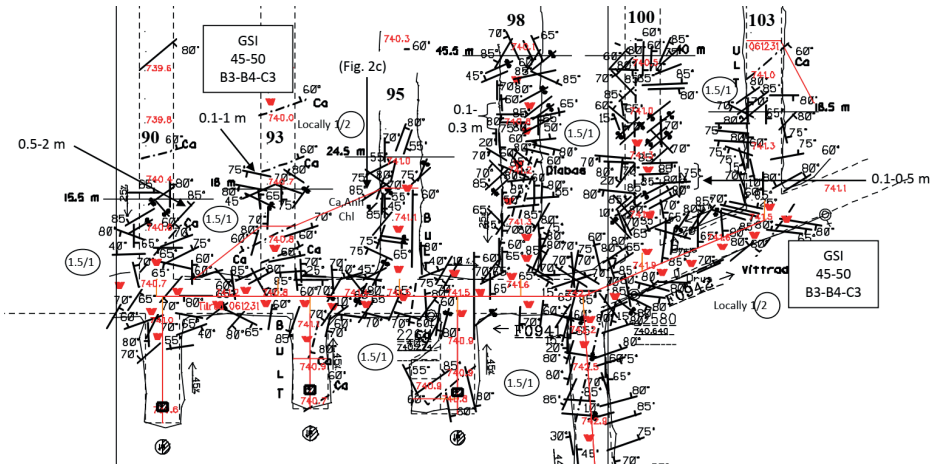

Figure 4-3. Measured joints in Block 9, level 741, Crosscuts 100 and 103. The red "V" indicates dripping water, the boxes indicate the estimated GSI values, the horizontal line with length indicate distance to mine dump fallout (Andersson, 2010).

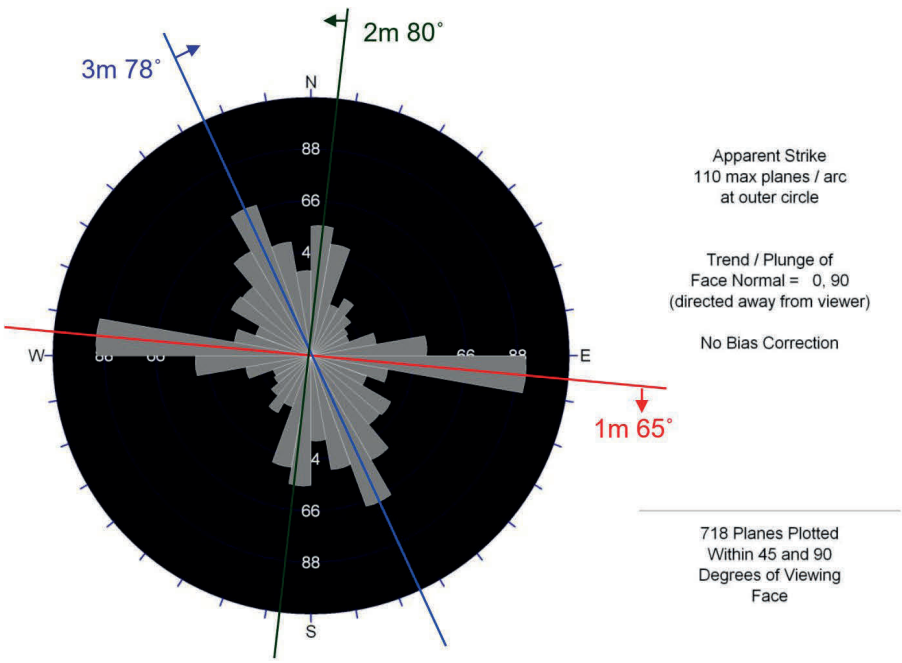

Figure 4-4. Rose diagram of the strikes of the joints in Blocks 9 and 12 at level 741 m (Andersson, 2010).

The primary objective of this study is to examine the behaviour of the rock mass and the effectiveness of dynamic rock bolts within the test areas. To achieve this goal, a detailed analysis of the joints in close proximity of Crosscuts 100 and 103 (as denoted by the blue markings in Figure 4-4) has been undertaken. Digitization of the geological mapping was conduct to extract pertinent information pertaining joint sets, joint orientation, and joint spacing. Three distinct joint sets, designated as JS_1, JS_2 and JS_3 (Figure 4-5), were identified. The average normal set spacing for each of these joint sets was determined to be approximately 3.4 m, 3.8 m and 4.8 meters, respectively.

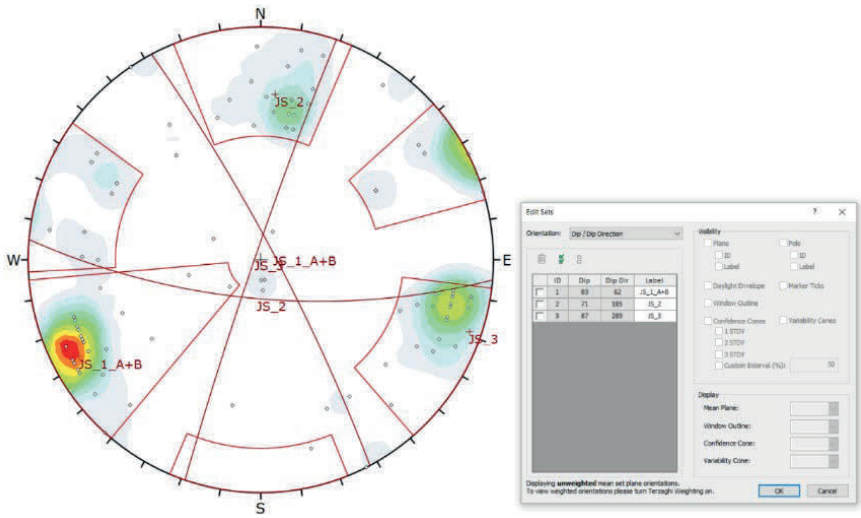

Figure 4-5. Pole diagram of the digitized joints in the proximity of Crosscuts 100 and 103.

4.2 Discrete Fracture Network

A Discrete Fracture Network (DFN) serves as a deterministic or stochastic representation of rock mass discontinuities (Vakili et al., 2014). Throughout this report, the terms "joint", "fracture" and "discontinuity" are used interchangeably to describe the same type of objects unless otherwise specified. The primary advantage of employing DFN lies in its ability to provide a physical representation of complex joint patterns, thereby enabling a more precise simulation of the behaviour exhibited by jointed rock masses. The general steps involved in generating a DFN model include data collection, data processing, joint characterization, parameterization, the realization of joint networks and subsequent validation.

The desired characteristics of a DFN model, as outlined by ITASCA Consulting Group (2023), may include:

- Modelling of joints using disks in three-dimensional space.

- Joint orientations derived from a combination of joint sets, typically comprising one sub-horizontal set, several sub-vertical sets, and additional “background” or “randomly” distributed joints.
- Background joints, which may represent a range of smaller joints, following a size distribution distinct from other joint sets, which usually have larger sizes.
- Assumption of joint positions throughout space.
- Specification of joint density for each joint set.

4.3 Determination of DFN parameters at Crosscut 100 and 103

The limited data set as mentioned earlier was collected through digitization of mapped joints according to Figure 4-3, where a total number of 99 joints in the areas including Crosscuts 101 and 103, and tunnels between these two, have been documented. Dip, dip direction and relative location of each mapped joint along assumed scanlines were determined for further process.

Some engineering judgements were made during the data process. For example, it is noted in Figure 4-5 that the JS_2 with sub-vertical orientation strikes likely parallel to the tunnel walls of Crosscuts 101 and 103, which is in line with the fact that very few joints within JS_2 were mapped along the crosscuts in Figure 4-3. Joints with similar orientation are more frequently observed along the pillar between Crosscuts 101 and 103 as well as on the opposite side of the pillar. Hence the joint set spacing for JS_2 was mainly estimated based on data from between the crosscuts, while joint set orientation was determined based on larger set of data.

Several assumptions have been made to quantify those parameters that could not be measured from field mapping such as joint persistence (Table 4-1). The shape and roughness of the joints are not the within the scope of this work, therefore simplified plane disk joints are assumed.

It is more commonly suggested that in natural condition, joint pattern follow a Fisher distribution function (Vakili et al., 2014), this suggestion for joint orientation is aligned with the data from the mapped joints within JS_1 and JS_3, while a uniform distribution is considered more fitting to describe JS_2. The joint density P_{10}, defined as the number of joints per meter, is estimated based on the calculated normal joint set spacing. Parameters used to generate the DFN realizations are summarized in Table 4-1.

Table 4-1. Joint set parameters and statistical models for DFN generation in the study area.

	JS_1	JS_2	JS_3
Orientation distribution	Fisher (Fisher coefficient 16.16)	Uniform	Fisher (Fisher coefficient 22.1)
Dip Direction	Mean: 66 Lower limit: 42 Upper limit: 80	Mean: 180 Lower limit: 163 Upper limit: 197	Mean: 283 Lower limit: 90 Upper limit: 318
Dip	Mean: 80 Lower limit: 60 Upper limit: 90	Mean: 72.5 Lower limit: 60 Upper limit: 85	Mean: 80 Lower limit: 65 Upper limit: 85
Normal Set Spacing	3.4	3.8	4.8
Density (P_{10})	0.28	0.26	0.2
Position Distribution	Uniform		
Persistence (Power-law distribution)	Mean: 5 Lower limit:3 Upper limit: 25		

It is vital to highlight that the density parameters as shown in the table above are applied to DFN generations in the study area around Crosscut 100 and 103 only, where the local joints individually and collectively are considered of great influence on stress distribution. Outside the study area, alternatively in the extended area, the existence of the joints is considered to have neglectable impact on the final stress distribution in the study area. Hence DFNs with lower density in term of joint spacing however with same values for other parameters are generated to represent the joints in the extended area, this is further discussed in Section 7.1.

5. NUMERICAL MODELLING OF BLASTING DAMAGE BY LS-DYNA

This chapter presents the FEM model prepared in the LS-DYNA platform to numerically investigate blasting. The results will be exported from this software to be used for dynamic wave propagation simulation in 3DEC, which will be presented in the next chapter.

5.1 Material properties and constitutive models

The NSP 711 explosive used in the field Test No. 6 at Kiirunavaara Mine is modelled in LS-DYNA by means of an explosive material model with the Jones-Wilkins-Lee (JWL) Equation of State (EoS) (Lee et al., 1968) as Equation (1):

$$p = A\left(1 - \frac{\omega}{R_1 V}\right)e^{-R_1 V} + B\left(1 - \frac{\omega}{R_2 V}\right)e^{-R_2 V} + \frac{\omega E}{V} \qquad (1)$$

where:

- p is the pressure
- A, B, R1, R2 and w are constants;
- ω is the Gruneisen coefficient;
- V is the specific volume;
- E is the internal energy.

A, B, and E have units of pressure while R1, R2, and ω are unitless. The parameters for characterizing NSP 711 explosive were calibrated (Helte et al., 2006) and listed in Table 5-1. ρ is the density of the explosive used, D is the velocity of detonation of the explosive and, E is the initial internal energy of the explosive.

The charge configuration in the blasthole is decoupled. The gap between the explosive and the wall of the blasthole is filled with air. Therefore, the line of coding "*MAT_NULL" is adopted in LS-DYNA for air and is combined with a linear polynomial EoS shown in Equation (2).

Table 5-1. Parameters of NSP 711 explosive (Helte et al., 2006)

ρ (kg/m^3)	D (m/s)	P_{CJ} (GPa)	A (GPa)	B *(GPa)*	R_1	R_2	w	E (KJ/cc)
1500	7680	21.15	759.9	12.56	5.1	1.5	0.29	7.05

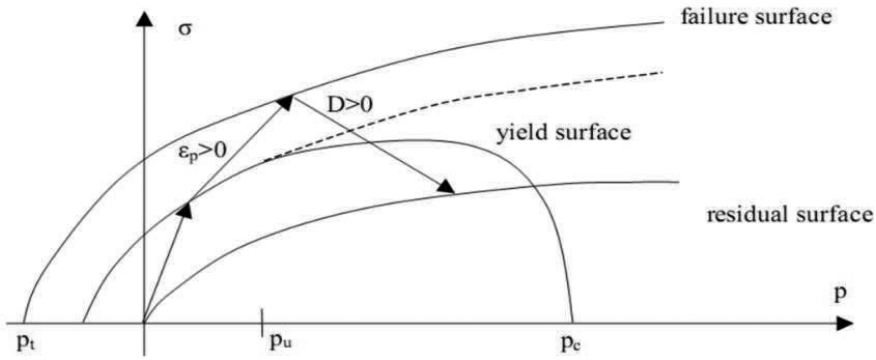

Figure 5-1. Stress limit surfaces and loading scenario in the RHT damage model **(Borrvall & Riedel, 2011)**.

$$P = \left[C_0 + C_1\mu + C_2\mu^2 + C_3\mu^3 \right] + \left[C_4 + C_5\mu + C_6\mu^2 \right] E_0 \qquad (2)$$

where:

- C_0, C_1, C_2, C_3, C_4, C_5, and C_6 are material dependent constants.

For the initial internal energy, under standard atmospheric pressure, and according to the Gamma-law calculation, at γ = 1.4, the initial internal energy is $E_0 = 2.5$ e5 J/kg and its initial density is 1.29 kg/m^3.

For the air in the interaction space, only the density of the material should be defined. A small value, 1.18 e-4 kg/m^3, is set to the density. This density is not a real density, it is only used to avoid numerical problems (zero mass) if external forces are applied to nodes belonging to air element.

The rock is modelled with the Riedel-Hiermaier-Thoma (RHT) material model (Riedel et al., 1999) in LS-DYNA, which is an advanced damage plasticity model for brittle materials such as concrete and rock. The material model involves three limit surfaces which describe the strength of the material shown in Figure 5-1: a yield, a failure and a residual surface. The yield surface is limited by a cap surface that can evolve with repeated cycles of loading and unloading. Beyond the yield surface, the material starts to deform plastically with a linear hardening description. When the material reaches the failure surface, the damage of the material starts to evolve from zero until the damage is equal to one and the residual surface is reached. Here, the material is considered to be fully damaged, and the strength is determined by the residual properties. The strain rate effect is also included in this model.

In the RHT damage model, the damage level is defined using the accumulation $D = \sum \frac{\Delta\varepsilon^p}{\varepsilon^f}$, where $\Delta\varepsilon^p$ is the accumulated plastic strain and ε^f is the failure strain. D=1 means the material is fully damaged while D=0 means undamaged. The values used for

the modelling of rock are shown in Table 5-2. The main parameters include elastic modulus (E), uniaxial compressive strength (σ_c), uniaxial tensile strength (σ_t) and Poisson's ratio (v) etc.

Table 5-2. Parameters used for the rock in LS-DYNA model.

ρ (kg/m^3)	E (GPa)	σ_c (MPa)	σ_t (MPa)	v
2800	70	267.3	16.5	0.27

5.2 Model geometry and boundary conditions

The blast design of Test No. 6 aimed at generating an almost planar wave front by using (i) a large burden and (ii) two blastholes. Since one of the blastholes did not detonate in Test No. 6, only one of the measures could be used to improve the wave front as tested in Shirzadegan et al. (2016b). The numerical model to obtain the crushed zone around the borehole is described by means of the damage model in Figure 5-1.

The dimensions of the LS-DYNA model are 25×10×10 m^3 (L×W×H). Two boreholes are in the model in preparation for Test No. 7 (not included in the present study), where the second borehole was blasted at a later time in the field experiment. The length of the boreholes is 20 m while the charge length is 10 m. The diameter of the borehole is 152 mm while the charge diameter is 120 mm, with a decoupling configuration. The gap between the wall of borehole and the explosive is filled with air. No stemming material was used to vent and reduce the effect of detonation gases. Only the explosive in the upper hole is initiated from the bottom of the borehole in the LS-DYNA model.

All boundaries except for the front of the model are defined as non-reflecting boundaries to prevent the stress wave reflection. Since the borehole length is 20 m long, a 5 m segment from the bottom of the borehole is generated to define a non-reflecting boundary to prevent the stress wave reflection from the borehole bottom side, so the length of the model is 25 m.

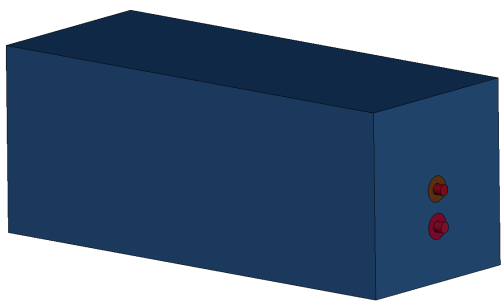

Figure 5-2. Numerical model of blasting Test No. 6 in LS-DYNA.

The rock is modelled with Lagrangian elements, while the explosive and the air are modelled with Arbitrary Lagrangian-Eulerian (ALE) elements to avoid large deformations. Additionally, a part which overlaps with the rock inside the model is defined to provide an interaction space for ALE parts and Lagrangian parts. This part is defined as vacuum material. So, there are four materials in the model: rock, explosive, air and vacuum.

To save computational time, two cylinders around the boreholes are defined to interact with the ALE elements. They are the portions of the rock mass and have the same properties as the main rock mass. The protruding red cylinders in Figure 5-2 are air domains outside the wall of the tunnel. The purpose of these is to define a domain that can cover the potential deformation of the rock at the borehole collar due to blasting.

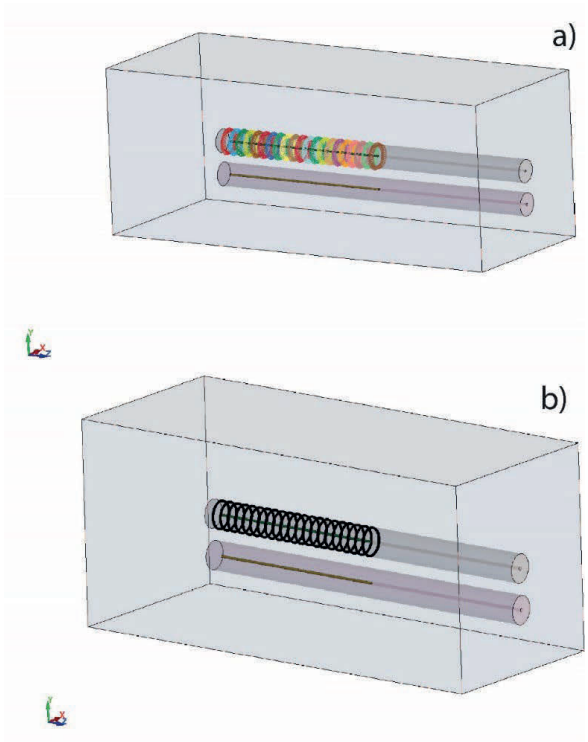

Figure 5-3. Nodes and elements in the LS-DYNA model: a) Nodes located on the selected cross-sections b) Elements located on the selected cross-sections.

To output the vibration velocity and stress at the crushed zone boundary (see Section 5.3) outside and along the borehole, eleven sections are defined to record the vibration velocity

and stress history in high resolution around Test No. 6. The interval distance of adjacent sections is 0.5 m. Each section includes 40 nodes and 40 elements (Figure 5-3).

5.3 Modelling results

The running time of the modelling is 6 milliseconds. The charge length is 10 m and the velocity of detonation is 7 680 m/s. The explosive can finish detonation in two milliseconds in this condition. The velocity of P-wave in the rock is around 5 000 m/s, and can propagate around 30 m in six milliseconds. So the stress wave can reach the boundaries of the model within the running time.

The blast-induced damage in the model is shown in Figure 5-4 and 5-5. The resulting diameter of the crushed zone is around 1.4 m. An example of the vibration velocity with components in three directions for one node on the crushed zone boundary is shown in Figure 5-6.

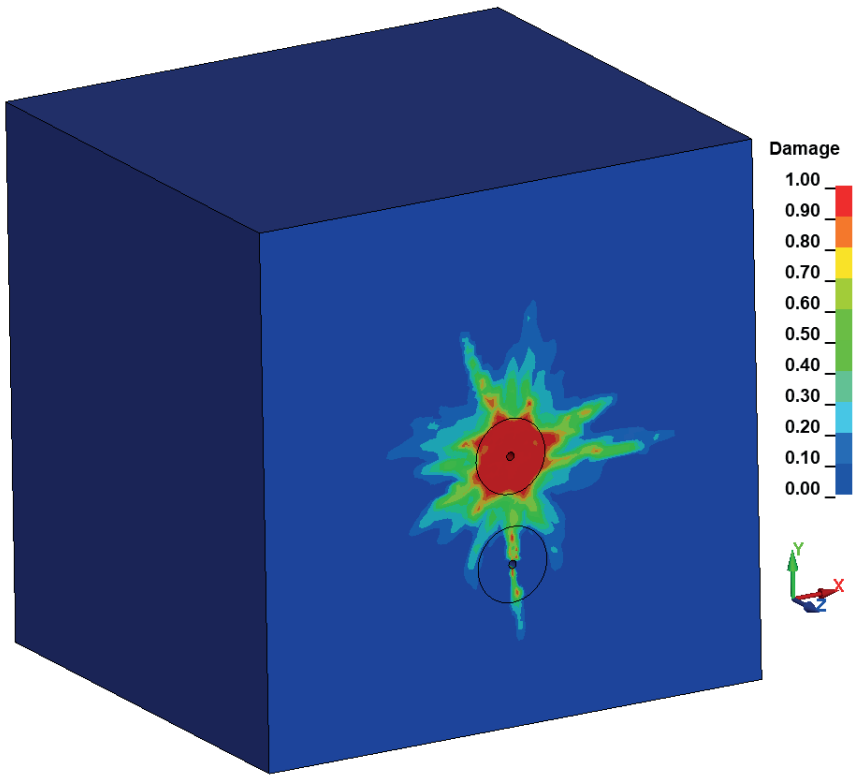

Figure 5-4. Damage around the blasthole for Test No. 6 with LS-DYNA**.**

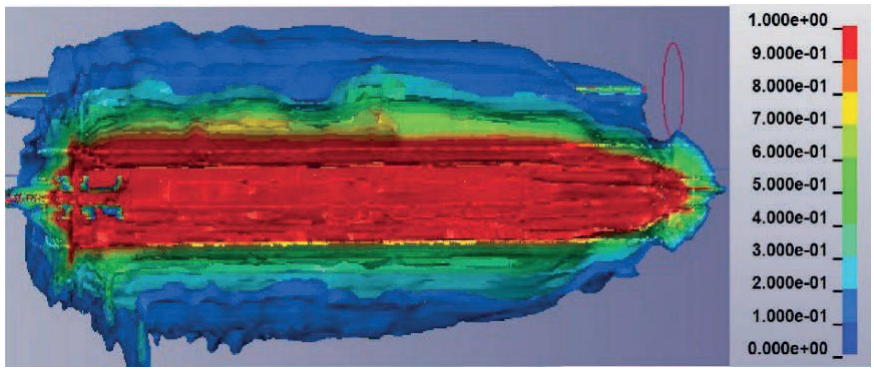

Figure 5-5. Damage area computed by LS-DYNA around the blast hole of Test No. 6.

An example of the vibration velocity with components in three directions for Node 75513 on the crushed zone boundary is shown in Figure 5-6. An example of the stress history of Element 113711 on the crushed zone boundary shown in Figure 5-7. The recorded vibration velocity history of the nodes at the periphery of the crushed zone will be introduced as the blasting boundary condition for later dynamic modelling after blasting in 3DEC.

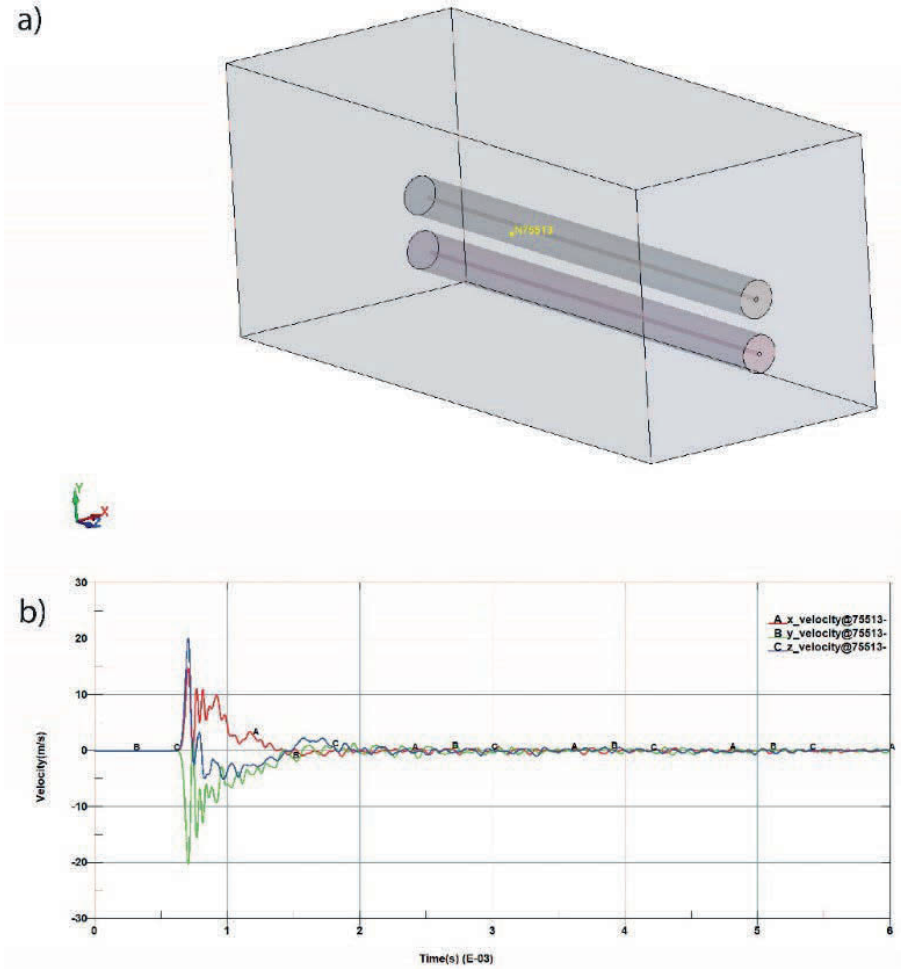

Figure 5-6. Vibration velocity history of Node 75513**:** a) its position in the model and b) vibration velocity history (x, y, z directions)**.**

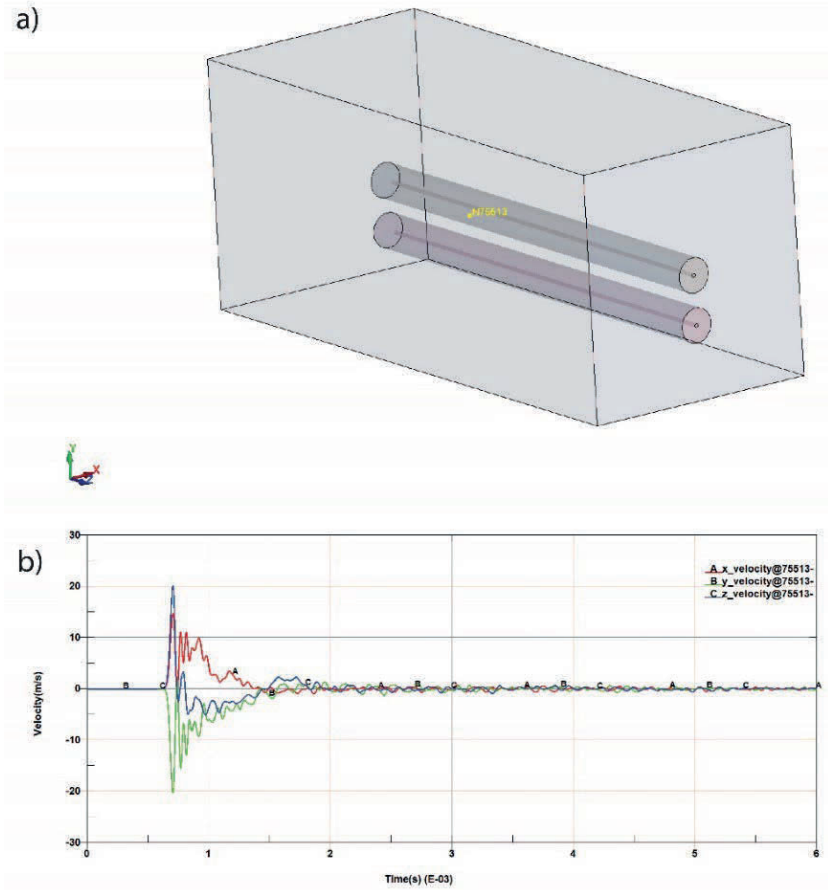

Figure 5-7. Stress history of Element 113711: a) its position in the model and; b) velocity history (x, y, z directions)**.**

6. 3DEC MODEL OF LARGE-SCALE FIELD TEST NO. 6

Prior to the 3DEC numerical analysis, modelling constrains need to be determined including choice of constitutive models, element types for the reinforcement system, material properties, model geometry and boundary conditions.

6.1 Constitutive models

Mohr-Coulomb constitutive models were adopted for simulating the shear failures in both rock blocks and along rock joints. The Mohr-Coulomb model assumes that the rock material behaves as a linear elastic material under low stresses, but it fails when the shear stress reaches a critical value, known as the Mohr-Coulomb failure criterion. The model describes the relationship between the normal stress, shear stress, and strain of the rock material, with elastic and plastic peak or residual properties.

6.2 Element types

For the rock blocks, elastic or rigid element type can be chosen in order to neglect the block solid material deformation. If the deformation of the blocks cannot be neglected, for computational modelling in 3DEC, two main methods can be used to include deformability. The direct method of introducing deformability involves dividing the body into either internal or boundary elements, which enhances the number of degrees of freedom and enables the representation of more complex deformation patterns. The level of complexity in the deformation process is contingent upon the number of elements into which the body is subdivided. In the elastic case, the formulation of these zones is analogous to that of constant-strain finite elements. Additionally, the zones can be defined by an arbitrary, nonlinear constitutive law. A drawback of this method is that it requires the division of a body of complex shape into numerous zones, even when a simple deformation pattern is desired.

3DEC includes four basic constitutive model groups for blocks and seven constitutive model groups for joints, used to capture a range of behaviours. The elastic, plastic, creep and dynamic are the four constitutive models available for blocks, while elastic, Mohr-Coulomb, softening-healing Mohr-Coulomb, bilinear Mohr-Coulomb, power law creep, continuously yielding and nonlinear are the seven joint constitutive models built in 3DEC (ITASCA Consulting Group, 2023).

The Mohr-Coulomb constitutive model is utilized for characterizing the behavior of the block material within the plastic model group. Additionally, the Mohr-Coulomb constitutive model is employed to depict plasticity in the joint modeling. The elastic joint model is the most fundamental and is specifically used for construction joints in the model.

Hybrid bolt structural elements (ITASCA Consulting Group, 2023) are adopted to simulate the dynamic bolts in the 3DEC models. These elements can encompass the

behaviour of cables and include an extra component to resist shearing perpendicular to the cable where the cable crosses a joint or interface. The cable can provide a pulling resistance by means of the rod and grout properties along the cable length, while shear resistance can be developed by the rock bolt rod via “dowel” section inserted at the intersections with the rock joints. Discontinuous rock masses are modelled in 3DEC as an assemblage of discrete blocks, with reciprocal boundary conditions defined by the discontinuities between them. The blocks can undergo large displacements along the discontinuities and rotate as necessary. Each block can be assigned a solid constitutive model, and a joint constitutive model determines the behaviour of the fractures at the faces of the blocks.

It is important to recognize that in practice, the contribution of dowel section to hybrid bolt performance can be highly bolt specific depending on the characteristic features designed along the bolt length to achieve its unique anchorage mechanism.

6.3 Material properties

Static and dynamic properties of intact rock and rock joints might be different and can affect the results of numerical modelling (Bazargan, 2022). However, dynamic mechanical properties of rock and joints were not available and are generally scarcely documented in the literature. It is important to highlight that one of the studied crosscuts was excavated before the blast impact and remained stable in its origin shape without the installation of any support system for some time. Even after the blasting impact, only minor fallout was observed. This indicates the presence of very stiff rock and relatively few joints in the studied area. The mechanical properties of intact rock and the joints as inputs for 3DEC modelling are presented in the following Table 6-1 and Table 6-2 based on earlier work (Shirzadegan, 2020).

The calibrated parameters for the Swellex Mn24 bolts and D-bolts are summarized in Table 6-3 and for the grout in Table 6-4. Some assumptions have been made for the calibration of bolt parameters considering that: a) bolts of different types are assumed to have the same length, i.e. 3 meters; b) the contribution of the dowel section to the bolt performance in 3DEC does not consider the real location of the dowel along the bolt, instead the location is simplified and numerically assigned where the bolt intersects a rock joint; c) certain parameters are not available through physical tests on bolts and grouting, and hence evaluated based on empirical equations, but are assigned according to values found in the literature. For example, the “dowel stiffness”, is suggested to be estimated based on different parameters including grout properties and borehole diameter according to (Gerdeen et al., 1977) same dowel stiffness has been assumed for both bolt types.

In general, other factors than the characteristic strength and deformability features of the bolts are not within the scope of this study, while insight into how the bolts respond to dynamic loading is intended to be studied. In our model we define yield-tension of the grout as 0 MPa due to not finding reliable values in the literature.

Table 6-1. Intact rock properties for 3DEC modelling.

Density (kg/m^3)	2800
Elastic modulus (Pa)	70
Poisson's ratio	0.27
Bulk modulus (GPa)	50.7
Shear modulus (GPa)	27.6
Cohesion (MPa)	31
Friction angle (°)	61
Tensile strength (MPa)	16.5
Uniaxial compressive strength (MPa)	267

Table 6-2. Rock joint properties for 3DEC modelling.

Friction angle (°)	Cohesion (MPa)	Tensile strength (MPa)	Normal stiffness (GPa/m)	Shear stiffness (GPa/m)
35	1	0.5	110	9

Table 6-3. Calibrated properties of dynamic bolts in Kiirunavaara Mine**.**

	Swellex Mn24 bolt	D-bolt
Cross-sectional area (m^2)	3.27e-04	3.87e-04
Elastic modulus (Pa)	2,00e+11	2.00e+11
Density (kg/m^3)	7800	7800
Tensile load (N)	2.40e+05	2.77e+05
Tensile failure limit	0.35	0.22
Dowel shear stiffness (Pa)	1.03e+09	3.39e+08

Table 6-4. Properties of grout for modelled dynamic bolts.

Type of bolts	Normal stiffness (N/m/m)	Normal cohesive strength (N/m)	Grout perimeter (m)
Swellex Mn24 bolt	1.00e+09	2.00e+09	0.151
D-bolt	1.00e+09	2.00e+09	0.119

6.4 Model geometry

The dimensions of the local model created in 3DEC are 100 meters in the directions of the x-axis and z-axis, and 150 meters in the direction of the y-axis (parallel to Crosscut 100 and 103). Figure 6-1a shows the full dimension of the local model and Figure 6-1b shows the tunnel system layout in the study area. The locations of crosscuts, footwall

drift, and upper borehole (Test No. 6) and lower borehole (Test No. 7) for blasting and their deviation with respect to the crosscuts, are included in the model. The footwall drift is intersected by the crosscuts at an angle of approximately 72 degrees (e.g. is not perpendicular to them).

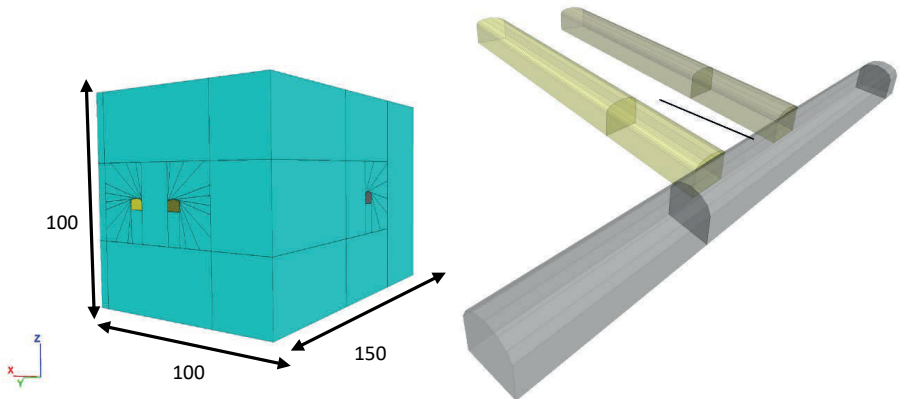

a b

Figure 6-1. Local 3D model of the research area at the level of 741 m: (a) local model dimension; (b) layout of footwall drift, crosscuts and blastholes deviation.

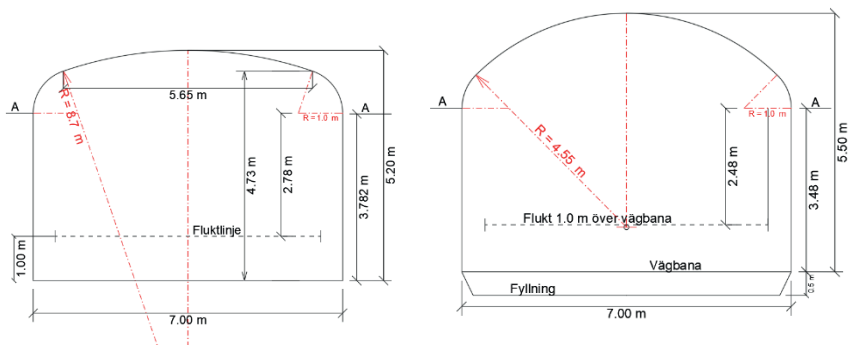

a b

Figure 6-2. Cross-sections of Kiirunavaara Mine tunnels: (a) Crosscuts (b) Footwall drift.

Figure 6-2 illustrates the cross-sections of the crosscut tunnels and footwall drift. The height of the footwall drift is about 5.5 m and that of the crosscuts about 5.2 m.

Figure 6-3 displays a cross-sectional view of the crosscuts, footwall drift, and two blastholes. The deviated blast holes are located on an average of 8.7 m from Crosscut 100, respectively 8.2 m from Crosscut 103, i.e. dimension of the “burden”. Figure 6-4

and Figure 6-5 also show the geometry of the transparent and solid view of the local 3DEC model.

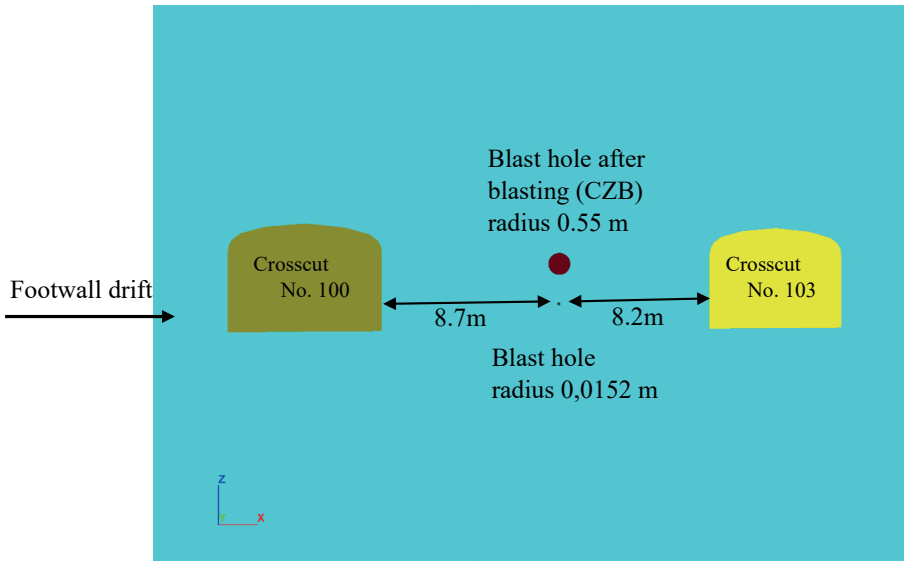

Figure 6-3. Front cross-cut view of the boreholes and crosscuts.

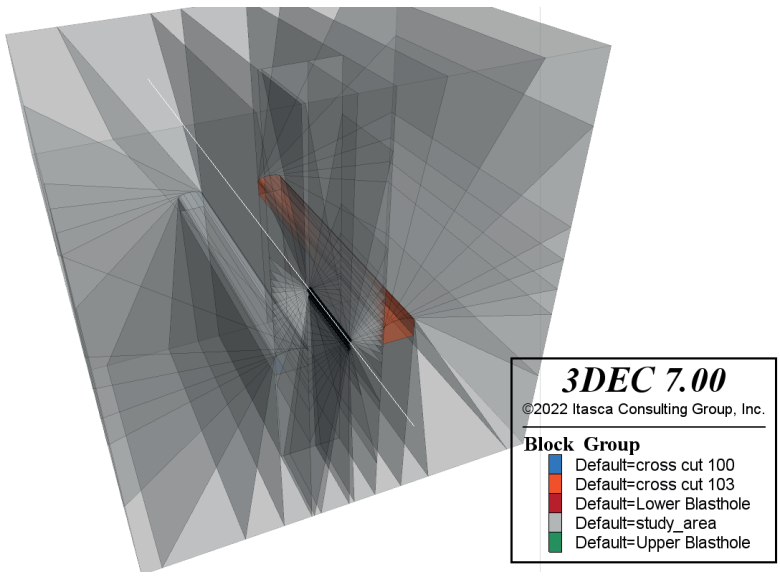

Figure 6-4. Geometry for the local model with 3DEC in transparent view.

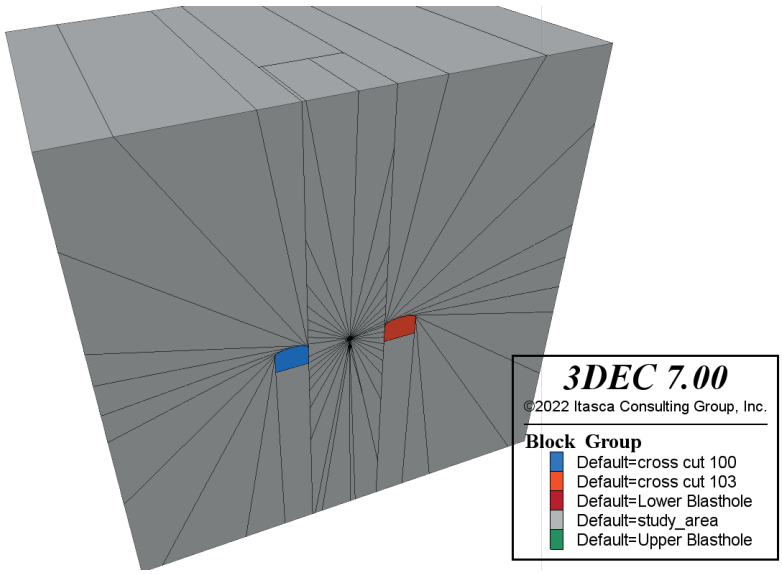

Figure 6-5. Geometry for the local model with 3DEC in solid view.

6.5 Boundary conditions

The production at Kiirunavaara Mine has been underway for a long time, started with an open pit and followed by underground mining. The stress induced by sublevel caving in the global model was computed using 3DEC. One of the assumptions in estimating the in-situ stress is that the rock mass can be treated as a homogenous, isotropic continuous, and linear elastic material. Previous studies (Sandström, 2003) sought to establish correlations that describes the original stress conditions prior to mining, with respect to depth. It is revealed that the primary principal stress should be a horizontal stress, which is almost perpendicular to the direction of the ore deposit. These correlations are employed to construct the initial stress conditions in the numerical model prior to mining.

Table 6-5. In-situ stresses at Kiirunavaara Mine (Sandström, 2003).

In-situ Stress Condition	
$\boldsymbol{\sigma_{H(ew)}}$ (MPa)	$0.037z$
$\boldsymbol{\sigma_z}$(v) (MPa)	$0.029z$
$\boldsymbol{\sigma_h}$(ns) (MPa)	$0.028z$

where:

- z is the depth below surface, m
- $\sigma_{H(ew)}$ is the tress in east-west (X axis) direction, MPa
- σ_z(v) is the stress in vertical (Z axis) direction, MPa

- σ_h (ns) is the stress in north-south (Y axis) direction, MPa.

A global 3DEC geomechanical model has been developed to study the stress redistribution in Kiirunavaara Mine for further optimization of the ore extraction and minimization of risks associated with mining induced rock failures (personal communication: Nikadat, 2022). This global model is adopted to derive the stress level in this study's specific level which is later converted into the boundary conditions for a local model, where the performance of dynamic bolts is numerically investigated.

For the continuous global 3DEC model, a mine-scale model was generated to account for the current mining levels and production progress. The stress conditions at Block 9 and Level 741 m were determined for the time of execution of Test No. 6, when the mining front had reached 780 m. The rock mechanics properties were assumed as suggested by Malmgren & Sjöberg (2006) and Malmgren, Sjöberg, & Krekula (2008). Relatively fine elements were assigned around the orebody and near the test drift, compared to those in the rest of the global model. The schematic plot of the global model is presented in Figure 6-6. Figure 6-7 shows the stress contour of the global model for Kiirunavaara Mine at the production level correspondent to the time when Test No. 6 was performed at the level of 741 m.

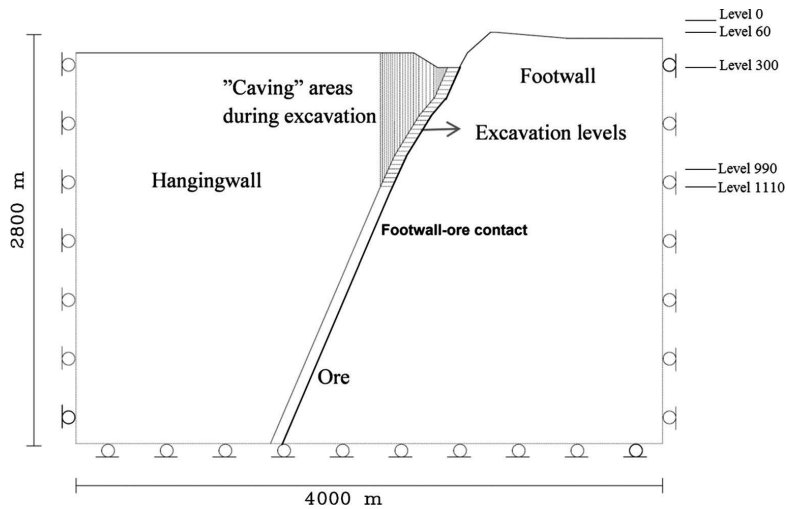

Figure 6-6. The schematic cross-section of global model of Kiirunavaara Mine.

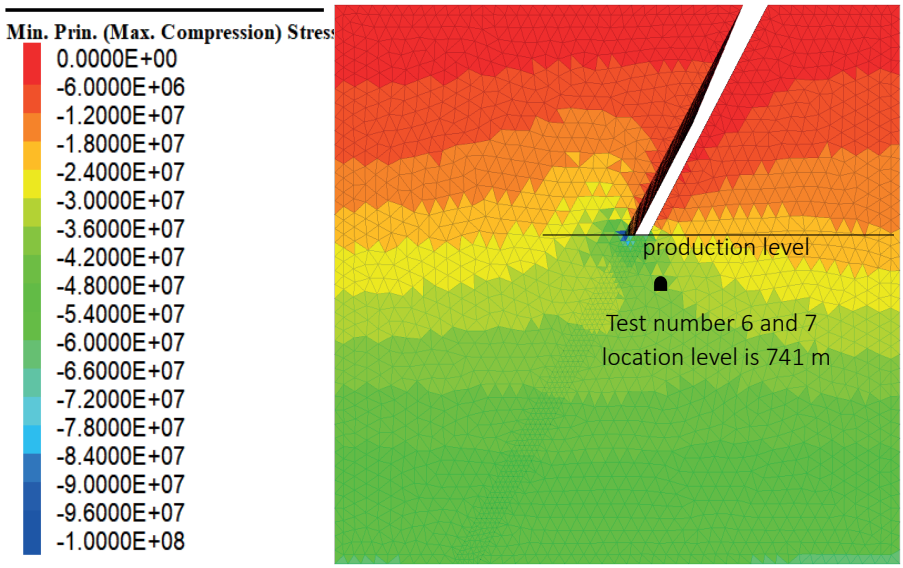

Figure 6-7. Global stress model for Kiirunavaara Mine for the conditions at Test No. 6.

The local model of the area around Test No. 6 was also constructed in 3DEC, in which the rock mass is treated as a discontinuum medium, with isotropic continuous blocks isolated by planar fracture features, and linear elastic, perfectly plastic materials. The local model features the footwall drift, two crosscuts, and blast holes. Table 6-6 presents the derived boundary conditions of the local model, where the vertical boundary at y = 100 m locally was assigned fixed boundary during static and dynamic analysis to prevent whole model rotation. Thus, other boundaries, except y = 100 m locally, were assigned stress boundary during static analysis.

During the dynamic analyses, the boundaries were set to act as non-reflecting (viscous) boundaries on all surfaces of the local model. The boundary condition of this setting prevents reflecting waves back into the model.

Since the study area is located at large depth below the ground surface, the stress gradients are judged to be insignificant, due to the small changes of location both horizontally and vertically within the local model. Therefore, in-situ stresses can be considered of constant magnitudes for the local model. The outcome of the derived stress in the study area are outlined in Table 6-6.

Table 6-6. Stress derived from the global model as local model boundary inputs**.**

Stress components	Stresses from 3DEC global model (MPa)
σ_H	-25.27
σ_h	-4.60
σ_{int}	-16.20
σ_{xx}	-16.90
σ_{xy}	7.82
σ_{xz}	-8.58
σ_{yy}	-15.15
σ_{yz}	-1.33
σ_{zz}	-11.14

The blasting boundary condition inside the blasthole in the 3DEC model are determined based on the results of LS-DYNA reported in Chapter 5.

6.6 Computational steps

The following computational steps were included in the 3DEC modelling:

1) Model equilibrium with elastic properties with joint element not activated
2) Opening of the crosscuts and borehole
3) Activation of the joints with plastic properties and model equilibrium to convergence (unbalanced forces not negligible, 1e-2)
4) Activation of the bolts
5) Model equilibrium to convergence in static conditions (negligible unbalanced forces, 1e-5)
6) Reset of displacements
7) Blasting input in the borehole
8) Model equilibrium to convergence in dynamic conditions (negligible unbalanced forces, 1e-5).

7. NUMERICAL MODELLING RESULTS OF LARGE-SCALE FIELD TEST NO. 6 BY 3DEC

In this chapter, the 3DEC results are presented in the form of velocity history of selected points on the crosscut walls and, the axial displacement of the installed bolts and the displacement of the rock blocks. Some considerations about the block displacement patterns are also provided.

The 3DEC models run in this study are summarized in Table 7-1 and described in the following sections.

Table 7-1. Categorization of the 3DEC models.

Bolt types / Joint patterns	Swellex Mn24 bolt	D-bolt
Regularly spaced joint sets	RSJS & Swellex Mn24 bolt	RSJS & D-bolt
Discrete Fracture Network	DFN & Swellex Mn24 bolt	DFN & D-bolt

7.1 Models with different joint patterns

Two different models were created by generating the joints in the study area under different assumptions: the first assumes a rock mass with regularly spaced joints and, the second with joints following a probabilistic distribution by means of one DFN realization. Outside the study area, an extended area was crated with joints generated by means of a coarser DFN realization based on the same joint parameters, but irrespective of how the joints in the study area were generated.

Figure 7-1 illustrates the model with regularly spaced joint sets in the study area and a coarse DFN realization in extended area. Figure 7-2 illustrates the model with DFN realization in the study area and a coarser DFN realization in the extended area.

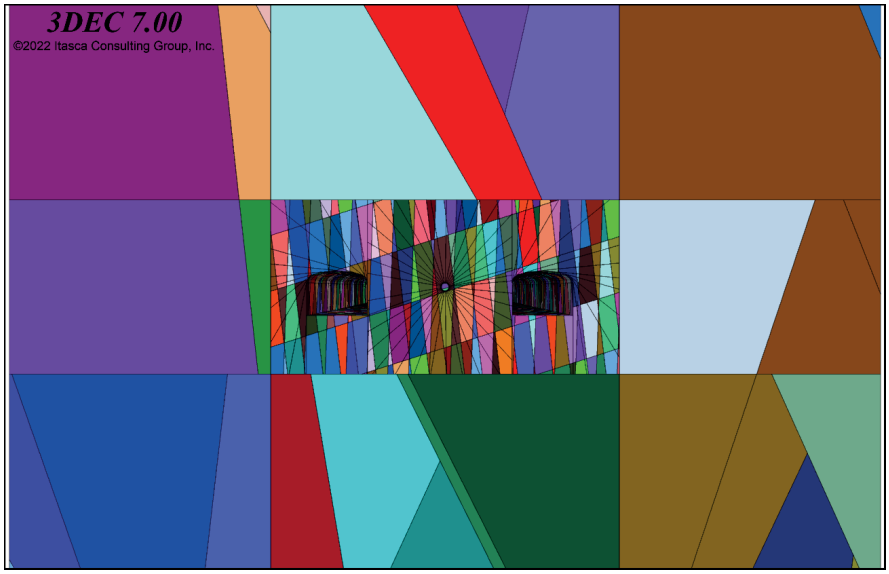

Figure 7-1. Geometry of host rock mass with regularly spaced joints in the study area and DFN in the surrounding extended area.

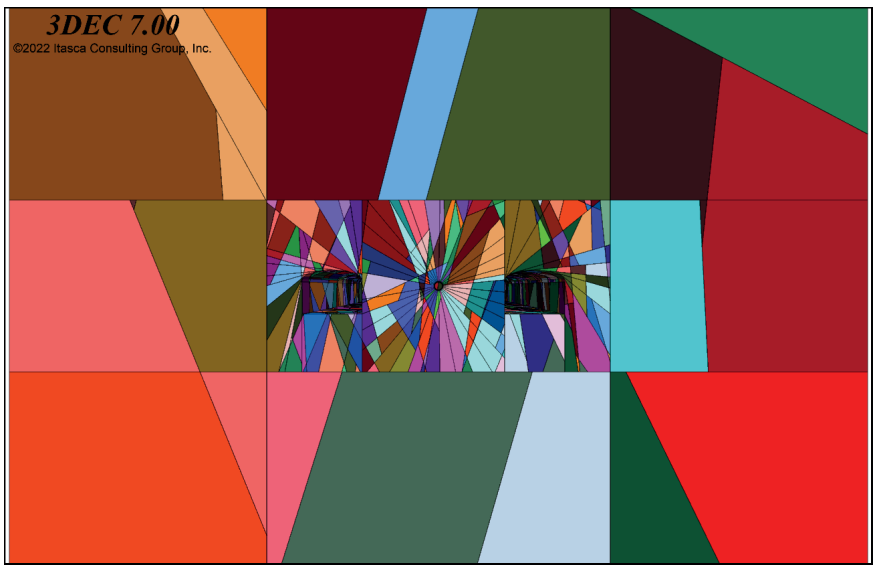

Figure 7-2. Geometry of host rock mass with DNF realizations in both the study area and extended area (the central part for the study area and the surrounding for the extended area)

7.2 Bolt types

This project is intended to investigate the performances of two types of dynamic bolts under dynamic load induced via blasting. The dynamic bolts have mechanical properties to simulate the Swellex Mn24 bolt and D-bolt. For each bolt type investigation has been separately implemented in the 3DEC model (Figure 7-3) respectively with regularly spaced joint model and discrete fracture network model. Hence the models have been categorised with respect to bolt types and the method applied to the generation of the joints.

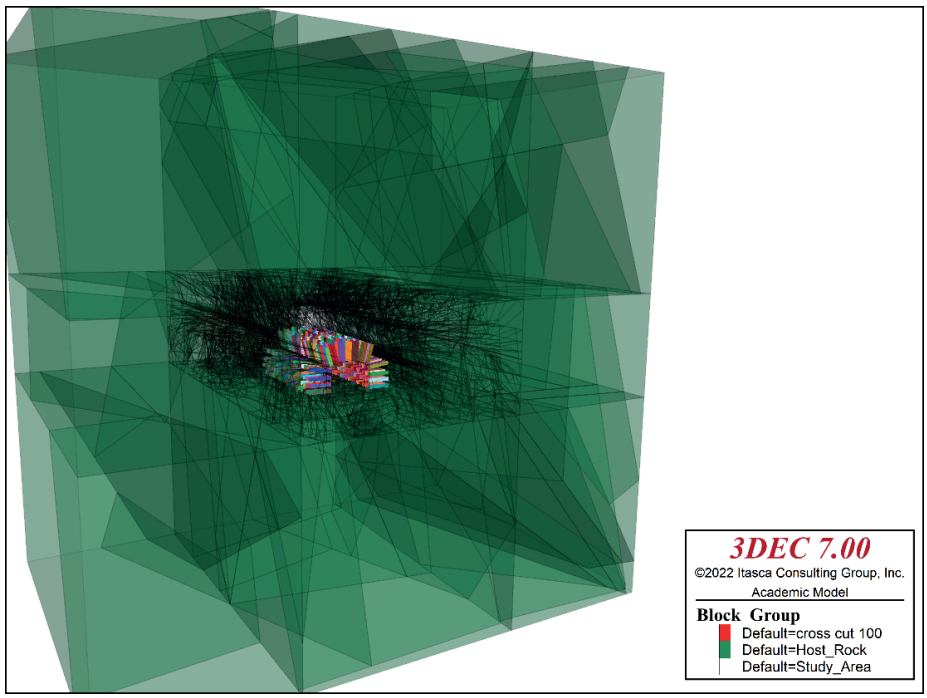

Figure 7-3. View of the installed bolts in Crosscut 100 in the 3DEC model.

7.3 Dynamic loads

The dynamic load induced by blasting is generated by LS-DYNA (Chapter 5) and imported into the 3DEC models to simulate the induced displacement and stress histories. Figure 7-4 shows an example of block displacement pattern 0.01 second after the initiation of the blasting. Changes in the shear force on the grouting of the bolts can be seen at the same point in time in Figure 7-5. The geological features in the models produce different behaviours of the propagating blasting wave (Figure 7-6 and figure 7-7).

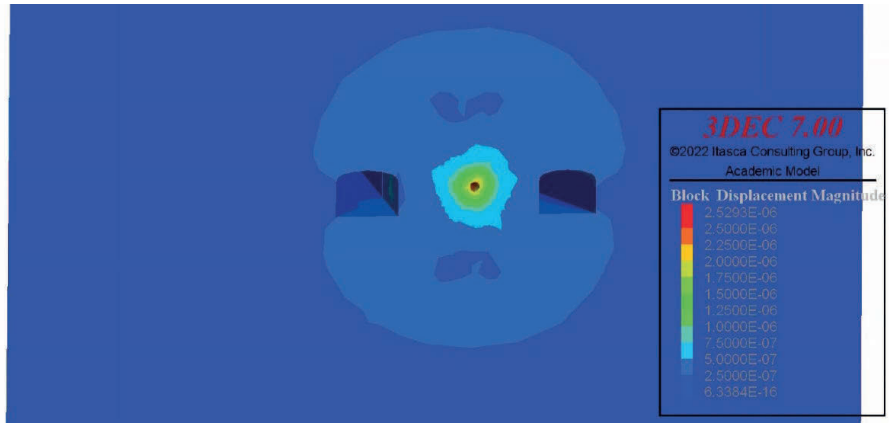

Figure 7-4. Block displacement around the blasthole 0.01 sec after initiation of the blasting for regularly spaced joint set model (displacements are in m**)** (3DEC model: RSJS & Swellex Mn24 bolt).

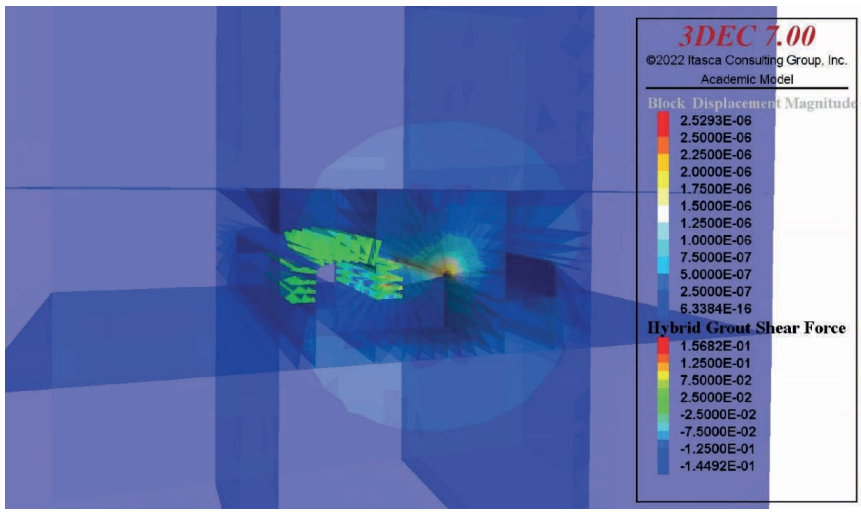

Figure 7-5. State of the bolt grout shear force **(**shear force in MN**)** and deformation of the rock blocks (displacements are in m) 0.01 sec after the blast impact for regularly spaced joint set model **(**3DEC model: RSJS & Swellex Mn24 bolt).

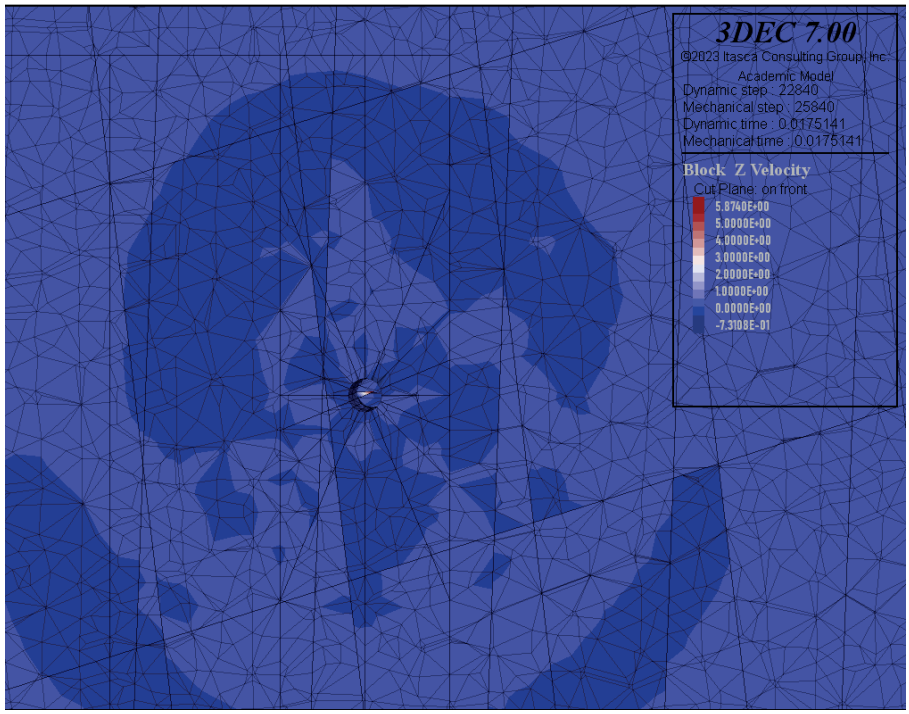

Figure 7-6. Block velocity in meter per second in the rock blocks around the blasthole after blasting for the model geometry formed with regularly spaced jointed rock (3DEC model: DFN & Swellex Mn24 bolt) at a time of 0.01 sec after the blasting.

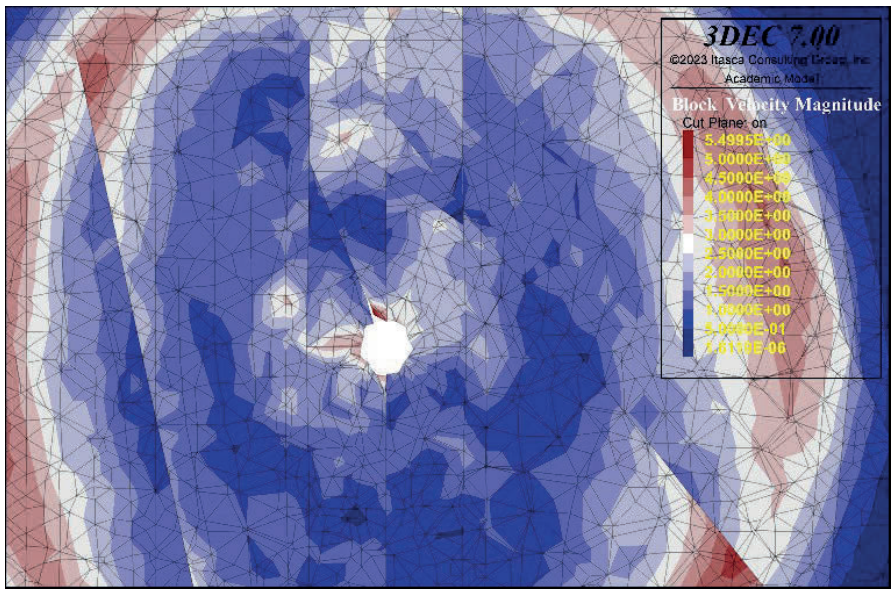

Figure 7-7. Block velocity in meter per second in the block around the blasthole after blasting for the model geometry with DFN realizations (3DEC model: RSJS & Swellex Mn24 bolt) at a time of 0.01 sec after the blasting.

7.4 Point probe velocity

In Crosscut 100 reinforcement including bolts was installed, while along Crosscut 103 no reinforcement was installed in Test No. 6. In the numerical models, the bolt arrangement was recreated.

Point probes are typically defined in the model at specific locations of interest to extract specific information or monitor certain variables such as point velocity, displacement, and stress values. Points along the tunnel wall of Crosscuts 100 and 103 are pre-selected in the 3DEC models order to collect the history data on velocity (Figure 7-8 and Figure 7-9) In each of the crosscuts, the spacing between the point probes is set to be one meter in both longitudinal direction (y-axis) and vertical direction (z-axis).

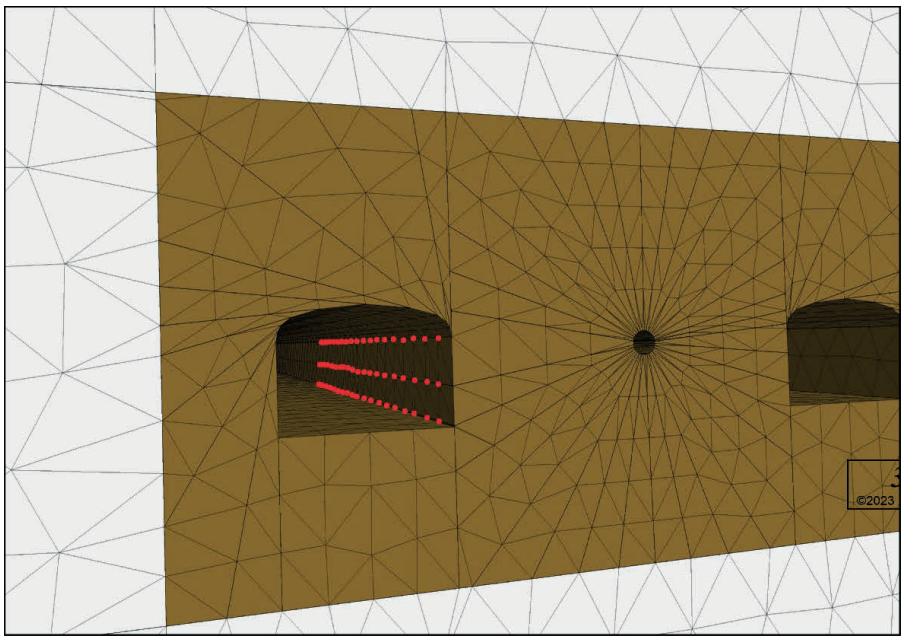

Figure 7-8. Pre-selected point probes (red dots) along the tunnel wall of Crosscut 100.

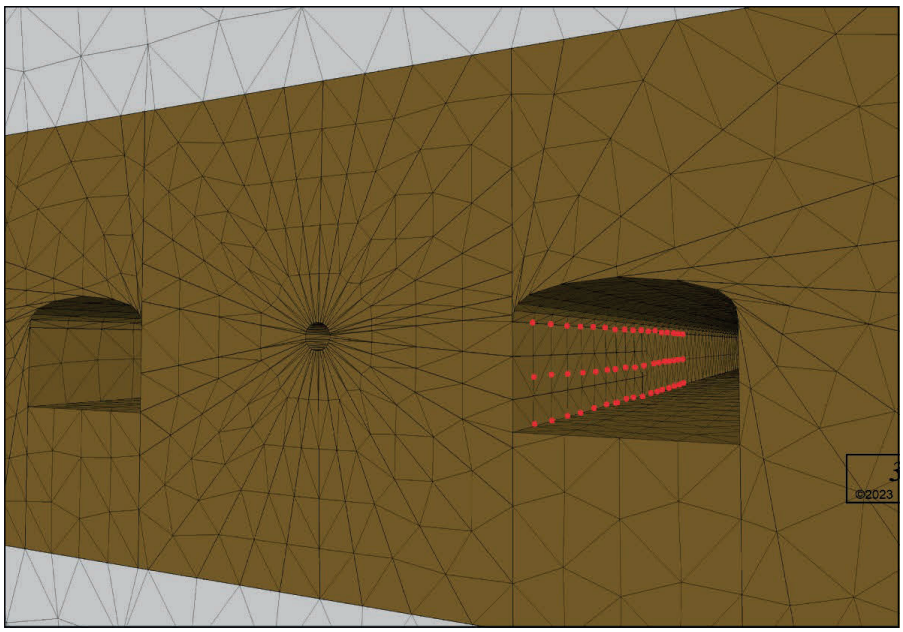

Figure 7-9. Pre-selected point probes (red dots) along the tunnel wall of Crosscut 103.

Velocities on the point probes in the model after blast impact are shown in the following sub-chapters. The velocity component in the transversal direction (x-axis) at the point probes is presented. The charts are generated with velocity values in meter per second (vertical axis in the charts) and for 0.5 seconds model runtime (horizontal axis in the charts).

To reach the computational time of 0.5 seconds, a considerable number of cycles are required. Average wave propagation velocities in rocks are reported to be between 1600 to 6000 meters per second. Thus, the propagation time value for the 8-meters space between the blast hole and the crosscut is between 1 to 5 milliseconds. Therefore, running the model for 0.5 seconds is believed to investigate the effect of the blast on the crosscuts and study the performances of dynamic bolts within a good computational framework.

Geometrically, the blast hole is placed between Crosscut 100 and 103. Crosscut 100 was placed in a negative X-direction from the blast hole, while Crosscut 103 was placed at a positive X-direction from the blast hole. Therefore, the peak particle velocity collected from the point placed on the wall of Crosscut 100 will show negative values when displacement occurs toward this tunnel, while the peak particle velocity collected from the point placed on Crosscut 103 will show positive values when displacement occurs toward this other tunnel.

The velocity collected at points on the wall of the crosscuts shows that the further we go from the blast hole, the lower the velocity values. This is in line with the physics of wave propagation in a medium with energy loss due to rock texture and travel distance. This can change based on the damping properties of the model. The velocity values numerically measured can also be compared to the field-collected data with a peak particle velocity between 2.5 to 4.5 m/sec (Shirzadegan et al., 2016a; Shirzadegan et al., 2016b).

It is observed that the influence of the blast on the velocity of the points diminishes over time, and the points return to their stable original condition once the blast impact has ceased. This illustrates the damping properties of the jointed rock mass and the convergency of the numerical simulations.

By comparing the results from Crosscut 100 with those of Crosscut 103, slightly different results can be observed. Velocity values from the crosscut that has dynamic bolts in place are lower than the velocity value on the crosscut with no reinforcement installed on the tunnel walls. This shows that dynamic bolts reduce the rock block velocity of the area close to the tunnel walls.

Dynamic bolts installed in the model with regularly spaced joints or in the model with the DFN realization illustrate similar performance results and have the same effect in reducing the rock block velocity during dynamic load induced via blasting on the reinforced tunnel wall. This result compares well with the collected field data of the crosscut before and after blasting and indicates that both the joint patterns are a good representation of the rock mass at the field experiment location of Test No. 6.

Point probe velocities from selected probe points on the walls of Crosscut 100 and 103 in the simulated 3DEC models presented in Table 7-1 are presented in the following sections.

7.4.1 3DEC model RSJS & Swellex Mn24 bolt

This section illustrates 3DEC models with regularly spaced joint sets and mechanical parameters of Swellex Mn24 bolts.

7.4.1.1 Supported Crosscut 100 (RSJS & Swellex Mn24 bolt)

Velocity-time history plots were generated for predefined points along the tunnel wall of Crosscut 100 from RSJS & Swellex Mn24 bolt model, as depicted in Figure 7-10, Figure 7-11, Figure 7-12 and Figure 7-13. The horizontal axis corresponds to the number of cycle steps, equivalent to 0.5 seconds in real time following the blasting impact.

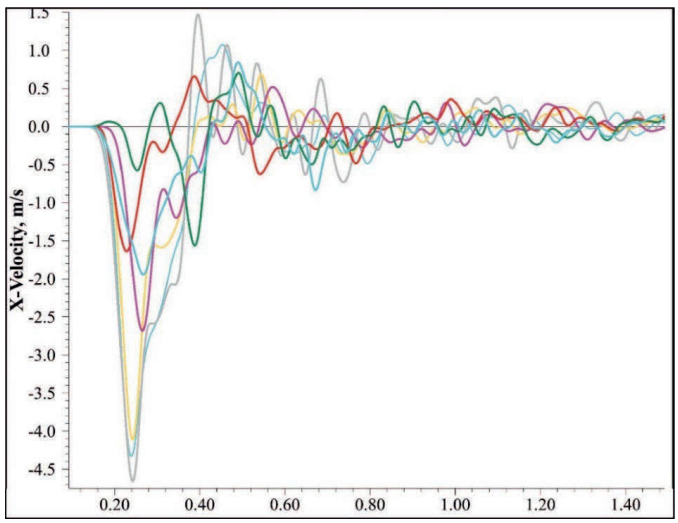

Figure 7-10. Velocity-time history for points between 5 and 10 meters from tunnel face of Crosscut 100, RSJS & Swellex Mn24 bolt model.

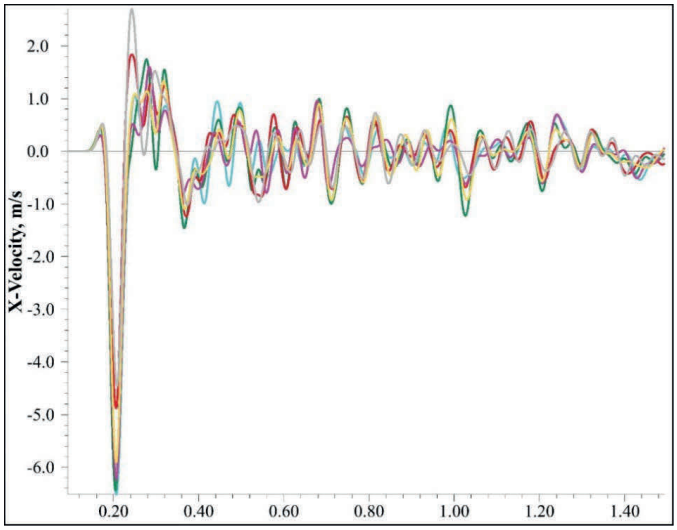

Figure 7-11. Velocity-time history for points between 10 and 15 meters from tunnel face of Crosscut 100, RSJS & Swellex Mn24 bolt model.

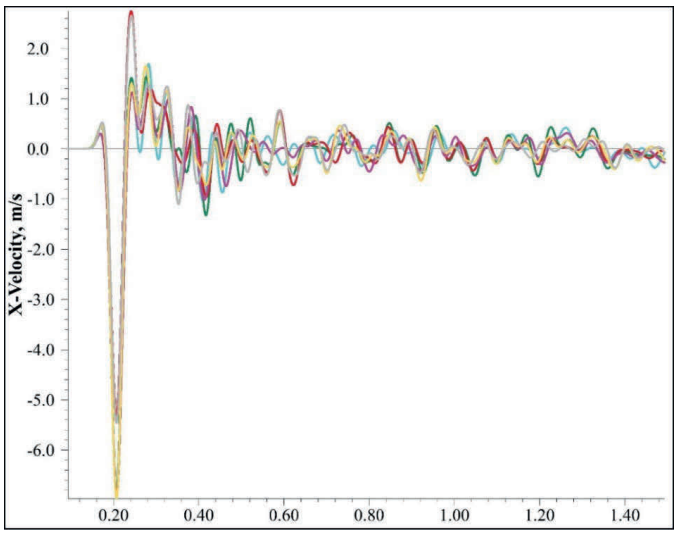

Figure 7-12. Velocity-time history for points between 15 and 20 meters from tunnel face of Crosscut 100, RSJS & Swellex Mn24 bolt model.

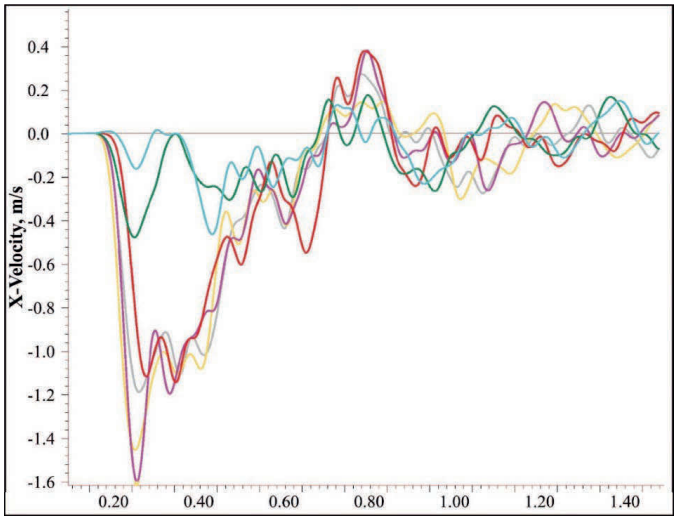

Figure 7-13. Velocity-time history for points between 20 and 25 meters from tunnel face of Crosscut 100, RSJS & Swellex Mn24 bolt model.

7.4.1.2 Unsupported Crosscut 103 (RSJS & Swellex Mn24 bolt)

Velocity-time history plots were generated for predefined points along the tunnel wall of Crosscut 103 from RSJS & Swellex Mn24 bolt model, as depicted in Figure 7-14, Figure 7-15, Figure 7-16 and Figure 7-17. The horizontal axis corresponds to the number of cycle steps, equivalent to 0.5 seconds in real time following the blasting impact.

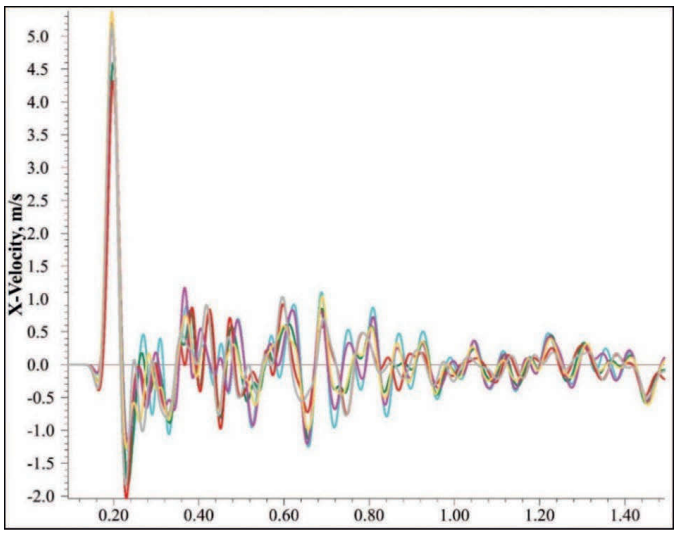

Figure 7-14. Velocity-time history for points between 5 and 10 meters from tunnel face of Crosscut 103, RSJS & Swellex Mn24 bolt model

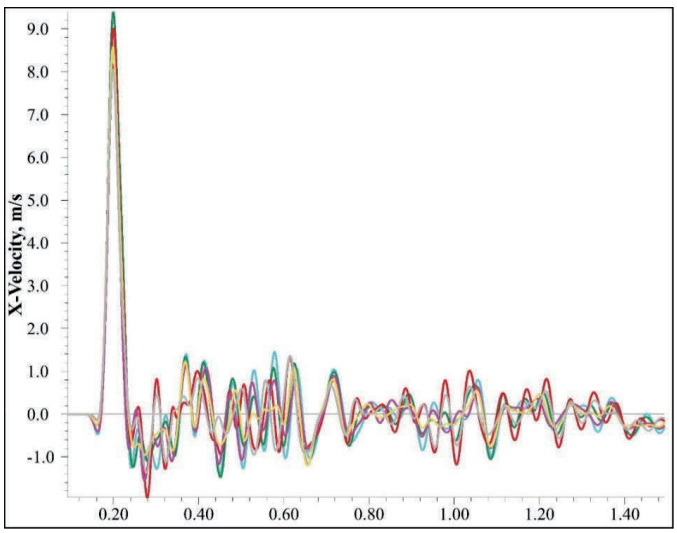

Figure 7-15. Velocity-time history for points between 10 and 15 meters from tunnel face of Crosscut 103, RSJS & Swellex Mn24 bolt model

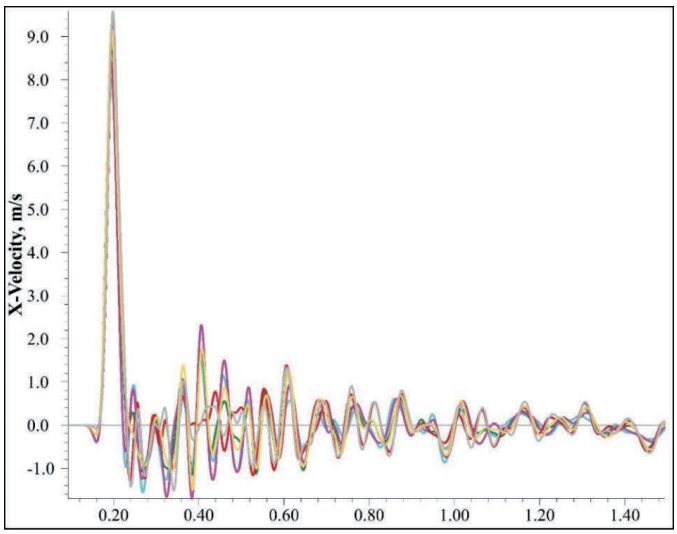

Figure 7-16. Velocity-time history for points between 15 and 20 meters from tunnel face of Crosscut 103, RSJS & Swellex Mn24 bolt model

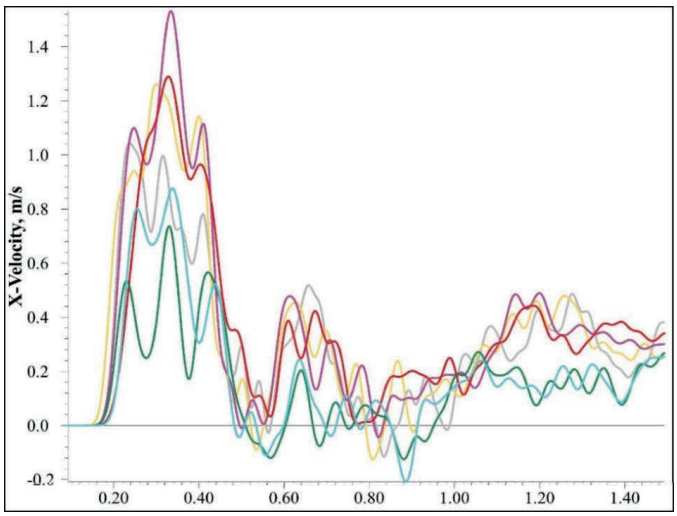

Figure 7-17. Velocity-time history for points between 20 and 25 meters from tunnel face of Crosscut 103, RSJS & Swellex Mn24 bolt model

7.4.2 3DEC model RSJS & D-bolt

This section illustrates 3DEC models with regularly spaced joint sets and mechanical parameters of D-bolts.

7.4.2.1 Supported Crosscut 100 (RSJS & D-bolt)

Velocity-time history plots were generated for predefined points along the tunnel wall of Crosscut 100 from RSJS & D-bolt model, as depicted in Figure 7-18, Figure 7-19, Figure 7-20 and Figure 7-21. The horizontal axis corresponds to the number of cycle steps, equivalent to 0.5 seconds in real time following the blasting impact.

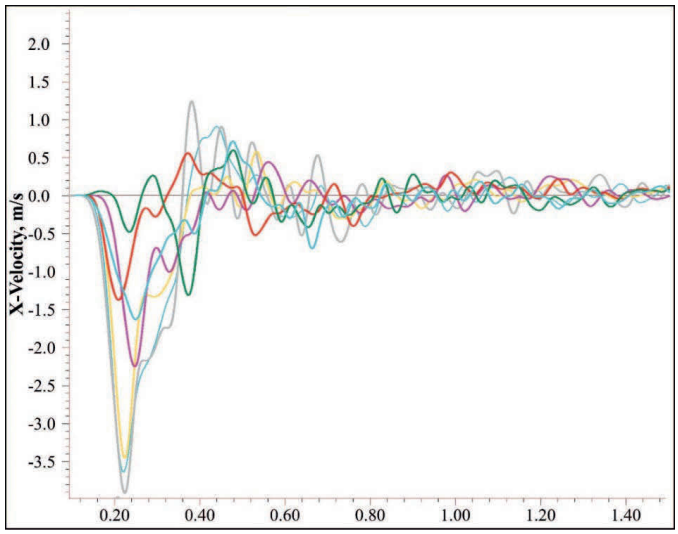

Figure 7-18. Velocity-time history for points between 5 and 10 meters from tunnel face of Crosscut 100, RSJS & D-bolt model

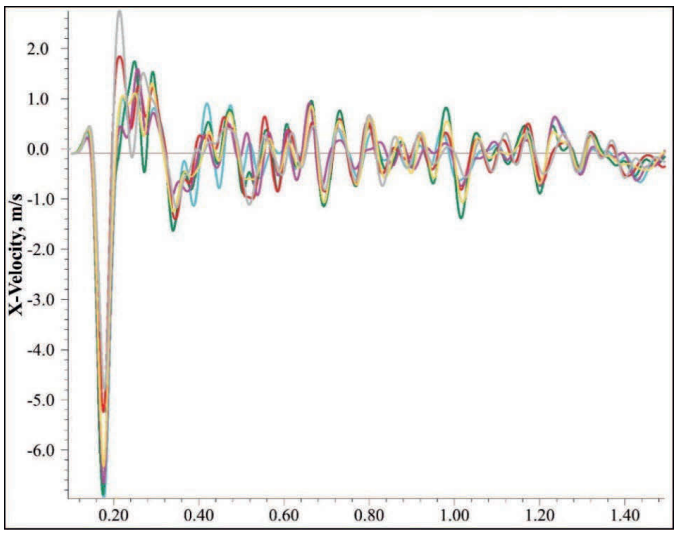

Figure 7-19. Velocity-time history for points between 10 and 15 meters from tunnel face of Crosscut 100, RSJS & D-bolt model

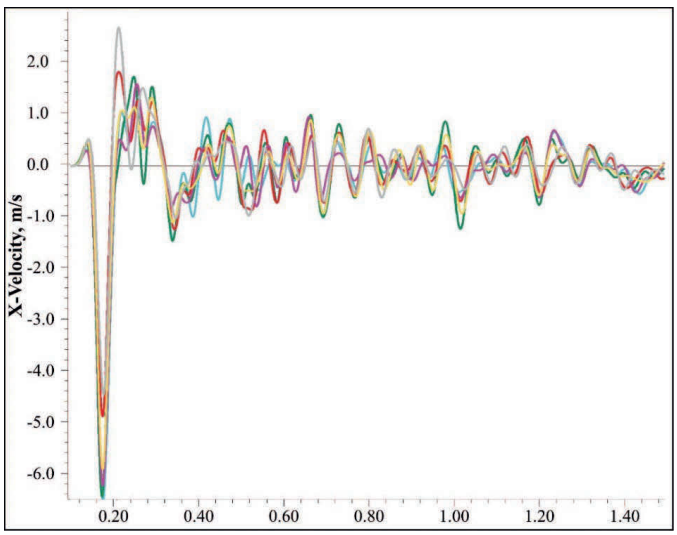

Figure 7-20. Velocity-time history for points between 15 and 20 meters from tunnel face of Crosscut 100, RSJS & D-bolt model

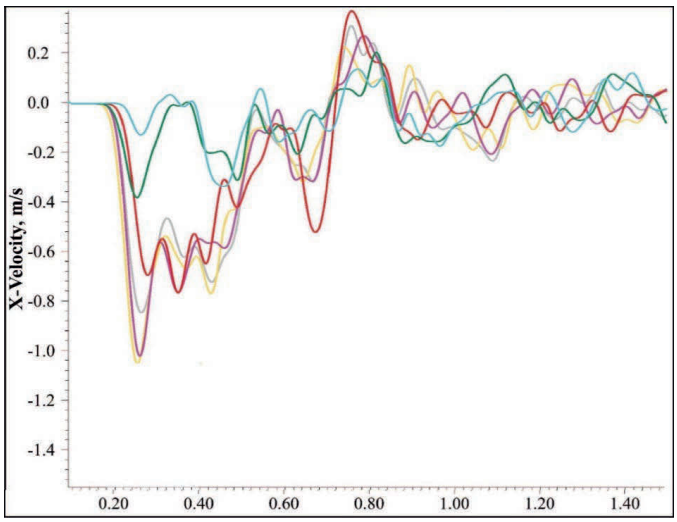

Figure 7-21. Velocity-time history for points between 20 and 25 meters from tunnel face of Crosscut 100, RSJS & D-bolt model

7.4.2.2 Unsupported Crosscut 103 (RSJS & D-bolt)

Velocity-time history plots were generated for predefined points along the tunnel wall of Crosscut 103 from RSJS & D-bolt model, as depicted in Figure 7-22, Figure 7-23, Figure 7-24 and Figure 7-25. The horizontal axis corresponds to the number of cycle steps, equivalent to 0.5 seconds in real time following the blasting impact.

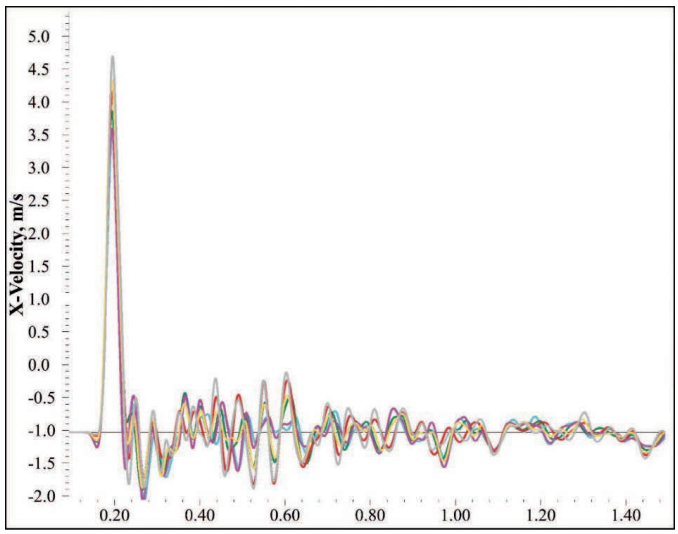

Figure 7-22. Velocity-time history for points between 5 and 10 meters from tunnel face of Crosscut 103, RSJS & D-bolt model

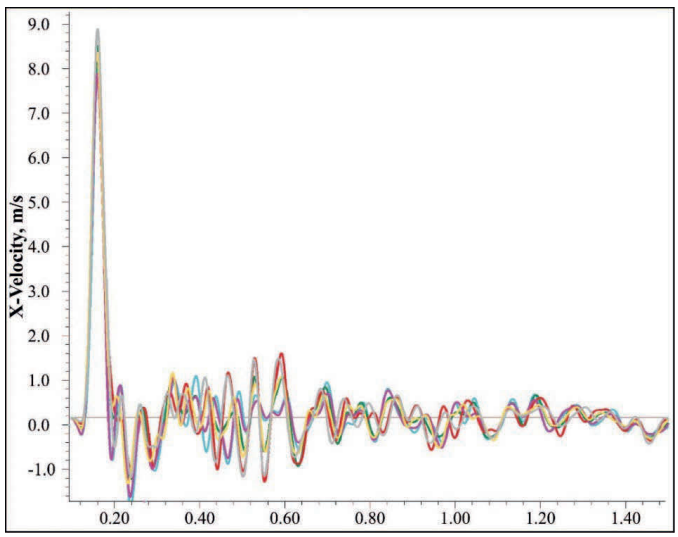

Figure 7-23. Velocity-time history for points between 10 and 15 meters from tunnel face of Crosscut 103, RSJS & D-bolt model

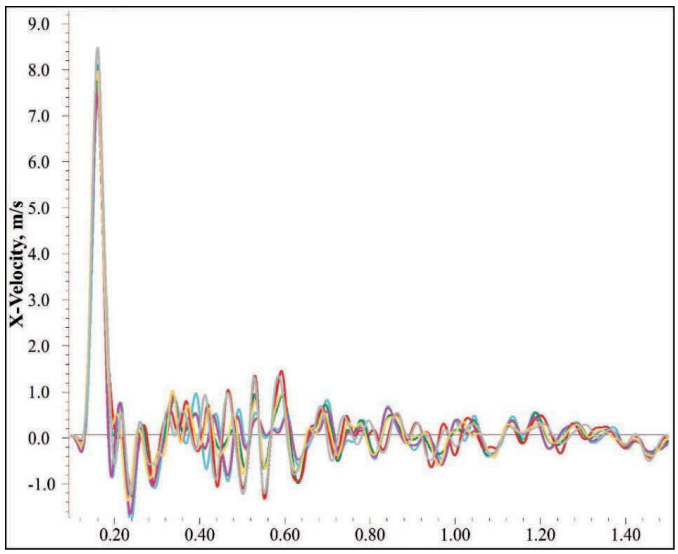

Figure 7-24. Velocity-time history for points between 15 and 20 meters from tunnel face of Crosscut 103, RSJS & D-bolt model

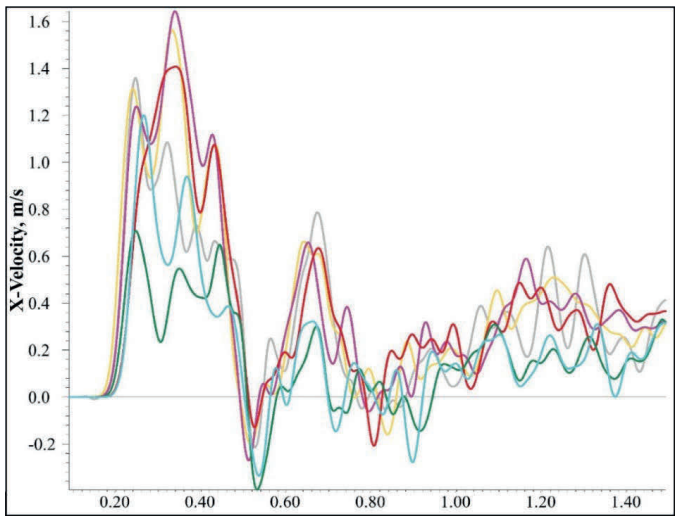

Figure 7-25. Velocity-time history for points between 20 and 25 meters from tunnel face of Crosscut 103, RSJS & D-bolt model

7.4.3 3DEC model DFN & Swellex Mn24 bolt

This section illustrates 3DEC models with Discrete Fracture Network joint sets and mechanical parameters of Swellex Mn24 bolts.

7.4.3.1 Supported Crosscut 100 (DFN & Swellex Mn24 bolt)

Velocity-time history plots were generated for predefined points along the tunnel wall of Crosscut 100 from DFN & Swellex Mn24 bolt model, as depicted in Figure 7-26, Figure 7-27, Figure 7-28 and Figure 7-29. The horizontal axis corresponds to the number of cycle steps, equivalent to 0.5 seconds in real time following the blasting impact.

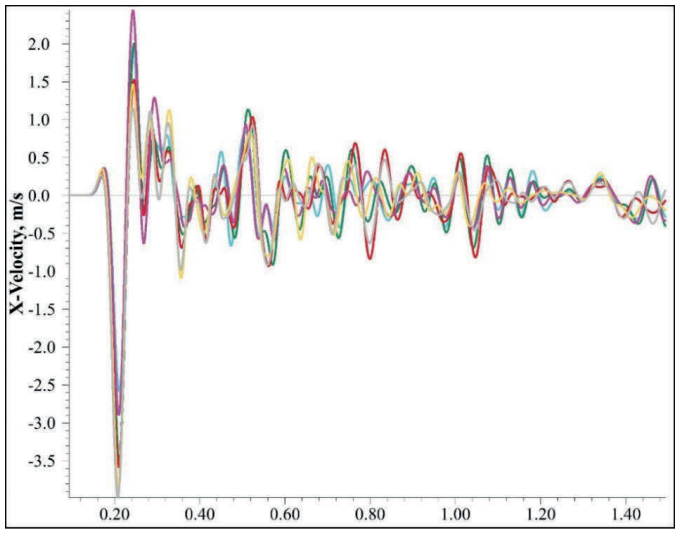

Figure 7-26. Velocity-time history for points between 5 and 10 meters from tunnel face of Crosscut 100, DFN & Swellex Mn24 bolt model

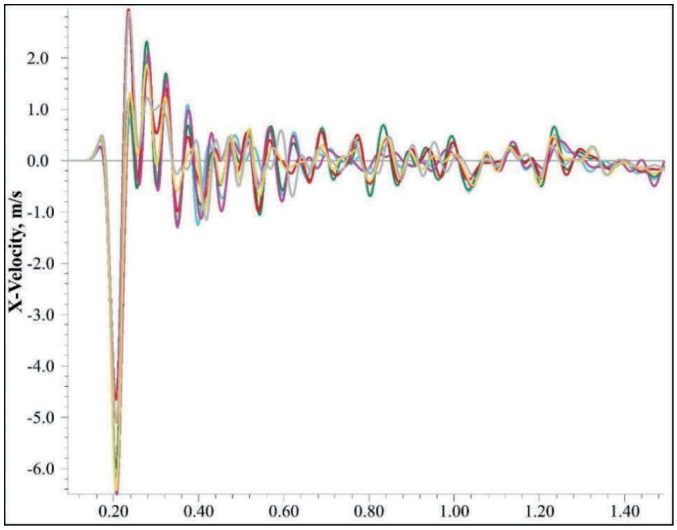

Figure 7-27. Velocity-time history for points between 10 and 15 meters from tunnel face of Crosscut 100, DFN & Swellex Mn24 bolt model

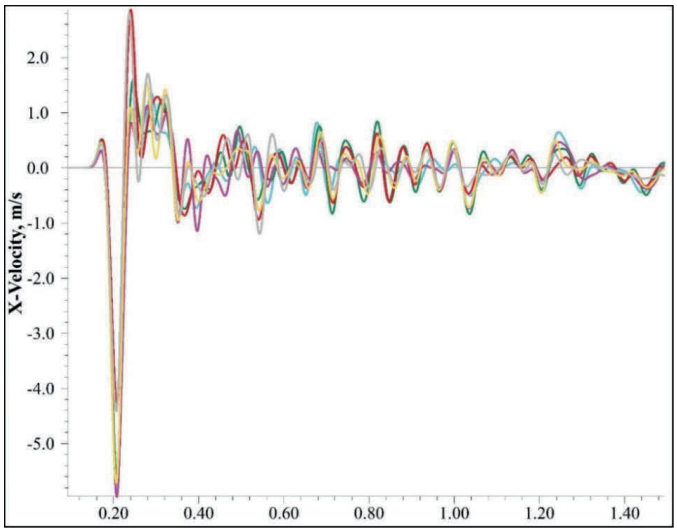

Figure 7-28. Velocity-time history for points between 15 and 20 meters from tunnel face of Crosscut 100, DFN & Swellex Mn24 bolt model

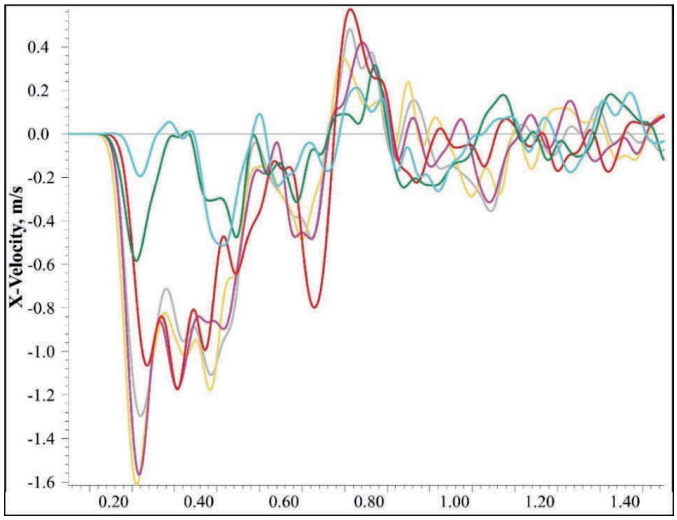

Figure 7-29. Velocity-time history for points between 20 and 25 meters from tunnel face of Crosscut 100, DFN & Swellex Mn24 bolt model

7.4.3.2 Unsupported Crosscut 103 (DFN & Swellex Mn24 bolt)

Velocity-time history plots were generated for predefined points along the tunnel wall of Crosscut 103 from DFN & Swellex Mn24 bolt model, as depicted in Figure 7-30, Figure 7-31, Figure 7-32 and Figure 7-33. The horizontal axis corresponds to the number of cycle steps, equivalent to 0.5 seconds in real time following the blasting impact.

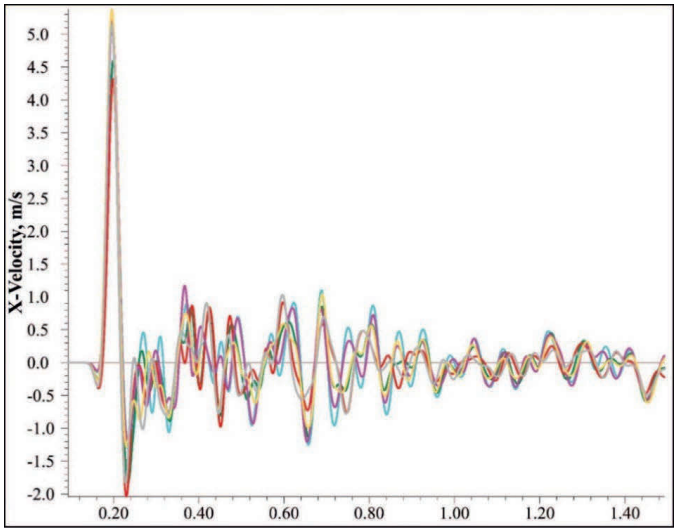

Figure 7-30. Velocity-time history for points between 5 and 10 meters from tunnel face of Crosscut 103, DFN & Swellex Mn24 bolt model

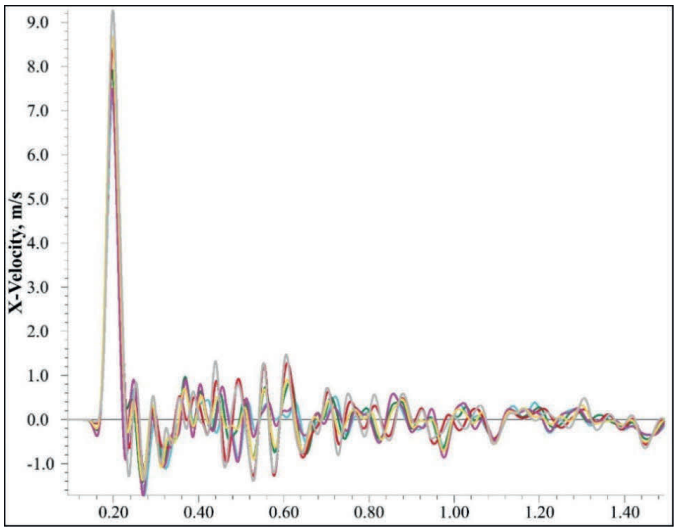

Figure 7-31. Velocity-time history for points between 10 and 15 meters from tunnel face of Crosscut 103, DFN & Swellex Mn24 bolt model

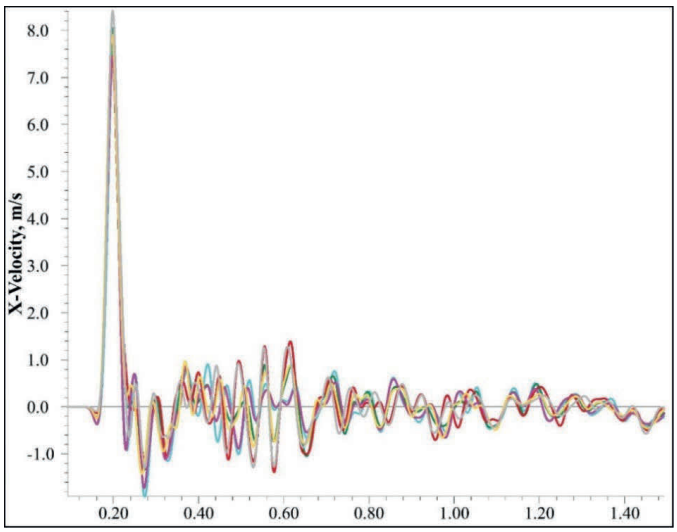

Figure 7-32. Velocity-time history for points between 10 and 15 meters from tunnel face of Crosscut 103, DFN & Swellex Mn24 bolt model

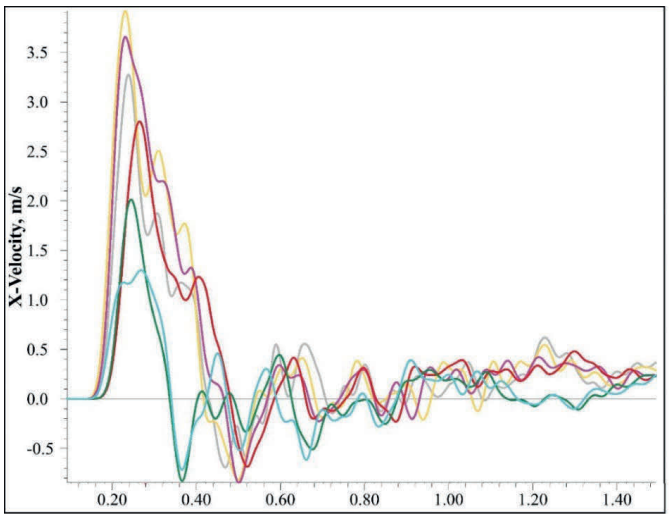

Figure 7-33. Velocity-time history for points between 20 and 25 meters from tunnel face of Crosscut 103, DFN & Swellex Mn24 bolt model

7.4.4 3DEC model DFN & D-bolt

This section illustrates 3DEC models with Discrete Fracture Network joint sets and mechanical parameters of D-bolts.

7.4.4.1 Supported Crosscut 100 (DFN & D-bolt)

Velocity-time history plots were generated for predefined points along the tunnel wall of Crosscut 100 from DFN & D-bolt model, as depicted in Figure 7-34, Figure 7-35, Figure 7-36 and Figure 7-37. The horizontal axis corresponds to the number of cycle steps, equivalent to 0.5 seconds in real time following the blasting impact.

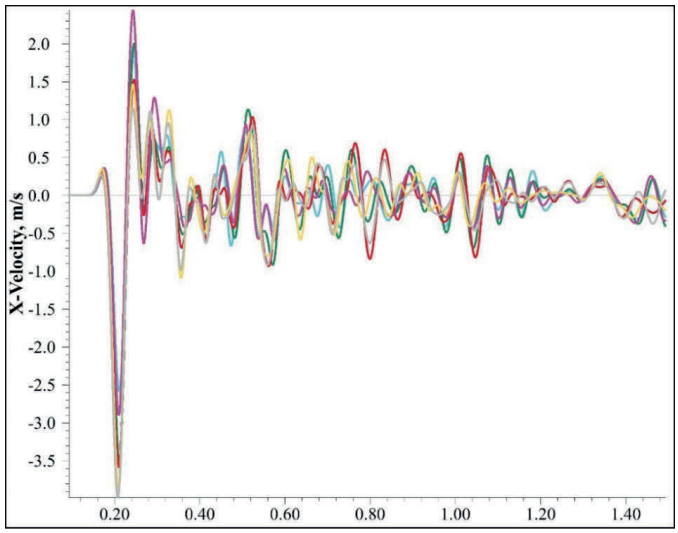

Figure 7-34. Velocity-time history for points between 5 and 10 meters from tunnel face of Crosscut 100, DFN & D-bolt model

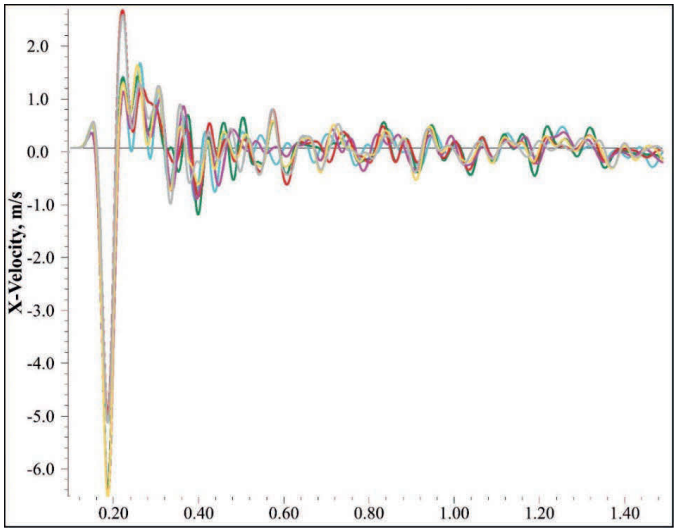

Figure 7-35. Velocity-time history for points between 10 and 15 meters from tunnel face of Crosscut 100, DFN & D-bolt model

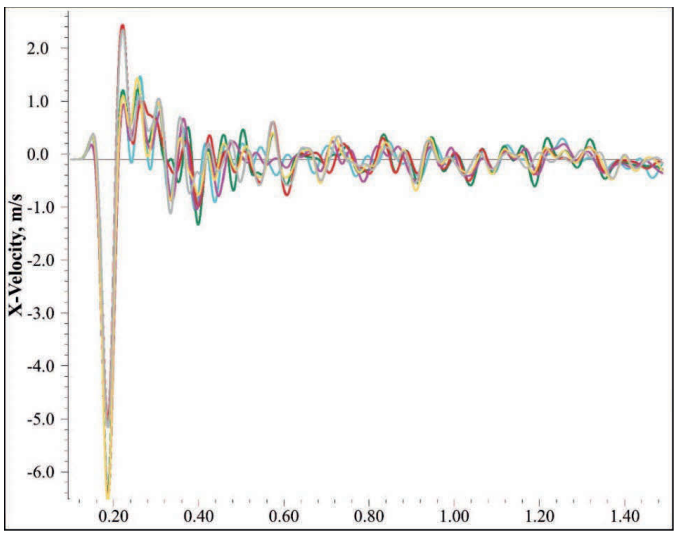

Figure 7-36. Velocity-time history for points between 15 and 20 meters from tunnel face of Crosscut 100, DFN & D-bolt model

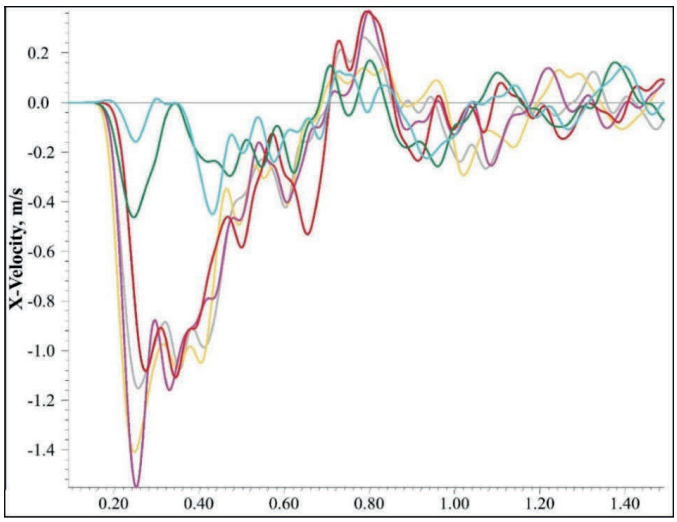

Figure 7-37. Velocity-time history for points between 120 and 25 meters from tunnel face of Crosscut 100, DFN & D-bolt model

7.4.4.2 Unsupported Crosscut 103 (DFN & D-bolt)

Velocity-time history plots were generated for predefined points along the tunnel wall of Crosscut 103 from DFN & D-bolt model, as depicted in Figure 7-38, Figure 7-39, Figure 7-40 and Figure 7-41. The horizontal axis corresponds to the number of cycle steps, equivalent to 0.5 seconds in real time following the blasting impact.

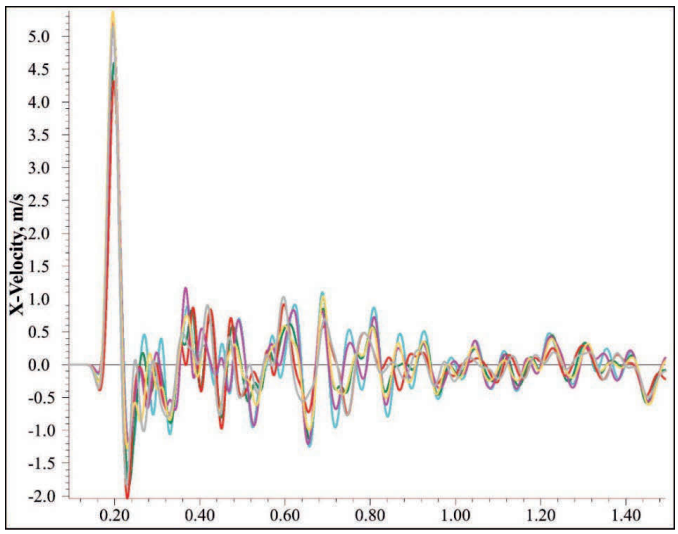

Figure 7-38. Velocity-time history for points between 5 and 10 meters from tunnel face of Crosscut 103, DFN & D-bolt model

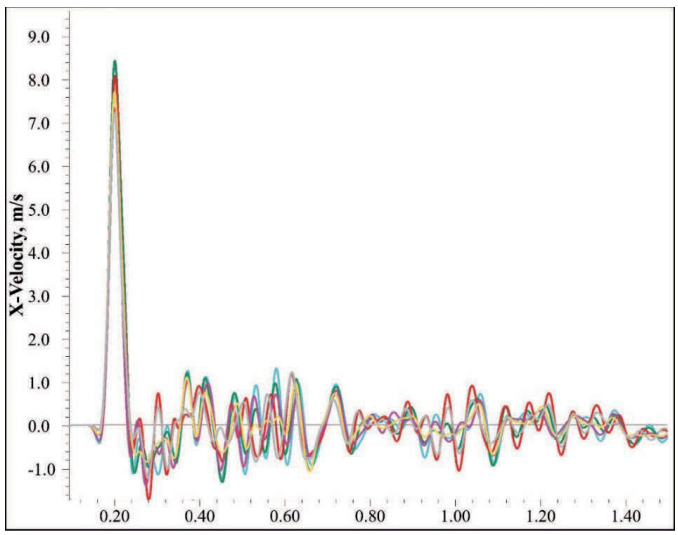

Figure 7-39. Velocity-time history for points between 15 and 20 meters from tunnel face of Crosscut 103, DFN & D-bolt model

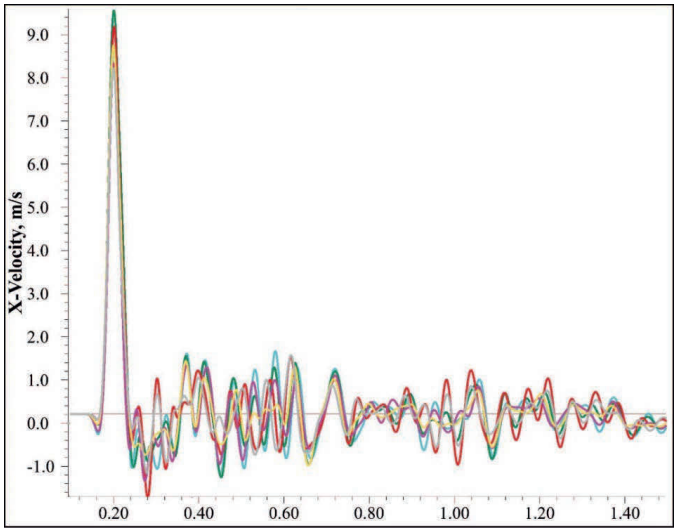

Figure 7-40. Velocity-time history for points between 15 and 20 meters from tunnel face of Crosscut 103, DFN & D-bolt model

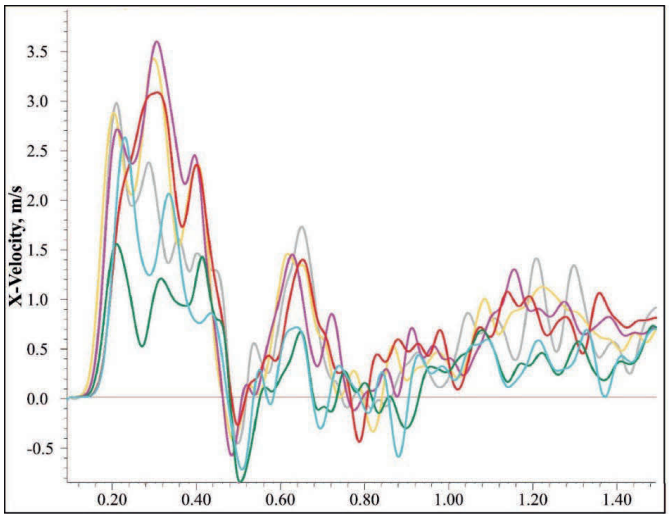

Figure 7-41. Velocity-time history for points between 20 and 25 meters from tunnel face of Crosscut 103, DFN & D-bolt model

7.5 Axial displacement of the bolts in Crosscut 100

In the 3DEC models as in the real Test No. 6, the bolts are installed in Crosscut 100 only.

7.5.1 Axial displacements in 3DEC model RSJS & Swellex Mn24 bolt

The axial displacement of the bolts is depicted for RSJS & Swellex Mn24 bolt model, see in Figure 7-42 the contour of the displacement before the blast impact and in Figure 7-43 after the blast impact.

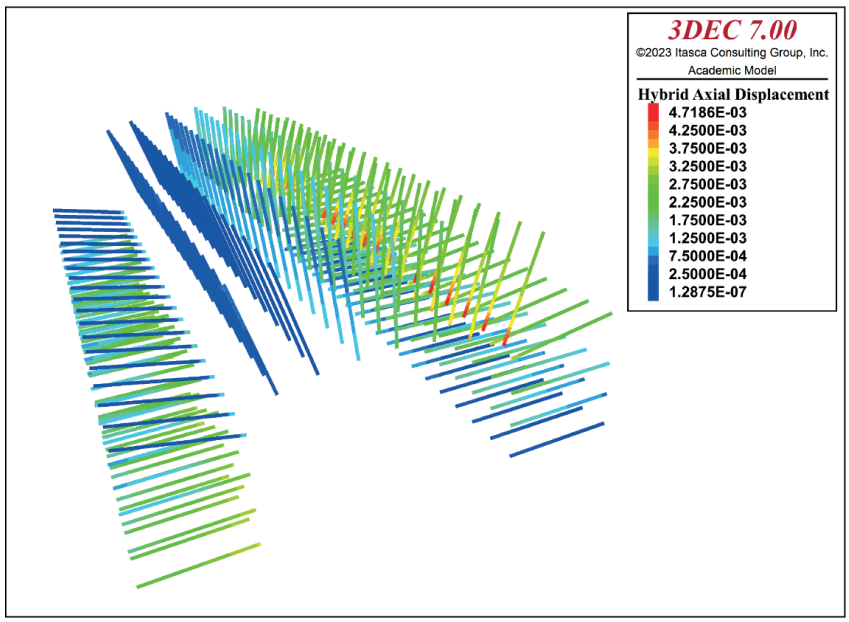

Figure 7-42. Axial displacements for bolts before the blast impact in RSJS & Swellex Mn24 bolt model.

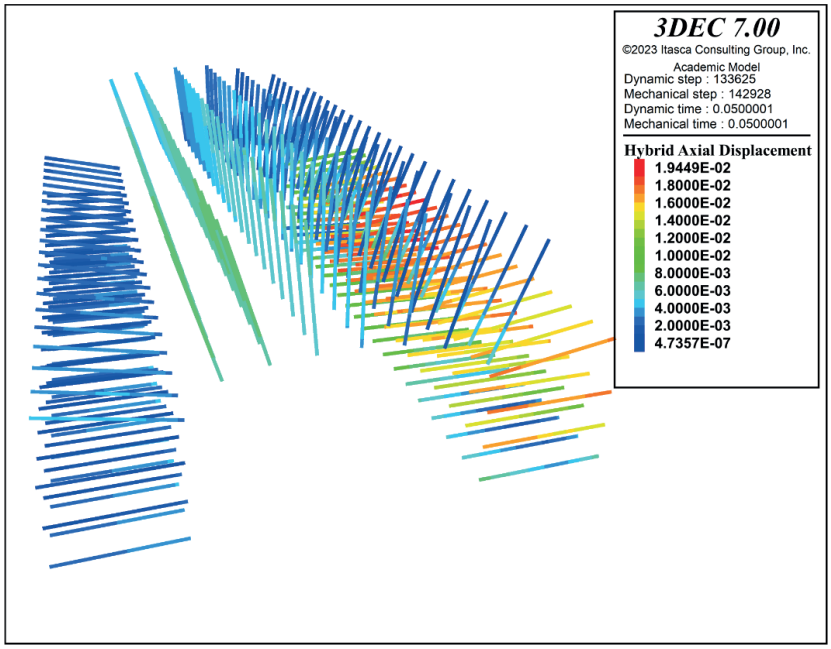

Figure 7-43. Axial displacements for bolts after the blast impact in Jset & Swellex Mn24 bolt model.

7.5.2 Axial displacements in 3DEC model RSJS & D-bolt

The axial displacement of the bolts is depicted for RSJS & D-bolt model, see in Figure 7-44 the contour of the displacement before the blast impact and in Figure 7-45 after the blast impact.

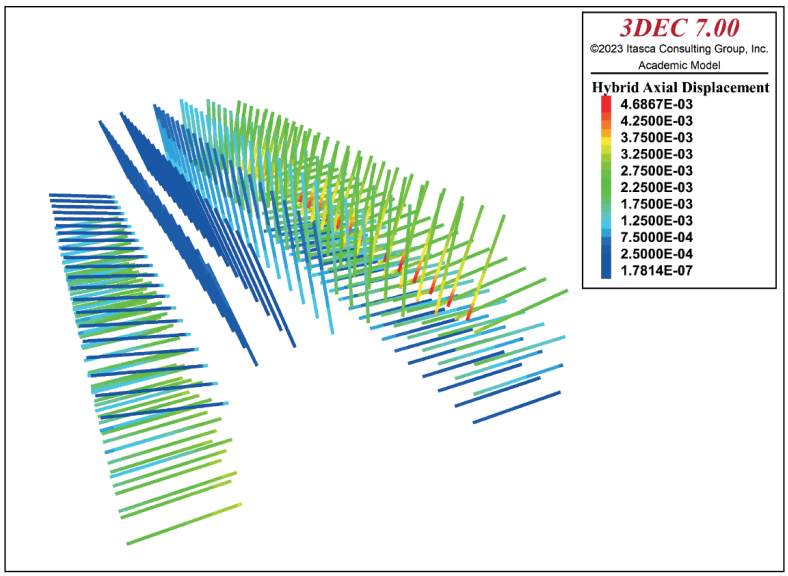

Figure 7-44. Axial displacements for bolts before the blast impact in RSJS & D-bolt model.

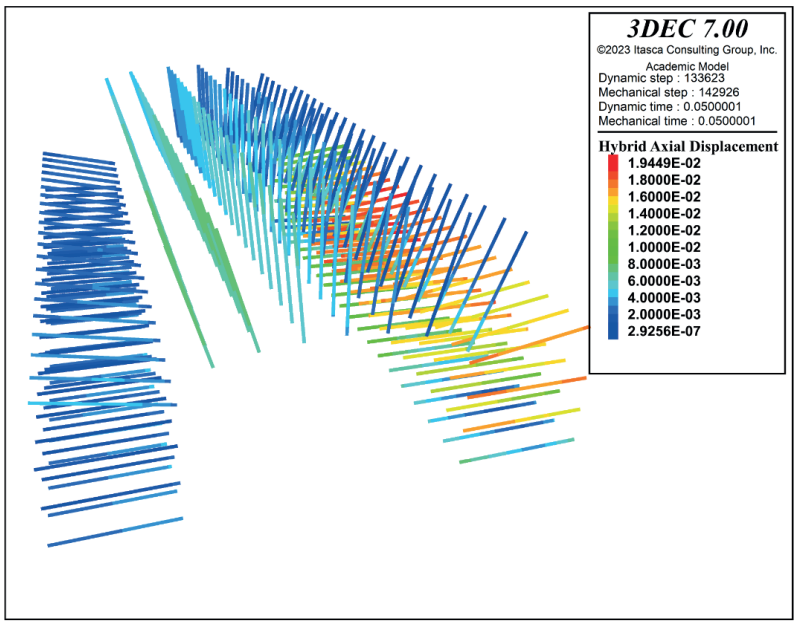

Figure 7-45. Axial displacements for bolts after the blast impact in RSJS & D-bolt model.

7.5.3 Axial displacements in 3DEC model DFN & Swellex Mn24 bolt

The axial displacement of the bolts is depicted for DFN & Swellex Mn24 bolt model, see in Figure 7-46 the contour of the displacement before the blast impact and in Figure 7-47 after the blast impact.

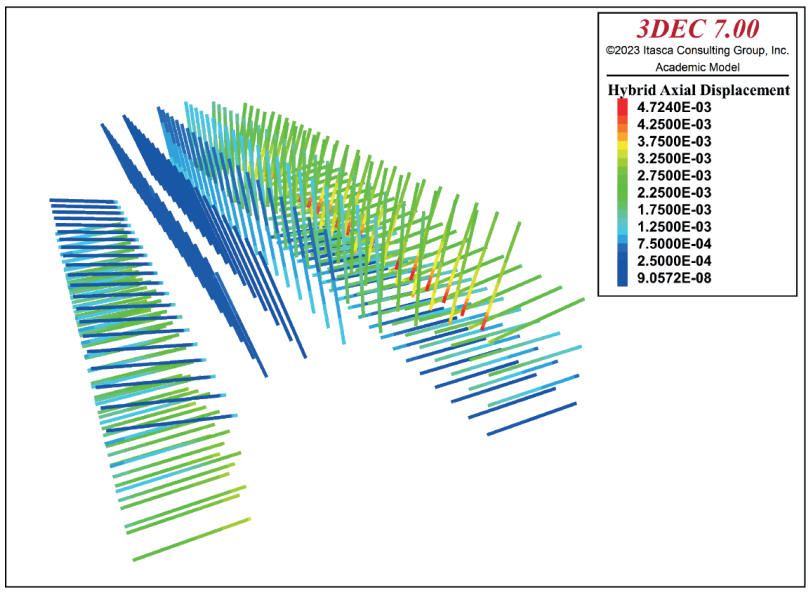

Figure 7-46. Axial displacements for bolts before the blast impact in DFN & Swellex Mn24 bolt model.

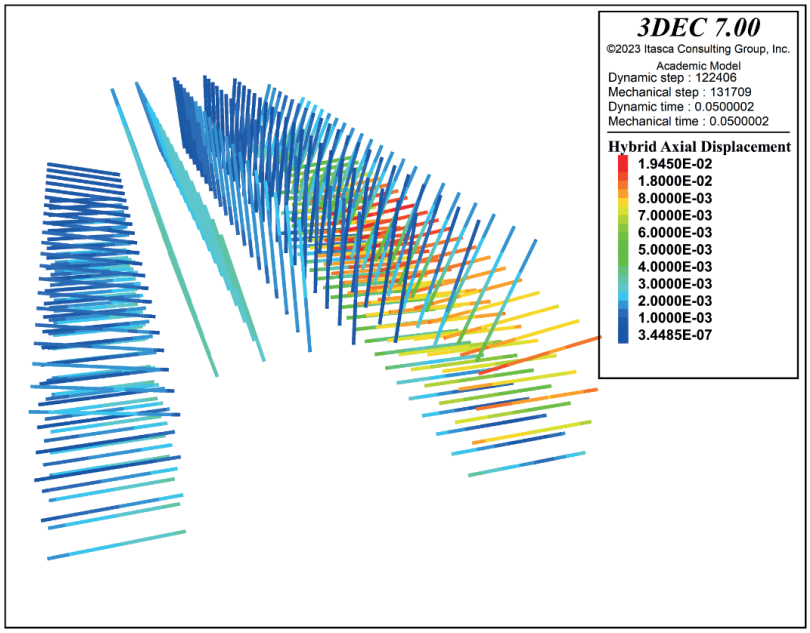

Figure 7-47. Axial displacements for bolts after the blast impact in RSJS & D-bolt model.

7.5.4 Axial displacements in 3DEC model DFN & D-bolt

The axial displacement of the bolts is depicted for DFN & D-bolt model, see in Figure 7-46 the contour of the displacement before the blast impact and in Figure 7-49 after the blast impact.

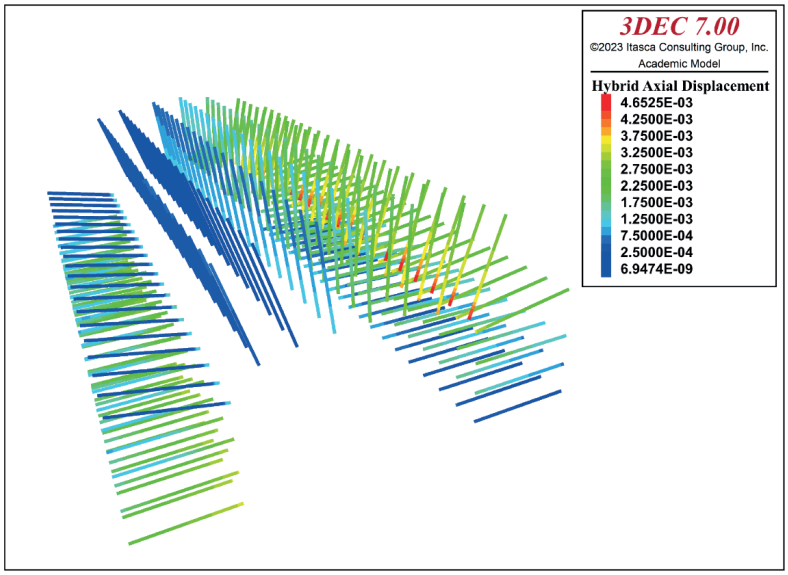

Figure 7-48. Axial displacements for bolts before the blast impact in DFN & D-bolt model.

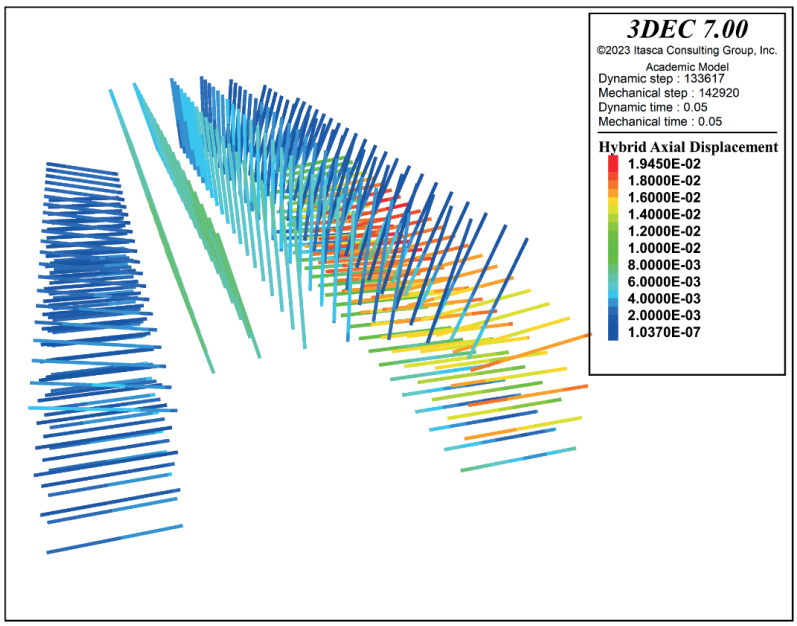

Figure 7-49. Axial displacements for bolts after the blast impact in DFN & D-bolt model.

8. DISCUSSION

In this chapter, the results as presented in Chapter 7 are discussed and compared with previously published results with UDEC (Shirzadegan, 2020). Considerations about the relation between results from LS-DYNA and 3DEC is provided. Finally, discussions on dynamic bolt performance under dynamic loads induced via blasting based on the numerical modelling are provided.

The data acquired from the field tests has been processed to obtain key information including peak particle velocity (ppv), frequency, duration of ground vibrations, and strains in the rock mass (Shirzadegan et al., 2016a; Shirzadegan et al., 2016b). This information serves as a basis for assessing the stability of the excavation and pinpointing areas of weakness or potential failure. These analytical techniques provide insights into the dynamic behaviour of the opening and allow for the identification of critical modes of vibration. The findings from the field tests can be used for optimization of blasting designs and excavation procedures. For instance, the results aid in determining sections of the excavation that require reinforcement or in evaluating the effect of modifications to blasting techniques.

The key findings of Test No. 6 (Shirzadegan, 2020) regarding point probes for Crosscut 100 and 103 are summarized as follows:

In Crosscut 100:

- New and fine cracks in the shotcrete
- Velocity range measured by accelerometers: 1.3 – 4.0 m/s
- Displacement measured by accelerometers: 4 – 7 mm
- Displacement measured by laser scanning: 2 – 31 mm
- Displacement measured by displacement measurement sensor: 10 mm

In Crosscut 103:

- Blocks of rock with varying thickness 0.1 – 0.8 m ejected
- Velocity range measured by accelerometers: 3.0 – 6.6 m/s
- Ejection velocity estimated by high-speed camera: 4.6m/s
- Ejection velocity measured by displacement measurement sensor: 3.17 m/s
- Displacement measured by accelerometers: -
- Displacement measured by laser scanning: -
- Displacement measured by displacement measurement sensor: -
- Depth of damage measured by borehole camera: 0.1 – 0.8 m.

Dynamic testing of bolt elements, either through laboratory tests or numerical simulations, as in this study, can provide valuable information about how bolts will perform under dynamic loading. This information can be used to design more effective reinforcement systems and to predict how these systems will perform under various loading scenarios. The pattern and density of rock bolts for instance can be optimized to

distribute the load more evenly across the rock mass, reducing the load on individual bolts and enhancing the overall stability of the rock mass.

Dynamic stresses and velocities from LS-DYNA were used as inputs in the 3DEC models. These induced waves that propagate through fractures and continuous medium in the models. Its energy is damped from its initial value until it reaches the crosscut walls. The stiffer the rock and fracture properties are, the longer the run time will be until the model converges at its desirable values. The stiffer the material is, the faster the wave can propagate through it.

8.1 Rock support performance under dynamic loading conditions

In the present study, only dynamic bolts were modelled with 3DEC, although shotcrete was also installed at the walls and roof of Crosscut 100 at the time of Test No. 6 was not modelled for simplicity and for a congruency with the earlier studies with UDEC.

Figure 7-42 to Figure 7-49 illustrate the rock bolt performance under dynamic load for the two different geometries and for the two dynamic bolt types are used in the present study, Swellex Mn24 bolt and D-bolts, respectively.

The axial displacement at the head of the bolts in the 3DEC models in static conditions, i.e. before blasting, is in general very low, less than one millimetre. The bolts along the spring line of the tunnel against the pillar experience larger displacements, with a maximum head displacement between 4.65 to 4.72 mm.

Assessing the changes in displacement for bolt heads before and after the blast impact provides insight into the potential stability or instability resulting from the blasting process. The models indicate maximum axial bolt head displacements ranging between 19.44 and 19.46 mm 0.5 seconds after the blasting. Comparative analysis with pre-blast static conditions reveals additional blast-induced displacements ranging from 14.72 mm to 14.80 mm displacement in certain bolt heads. Notably, the D-bolt in the model featuring DFN realization exhibits the highest axial displacement. While these displacements are permanent in nature, they remain relatively small compared with the tensile failure limit of the dynamic bolts, which can reach up to 0.35. This indicates the competent performance of the bolts in withstanding the loading induced by the blasting.

8.2 Effect of blast on the tunnel walls

In this study, the stability of the bolted tunnel Crosscut 100 is checked and compared with the unsupported tunnel Crosscut 103. The stability analysis is conducted by measuring displacement magnitude after blasting in Crosscut 100 and Crosscut 103. Displacements as high as 7.5 to 22.5 mm were observed in the tunnels. Displacement values in the Crosscut 100, in which the support system was installed, are smaller than the unsupported Crosscut 103.

8.2.1 Point probe velocity

The figures in Section 7.4 show the point probe velocity history following the blast impact in the 3DEC models. The fluctuations of the velocity over time were mainly attributed to the vibrating effect of the blasting. An abrupt increase in the velocity that reached approximately 9 m/s at the highest was observed for monitoring points pre-defined on the tunnel walls of Crosscuts 100 and 103, followed by gradual decrease over time.

It should be noted that in each plotted figure, only a minor number of the monitored points were recorded with x-velocity that exceeded 1 m/s. Overall, even for the points with such exceedance, the velocity had a tendency to gradually decrease over time towards zero, indicating neglectable motion at monitored points in the final stage of the model runtime and stability of its corresponding block.

According to Kaiser et al. (1996) the intensity of the failure process is best described by the anticipated ejection velocity of rock blocks from the walls and roof of the excavations, and the ejection velocity is used to determine whether:

- no ejection is expected (i.e. ejection velocity lower than 1.5 m/s);
- support would withstand (i.e. ejection velocity between 1.5 m/s and 5 m/s); or
- ejection velocities could be excessive (ejection velocity higher than 5 m/s) and support cannot prevent major damage to the excavation.

Based on empirical analyses (Cai et al., 2019; Kabwe, 2023) the required elastic strain energy to thrust the rock fragment for infinitely stiff rock mass can be expressed by the lower and the upper bound velocities as shown by Equation 3:

$$\frac{\sigma_1}{\sqrt{\rho E}} \leq v \leq \sqrt{\frac{2\sigma_1}{\rho}} \tag{3}$$

where σ_1 is major principal stress, ρ is the rock mass density, E is the Young's modulus of the rock mass. For intact rock with the properties as presented in Table 6-1, the minimum magnitude of 21 MPa for the major principal stress is anticipated for the ejection to occur without installed rock support and, the magnitude of 70 MPa for to result in damage of the support system and ejection of rock blocks.

The analyses based on vibration measurements at Malmberget mine during 2003 (Larsson, 2004) indicate that the accelerations are likely to range between 0.1 m/s^2 and 1.1 m/s^2 due to the production blast, while induced accelerations during seismic events are often in the range of 0.1 to 1 times of the gravity acceleration.

A coarse estimation of the transient major principal stress due to the seismic events at Test No. 6 is around two times of the original in situ stress in Table 6-6, i.e. a magnitude of about 50 MPa, which is below the level of 70 MPa for inevitable support system failure according to Kaiser et al. (1996).

The point probe velocities based on the modelling results indicate no dominant evidence of real rock ejection concerning that the generalized block size is over 3 meter in edge length and the spacing between the monitored points is 1 meter. This means that there are little chances to have smaller blocks in the 3DEC models.

The peak stress σ_d caused by seismic event is proportional to the peak particle velocity (*ppv*) of the seismic wave and can be calculated for planar wave. (Kaiser et al., 1996):

$$\sigma_d = \rho \, c \, ppv \tag{4}$$

where c is the propagation velocity of a compression wave and ρ is the rock mass density, *ppv* is the peak particle velocity. For a typical magnetite-apatite rock type, the compression wave velocity can fall in the range of 5 000 to 8 000 m/s. According to Equation 4, the peak stress magnitude of 126 MPa results for an equivalent seismic event is obtained for the borehole blasting, a compression wave velocity of 5 000 m/s and the observed maximum *ppv* = 9 m/s. In the extreme case the peak stress is roughly five times of the undisturbed major principal stress and 50% of the UCS for intact rock as presented in Table 6-1.

The gradual decrease in the monitored velocity down to very low lever for each point is a sign of the blasting energy dissipation and absorption in terms of rock mass and rock bolt deformation.

In general, the absolute value of peak x-velocity as recorded in the supported Crosscut 100 for the same sections are lower than that in the unsupported Crosscut 103, given the same joint patterns and bolt type in the models. This is in line with the anticipation that the installed dynamic bolts interact with the surrounding rock mass and provide resistance to loading due to the designed borehole blasting between the two crosscuts.

For each model, the section between 10 and 15 m from the crosscut tunnel faces, as well as between 15 and 20 m, recorded the higher peak x-velocity than the rest of the sections between 5 and 10 m, as well as between 20 and 25 m along the test tunnel wall of respective crosscut.

It should be noted that the bottom 10 meter out of the 20-meter long blasthole was charged with explosive, consistently the test wall sections closest to the charge length recorded the highest x-velocities. The plotted figures also indicated that the non-charged part of the blasthole resulted in higher vibrations than in the rock mass beyond the blasthole bottom. This can be also explained by the fact that the pillar end towards the footwall drift is less mechanically constrained than the rock mass beyond the blasthole bottom.

No significant difference for the modelled peak velocity had been observed, that is, irrespective of how the joint patterns had been generated for the models: regularly spaced joint sets or DFN. For observed points in the same section, no dominant capabilities of restricting the peak velocities had been manifested regardless of the generation of joint patterns.

Several aspects could account for these insignificant differences between models with different bolt types and joint patterns:

- Rock mass quality: the digitization results of the mapped joints indicate that the blocks due to the categorized three joint sets have roughly block size of 3 m in length, although there is no track of which of these mapped joints are existing ones prior to the production blasts and which are blast induced during the production stage. However, given such large block structure as mapped and under the assumption of considerably good joint conditions, the surrounding rock mass between the two crosscuts is likely of better quality than the suggested GSI-value between 45 and 50 for a larger area of Block 9 and Block 12 as mentioned in Section 4.1. The estimated low rock mass quality could be explained by including excavation damage during the mapping of the tunnels. This interpreted good rock mass quality is in line with the fact that the Crosscut 100 had not encountered any stability problems during the Test No. 6, while Crosscut 103 had been unsupported all the time since its excavation.
- Model uncertainty: the limited information on the geological data including the joint patterns is always a challenge in the model build-up, although efforts have been made to optimize the model, e.g. by verifying the model through comparison between the DFN generated joints and the mapped joints in the excavation, especially in areas close to the test tunnel walls, since the velocity history at particular monitoring points is influenced by the occurrence of joints in the immediate vicinity of the point.

8.2.2 Bolt behavior

After the blast impact, larger displacement in the models occurred where the bolts had been installed sub-horizontally on the tunnel wall along Crosscut 100. This was particularly true for the bolts at the top and middle rows of the tunnel wall towards the blasthole. The modelled bolts at the top and middle rows of the tunnel were installed in the direction parallel to the wave propagation and spatially closest to the detonated blasthole. The length of the blasthole where the charge detonated appeared to play a role in the axial displacement. A common trend had been observed for large axial displacement of the bolts installed closer to the charge length, highlighted by red colour in the figures of Section 7.5 related to the time after the blast impact.

8.2.3 Block displacements

Figure 8-1 presents an example of block displacement plot derived from the 3DEC DFN & D-bolt model. Specifically, it illustrates the contour of the displacement on the walls and roof of Crosscuts 100 and 103 following the blast impact. These displacements are solely attributed to the blasting effect, as they were reset to zero upon reaching static equilibrium in the 3DEC models after bolt activation.

Surface displacement values calculated for Crosscut 100 are comparable in magnitude to those collected from Test No. 6. However, the displacement values calculated for

Crosscut 103 are lower than field measurements. Despite a documented rockfall in Crosscut 103 observed through laser scanning, the numerical modelling with 3DEC does not replicate a rockfall following propagation of the blasting wave.

The thickness of the ejected blocks of rock varied between 0.1 and 0.8 m (Shirzadegan, 2020). Although the 3DEC models did not depict detachment and fallout of rock blocks, enhanced permanent displacements in Crosscut 103, particularly at the junction with the footwall drift, can be numerically simulated (Figure 8-1b). Additionally, Figure 8-1b illustrates permanent displacements on the wall opposite to the borehole location in the unsupported Crosscut 103. a phenomenon not observed in Figure 8-1a for Crosscut 100.

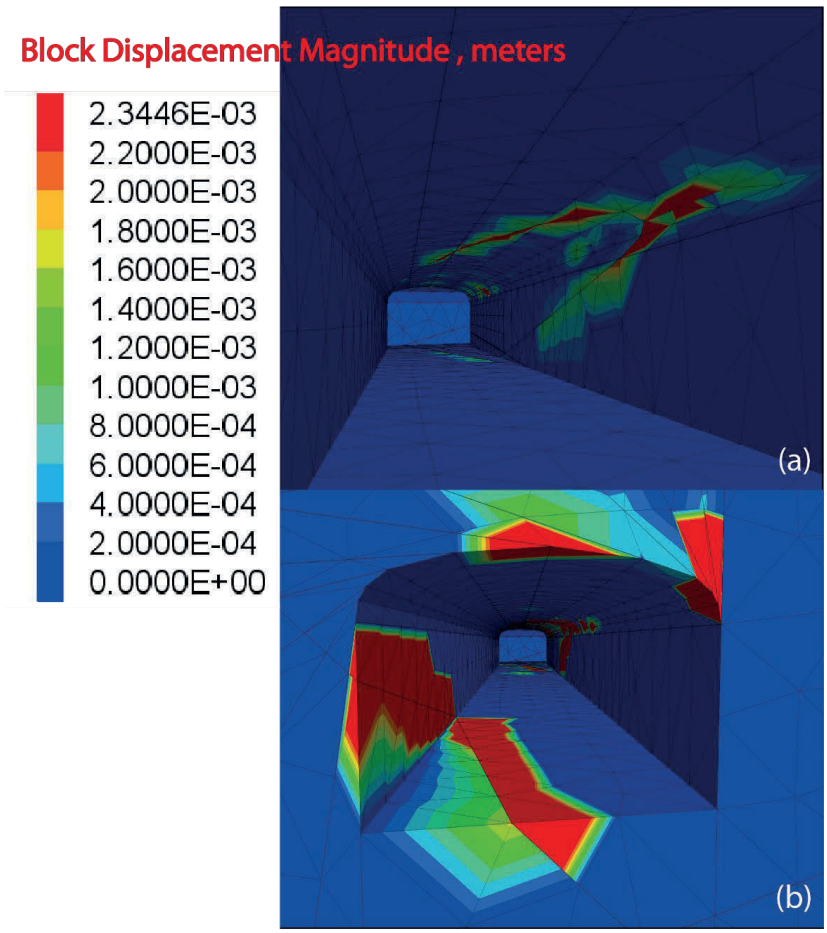

Figure 8-1. Contours of block displacement for 3DEC model DFN & D-bolt model after blast impact: a) Crosscut 100 and; b) Crosscut 103.

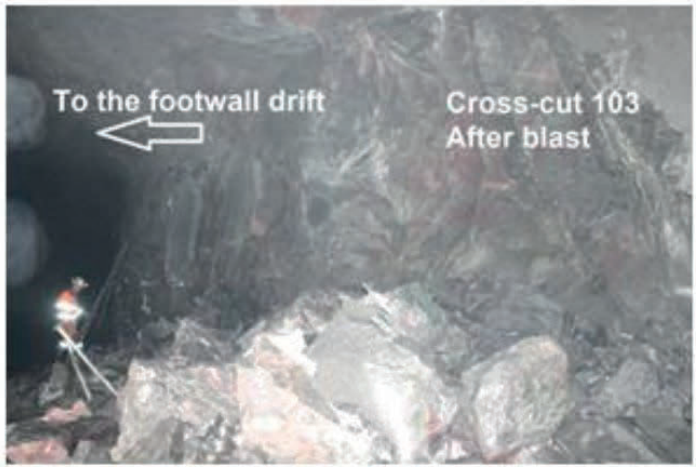

Figure 8-2. Photographic documentation of Test No. 6 and Crosscut 103. The photo shows a block fall out close to crossing with the Footwall drift (left side).

The differences between numerically calculated results and field measure data for the unsupported Crosscut 103 can be due to the mechanical properties of the fractures and joints. Similar results from discrete fracture networks are observed for the regularly spaced joint sets. Mechanical properties of the joints, spacing between the major joint sets and plausible interactions between those joints and form an unstable wedge is an important part of the investigation.

8.3 Comparison of bolt performances

Providing material properties for modelling of dynamic bolts poses challenges, as many parameters listed in Table 6-3 and Table 6-6 are derived material properties of steel and grout using theoretical values and analytical equations. To obtain more reasonable data, conducting dynamic pull-out and shear tests on bolt type is desirable. The properties obtained from those tests can serve as inputs for numerical modelling.

Material properties were derived for Swellex Mn24 bolt and D-bolt and compared with provided Itasca documentation (Itasca Consultants Group, 2023) for dynamic bolts in 3DEC. Certain parameters that are not provided by the producer or available in literature are therefore assigned based on empirical assumptions. Hence, numerical shear tests were conducted on a Swellex Mn24 bolt modelled in 3DEC, with dowel yield tension 0 kPa and 64 kPa respectively, the latter according to an example by Itasca (Itasca Consultants Group, 2023). The axial displacement of the bolt was compared under identical numerical configurations and boundary conditions kept equal.

A bolt located in the centre of two blocks is sheared by moving one block downwards. The axial displacement is recorded in the models, and result in 66.83 mm with the properties used in the present study, and 64.07 mm with the properties from Itasca manual

(ITASCA Consulting Group, 2023). The two models presented a difference of only 4% in the value of the axial displacement, which was considered acceptable.

Both Swellex Mn24 bolt and D-bolt demonstrated effective performance in relation to the convergent point probe velocity observed along Crosscut 100 in numerical models. However, no significant difference could be discerned in peak velocity between the two bolt types.

The plotted figures in Section 7.5 illustrate the bolt displacement before and after the blast impact. Both bolt types exhibited similar maximum axial displacement magnitudes, approximately 5 mm before the blast impact and 2 cm after the blast impact.

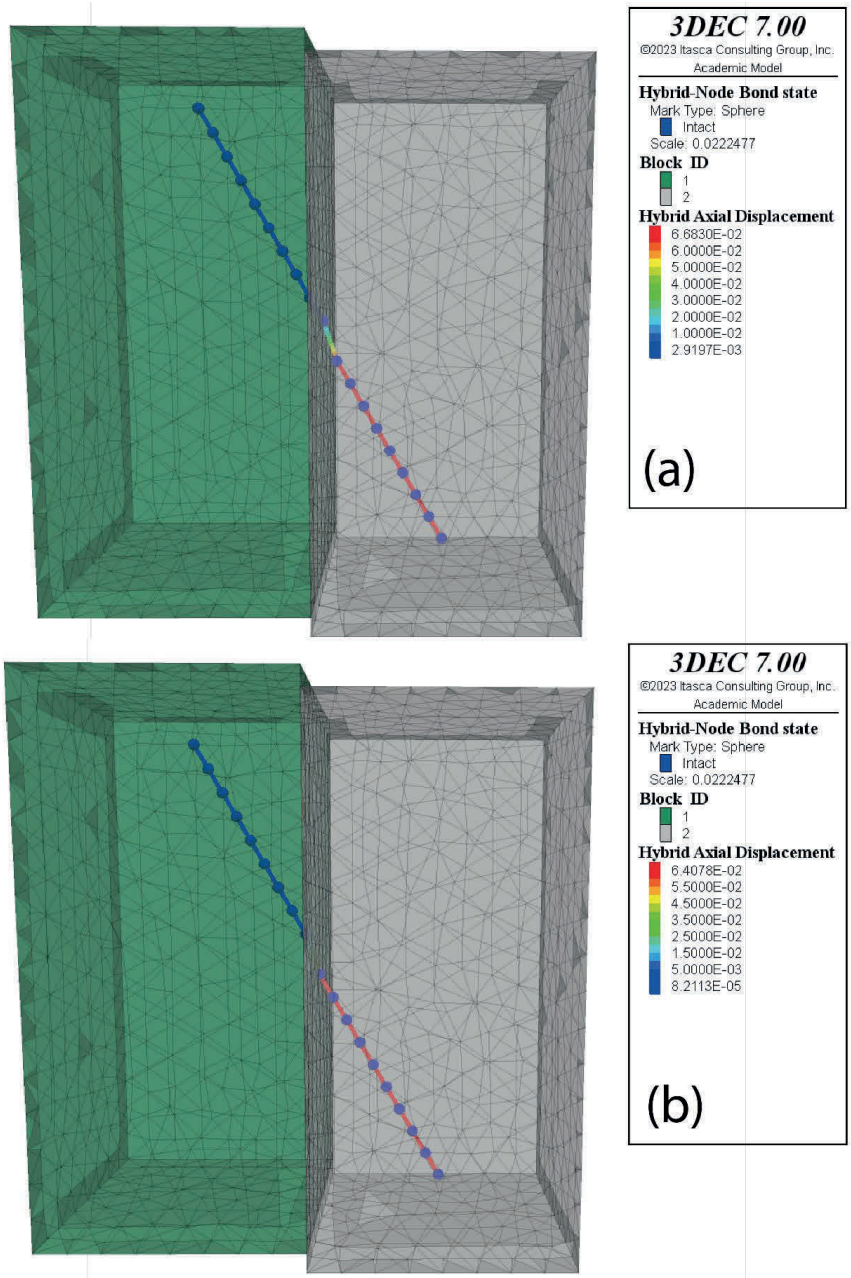

Figure 8-10. Numerical shear test of a Swellex Mn24 bolt with a) dowel yield tension 0 kPa, and b) dowel yield tension 64 kPa.

8.4 Comparison between 3DEC, UDEC and field collected results for Test No. 6

When comparing the results obtained from 3DEC with UDEC (Shirzadegan, 2020), and 3DEC with field-collected results, it is essential to consider the specific limitations and specifications of each environment being analysed, the material behaviour, and the modelling assumptions made in each software.

8.4.1 3D (3DEC) versus 2D (UDEC)

The geometry of the models in UDEC was formed out of regularly spaced joint sets, and due to the two-dimensionality it only accounts for the dip but not the strike of the joints. In 3DEC geometries in three dimensions could account explicitly for multiple joint sets either generated as regularly spaced joints, or as one realization of discrete fracture network.

Other than the introduction of the third dimension during the creation of joints in the models, variations in wave propagation, the performance of dynamic bolts and, the damping conditions have been observed when transitioning from a two-dimensional (2D) to a three-dimensional (3D) environment. The inclusion of the third dimension can lead to a range of disparities in modelling, such as the activation of motion in joints along the additional axis. The interaction between waves generated through blasting and geological features, such as joints, remains an active area of investigation as depicted in Figure 8-3 (Warema et al., 2023). Geological features aligned parallel to the direction of wave propagation are likely to exert minimal influence on wave propagation speed and energy dissipation during dynamic impacts, whereas those perpendicular to the direction will exert the greatest impact.

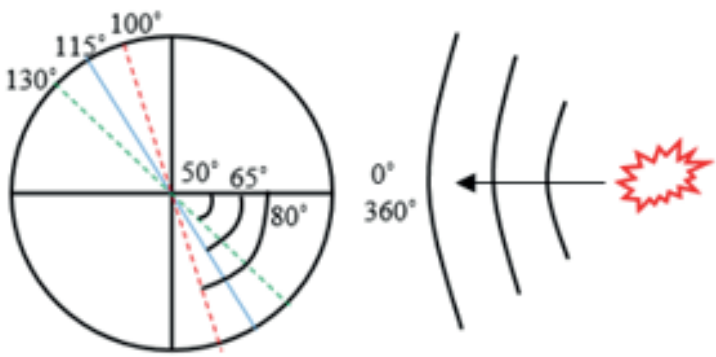

Figure 8-3. Influence of the inclination of fractures on the wave propagation (Warema et al., 2023). Waves will be led upwards and hindered downwards.

8.4.2 Assumptions on in-situ stresses

In a mine context, the orientations of in-situ stresses experienced during excavation are not solely influenced by gravitational force; due to continuous ore extraction at depth, the orientations of principal in-situ stress undergo rotate.

When comparing field-collected data with numerical simulations, it is imperative to replicate conditions as close to field condition as possible. In this study, the far-field in-situ stresses at the mining site were incorporated into a 3DEC global model to ascertain realistic stress component values at the location of Test No. 6, as described in Section 6.5. Subsequently, the application of far-field stresses to the 3DEC local model resulted in a rotated stress field compared to lithostatic conditions, as shown in the plot of the vertical displacement in static equilibrium condition (Figure 8-4).

Within the UDEC model, in-situ stresses as specified in Table 6-6 were employed instead of those listed in Table 6-5, implying a difference in assumption on the boundary conditions between the two analyses.

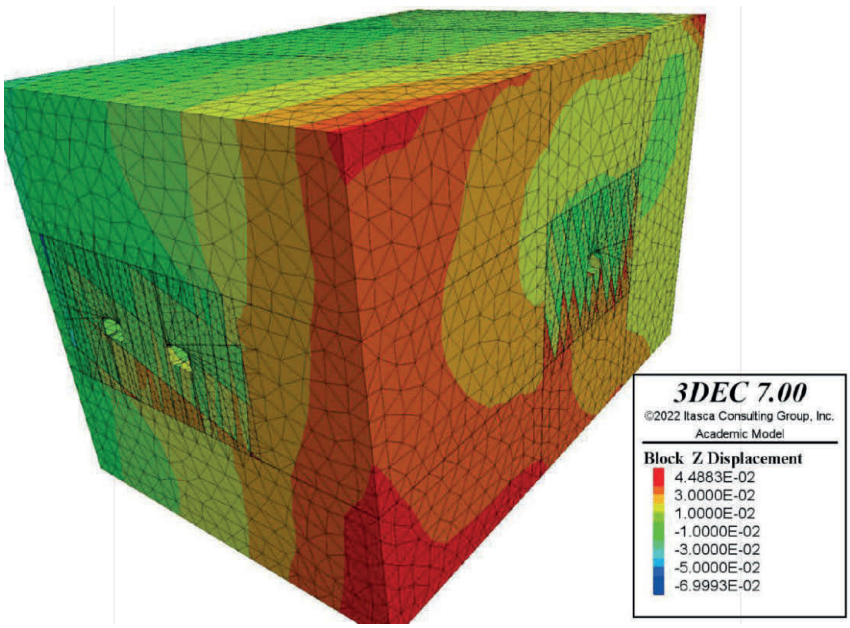

Figure 8-4. Vertical displacement in the 3DEC models of Test No. 6 in static equilibrium condition.

8.4.3 Discrete Fracture Network

For the 3DEC model, the Discrete Fracture Network (DFN) was used for generating realizations of the fracture pattern at the Kiirunavaara Mine. This feature provides a more

accurate representation of the rock mass compared to regularly spaced joint network and can be used for a variety of applications in underground engineering.

The DFN model prepared in this study is based on geological field mapped fractures at the location of Test No. 6. This was not formerly carried out for the UDEC models.

The 3DEC modelling results with regularly spaced joints and DFN did not show very different behaviour. The fact that the joint sets were oriented at an angle with the direction of the crosscuts and footwall tunnel, produced in both joint models a variety of block sizes, shapes and orientations close to the tunnel surfaces, which also resemble well the fracture patterns at the site as commented in Section 8.2.3.

8.4.4 Observations at point probes

Field results at Test No. 6 were previously compared with 2D model results by means of UDEC (Shirzadegan, 2020). The main findings are summarized in Figure 8-5. In comparison with point history by 3DEC illustrated in Section 7.4, similar amplitudes could be observed after borehole blasting from UDEC and 3DEC models. The velocity amplitude collected from accelerometers at the site, however, is much smoother than typically observed in UDEC and 3DEC numerical results (Figure 8-5 and Figure 8-6, respectively), which can depend on various parameters and particularly stiffnesses and damping parameters.

The recent numerical analysis conducted by Warema et al. (2023) utilizing UDEC for rock mass characterized by two regularly spaced joint sets suggests that when waves approach a joint set at a closer to perpendicular angle to its propagation direction, it results in higher point probe velocities. Conversely, when waves approach a joint set at a smaller angle, lower point probe velocities are observed. The complexity of wave patterns increases with the number of joint sets. These findings also indicate that the point probe velocities history exhibit local specificity, depending on factors such as the length and orientation of the nearest joints. This observation aligns with the results obtained from the bottom row of point probes in the UDEC model in Crosscut 100 (Figure 8-5c) characterized by higher and more persistent peak velocity monitored at point A12 and A13 at the site. However, no significant higher and more persistent peak velocity at the bottom point probe rows were observed in the 3DEC modelling results. Each curve in Figure 8-6 represents velocity history for monitoring points at the low row in Crosscut 103.

The numerical findings presented in Section 7.4 suggest that higher peak velocities, ranging from approximately 6 m/s to 9 m/s, are more likely to manifest in the sections of the tunnels nearest to the dynamite-loaded part of the blasthole. This phenomenon could be replicated by the 3DEC models but not by UDEC models previously. Moreover, this discrepancy can be attributed to the following factors:

- The joint patterns: in UDEC models sensitivity analysis was performed assuming various joint spacing for either of the joint sets respectively (1, 2, or 3 m); in 3DEC models, more realistic joint patterns were generated with wider joint spacing derived from joint mapping results. The rock at the bottom row had a higher chance to be geometrically constrained because of larger block size and higher energy needed to move the block.
- The charge length: the introduction of charge length along the blasthole in 3DEC model enables energy dissipation longitudinally and radially while in UDEC only radial dissipation can be considered.
- 3D effect: the layout of the structures including the void spaces such as the crosscut and footwall tunnels and blasthole affect the results. The free surfaces of the tunnel walls provide positions of wave reflections, close to which the rock mass tends to be subject to higher loading.

In general, the exact location of the joints in numerical models is important since it can affect wave reflection and refraction to a large extent. It also affects the shape and position of the blocks prone to move at the wall of the crosscut, influencing the occurrence of tensile yielding and point probe velocity in those positions.

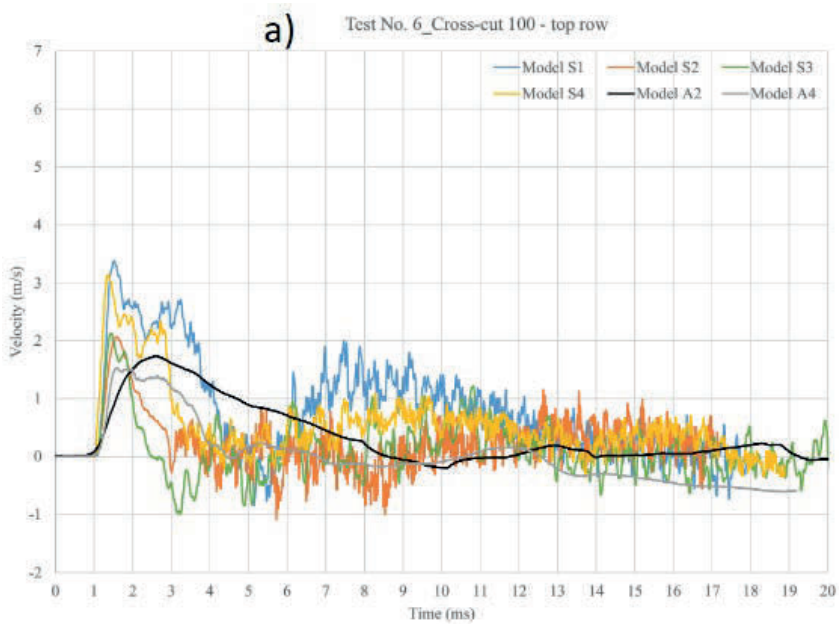

b)

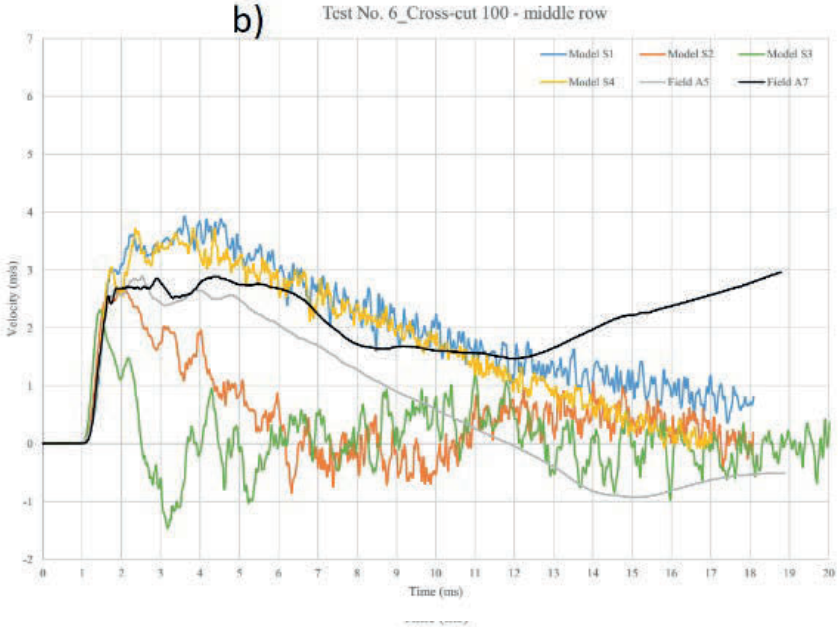
Test No. 6_Cross-cut 100 - middle row
Model S1
Model S2
Model S3
Model S4
Field A5
Field A7
Velocity (m/s)
Time (ms)

c)

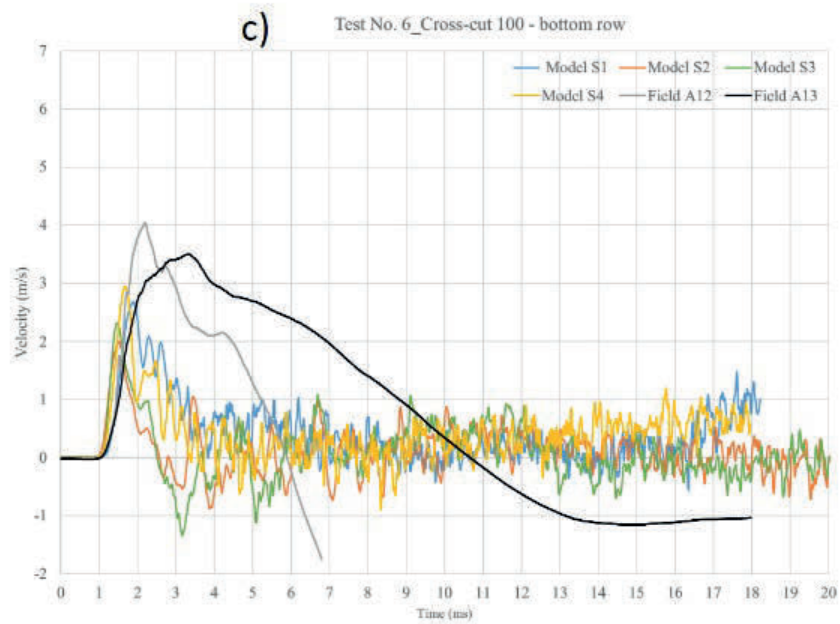
Test No. 6_Cross-cut 100 - bottom row
Model S1
Model S2
Model S3
Model S4
Field A12
Field A13
Velocity (m/s)
Time (ms)

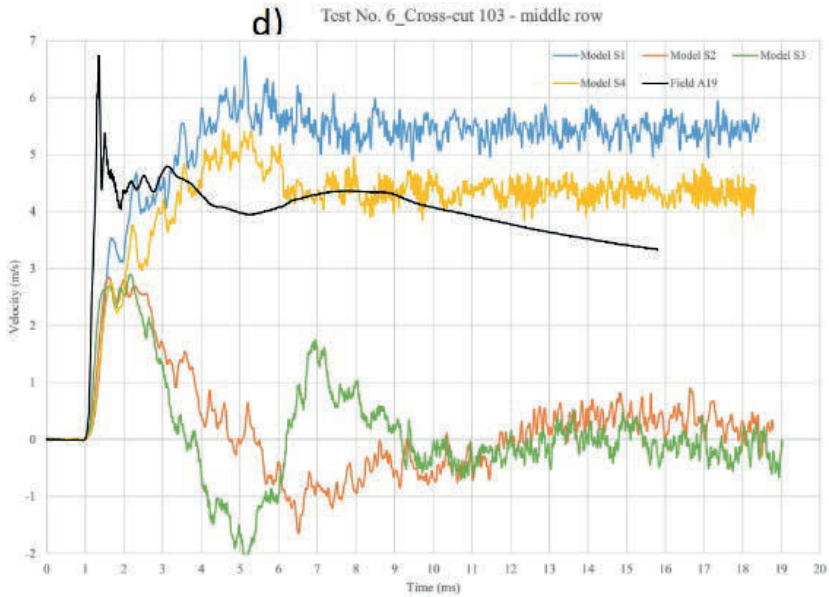

Figure 8-5. Comparison of velocity history obtained in Test No. 6 and UDEC models **(Shirzadegan, 2020)**: a) top row in Crosscut 100, b) middle row in Crosscut 100, c) bottom row in Crosscut 100 and, d) middle row in Crosscut 103.

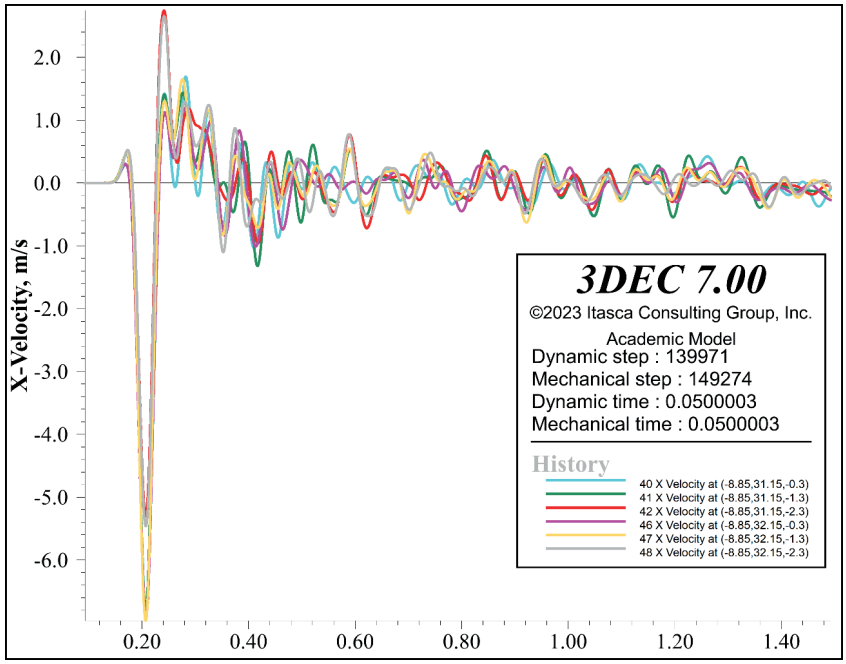

Figure 8-6. Point velocity history near the placed accelerometers between 15 and 20 meters from tunnel face of Crosscut 100 (RSJS & Swellex Mn24 model).

9. CONCLUSION

In this chapter, we present the main findings and conclusions of this study.

The study shows that numerical simulations can be used to analyse the behavior of rock masses and rock support systems under dynamic loading conditions. The simulations performed with a combination of the codes LS-DYNA and 3DEC can provide better understanding of the response of the rock mass subject to dynamic loading. These results can be used as a tool to optimize the design of rock support systems in deep underground mine, saving the effort of expensive field tests.

The numerical results aimed to evaluate different rock support performance (Swellex Mn24 bolt and D-bolt) under dynamic loading conditions and made it possible to conduct numerical analysis for large-scale tests of rock support for Kiirunavaara Mine.

The main findings and observations from this study are as follows:

- The major challenge in setting up the 3DEC models is the generation of the geometry, placing the bolts and the assignment of the in-situ stresses in relation to the geometry.
- 3DEC modelling calculated velocity patterns match well those observed in the field for Test No. 6.
- Calculated results in 3DEC are comparable with UDEC results in the sense of point velocity amplitude of around 5 m/s.
- In 3D, the rock bolt performance in full could be captured and a reliable stress wave propagation induced by blasting through the model geometry could be achieved.
- The results showed that the larger the distance between the blasthole and the test wall, the higher the chance of producing a more planar wave front can be obtained.
- The results also illustrate that the larger the distance between the blasthole and the test wall, the lower the point probe velocity is produced.
- Results show that the crosscut with installed bolts will experience lower peak particle velocity after blasting induced waves reach the tunnel walls in comparison to the crosscut with no rock support installed.
- The performance of rock bolts under dynamic condition is a challenge in rock engineering due to uncertainties in bolt dynamic properties and damping conditions.
- The calculated axial displacement of the bolts showed that both Swellex Mn24 and D-bolt experienced below 4% elongation, which is very moderate with respect to the bolt capacity. Similar result was also observed in Crosscut 100 during the field test when there was not rock fall or failed bolt after blasting.

- A discrepancy between the documented fallout in Crosscut 103 and 3DEC numerical results was observed for the particular DFN realization in this study.
- After providing a calibrated numerical model in 3DEC, it is possible to test the performance of different support systems, other than just Swellex Mn24 and D-bolts, using the same boundary conditions in future studies.
- 3DEC results suggest that numerical analysis can be used as an important tool for the design of large-scale tests on dynamic rock support. Performing and calibrating the numerical analysis can significantly save time, budget and energy while searching for an optimum design of the burden.

10. FURTHER STUDIES

Despite the advancements shown in this report, challenges remain in predicting and managing the performance of rock bolts under dynamic loading. As we continue to push the boundaries of engineering in challenging environments, such as deep underground or seismically active areas, the need for advanced research and technologies in this area will only increase.

Test No. 7 was conducted at the same location of Test No. 6. In this test, two blastholes were charged and detonated at the same time, but a lower range of velocity was measured than for Test No. 6. Therefore, numerical analyses of Test No. 7 are recommended, to investigate why a lower range of velocity was measured despite two blastholes were detonated.

Although the focus of this project was not to investigate the effect of geological structures on wave propagation and velocity amplification in general, the numerical models with simulated joints for Tests No. 1, 2, 4, 5 and 6 (presented in Chapter 5) show that the geological structures have an important effect on the calculated velocity on the surface of the tested walls. Joint parameter studies can be performed to study the effect of mechanical and spatial properties of the geological structures that can affect the wave propagation in the burden and velocity variation on the surface of the test wall. If site conditions allow, accurate field mapping of the geological structures in the study areas of the tests is recommended as a verification of the digitized joints.

Laboratory testing can be used to evaluate the performance of rock support systems under dynamic loading conditions. The testing can provide valuable information about the dynamic parameters and behaviour of the rock mass and rock support system under various loading conditions and can be used to validate numerical simulations.

The development of advanced materials for rock bolts is an active area of research. For example, fibre-reinforced polymer (FRP) bolts have been developed as a corrosion-resistant and lightweight alternative to traditional steel bolts. FRP bolts also have a higher strength-to-weight ratio than steel. Their behaviour under dynamic loading is different from steel bolts and requires further study.

ACKNOWLEDGEMENT

This project is the result of a cooperation between different organizations: Rejlers Sverige AB, Ramboll Sweden AB, Luleå University of Technology (LTU), and RocWise AB.

Rejlers team consists of:

- Pin Zhou, Tek. Lic., project leader and editor;
- Mohsen Bazargan, PhD, responsible for parts of literature review, running and processing of the numerical model results;
- Flavio Lanaro, PhD, advisor and technical reviewer.

Ramboll Sweden AB team has the main force by:

- Shahin Shirzadegan, PhD, researcher, responsible for coordination of the project and data sources.

Luleå University of Technology's team consists of:

- Noorraddin Nikadat, research engineer, model geometry and boundary stresses, assistant in preparation for some of the numerical work;
- Senzia Warema, research engineer, assistant in preparation of rock fracture data and for some of the numerical work;
- Changping Yi, PhD, Assistant Professor, researcher, responsible for the LS-DYNA analyses.

RocWise AB team:

- Erling Nordlund, PhD, Professor, Luleå University of Technology and RocWise AB, advisor and technical reviewer.
-

The research team would like to thank Reza Mohammadi from FS-Dynamics for his contribution in quality checking and improving the LS-DYNA results. We would also like to thank ETH Zurich for their advisory contribution and providing access to their computer cluster for faster computing time. We would like to thank our reference group for their inputs and comments during our evaluation meetings and to the report.

11. REFERENSER

Alibadian, Z., Sharafisafa, M., Mortazavi , A., & Maarefvand, P. (2014). Wave and fracture propagation in continuum and faulted rock masses: distinct element modeling. *Arabian Journal of Geosciences*, 5021-5035.

An, H., Liu, H., & Han, H. (2020). Hybrid finite-discrete element modelling of excavation damaged zone formation process induced by blasts in a deep tunnel. *Advances in Civil Engineering*, 1-27.

An, X. M., Zhao, Z. Y., Nie, W., & He, L. (2013). Dynamic rock bolt modeling in 2-D discontinuous deformation analysis. In J. Zhao, & J. C. Li, *Rock Dynamics and Applications - State of the Art.* CRC Press.

Andersson, U. B. (2010). *Geology and structures, level Z741, blocks 9 and 12.* Internal Report LKAB Kiruna, Sweden, p10.

Andersson, U. B. (2011). *Tättkartering runt skjutskador ort 93 och 95 Z741.* Internal Report LKAB Kiruna, Sweden, p2.

Andrieux, P. P., Turichshev, A., OConnor, C. P., & Brummer, R. K. (2005). *Dynamic Testing With Explosive Charges of Rockburst-Resistant Ground Support Systems at the Fraser Nickel Mine.* Itasca Consulting Company Inc. Sudbury, Canada.

Ansell, A. (1999). *Dynamically loaded rock reinforcement.* PhD Thesis, Institutionen för byggkonstruktion - KTH Universitet.

Ansell, A. (2004). In situ testing of young shotcrete subjected to vibrations from blasting. *Tunnelling and Underground Space Technology*, 587-596.

Ansell, A. (2005). Laboratory testing of a new type of energy absorbing rock bolt. *Tunnelling and Underground Space Technology*.

Archibald, J. F., Baidoe, J. P., & Katsabanis, P. T. (2003). Rockburst damage mitigation benefits deriving from use of spray-on rock lining. *Proceedings of Third International Seminar on Surface Support Liners: Thin Spray-on Liners, Shotcrete and Mesh*, (pp. 169-178). Quebec.

Atlas Copco. (2023). *Swellex Mn 24 spec sheet - Atlas Copco.* Retrieved from https://www.yumpu.com/en/document/read/16734887/swellex-mn24-spec-sheet-atlas-copco

Banadaki, M. D., & Mohanty, B. (2012). Numerical simulation of stress wave induced fractures in rock. *International Journal of Impact Engineering*.

Barla, G., & Barla, M. (2000). Continuum and discontinuum modelling in tunnel engineering. *Rudarsko Geolosko Naftni Zbornik*, 45-57.

Bazargan, M. (2022). *Numerical and laboratory studies of seismic properties and elements of rock fabric from the microscale to the macroscale.* Uppsala Universitet.

Borrvall, T., & Riedel, W. (2011). The RHT concrete model in LS-DYNA. *8th European LS-DYNA users conference.* Strasbourg.

Cai, M., Champaigne, D., Coulombe, J. G., & Challagulla, K. (2019). Development of two new rockbolts for safe and rapid tunneling in burst-prone ground. *Tunnelling and Underground Space Technology*.

Charette, F., & Plouffe, M. (2007). Roofex-results of laboratory testing of a new concept of yieldable tendon. *Fourth International Seminar on Deep and High Stress Mining.*

Chen, L., Gang, S., & Gang, C. (2014). Investigation of impact dynamics of roof bolting with passive friction control. *International Journal of Rock Mechanics & Mining Sciences*, 559-568.

Chen, S., & Zhao, J. (1998). A study of UDEC modelling for blast wave propagation in jointed rock masses. *International Journal of Rock Mechanics and Mining Sciences*, 35(1): 93-99.

Chen, S., Zhao, J., & Zhou, Y. (2000). UDEC modeling of a field explosion test. *International Journal for Blasting and Fragmentation*, 4(2): 149-163.

Cundall, P. A. (1980). *UDEC—a generalized distinct element program for modelling jointed rock.* Peter Cundall Associates, European Research Office, US Army Corps of Engineers.

Deng, X., Chen, S., Zhu, J., Zhou, Y., Zhao, Z., & Zhao, J. (2015). UDEC–AUTODYN hybrid modeling of a large-scale underground explosion test. *Rock Mechanics and Rock Engineering*, 48(92): 737-747.

Eldert, J. V. (2018). *Analysis of Excavation Damage, Rock Mass Characterization and Rock Support Design using Drilling Monitoring.* Luleå tekniska universitet.

Espley, S. J., Heilig, J., & Moreau, L. H. (2002). Assessment of the dynamic capacity of liners for application in highly-stressed mining environments at INCO Limited. *Proceedings of the International Seminar on Surface Support Liners*, (pp. 187-192). Johannesburg.

Fakhimi, A., & Lanari, M. (2014). DEM–SPH simulation of rock blasting. *Computers and Geotechnics*, 158-164.

Gerdeen, J., Snyder, V. W., Vieghlahn, G. L., & Parker, J. (1977). *Design Criteria for Roof Bolting Plans Using Fully Resin-Grouted Nontensioned Bolts to Reinforce Bedded Mine Roof.* Washington, DC: Bureau of Mines.

Hagan, T. O., MILEV, A. M., Spottiswoode, S. M., Hildyard, M. W., Grodner, M., Rorke, A. J., . . . Grave, D. M. (2001). Simulated rockburst experimwent - an overview. *The journal of The South African Institute of Mining and Metallurgy*, 217-222.

Han, H., Fukuda, D., Liu, H., Salmi, E. F., Sellers, E., Liu, T., & Chan, A. (2020). FDEM simulation of rock damage evolution induced by contour blasting in the bench of tunnel at deep depth. *Tunn. Undergr. Space Technol. 103, 103495.*

Harrison, J. P., & Hudson, J. A. (2000). *Engineering rock mechanics. Part 2: Illustrative Worked Examples.* Oxford: Pergamon.

Harvey, S., & Ozbay, U. (2009). *In-situ Testing of Roofex Yielding Rock Bolts. A Report Submitted to NIOSH.* WA: Spokane Research Laboratory: Spokane.

He, M. C., Tao, Z. G., & Zhang, B. (2013). *Constant-resistance and large deformation anchor cable and constant resistance device.* China.

He, M. C., Tao, Z. G., & Zhang, B. (2014b). *Constant-resistance and large deformation anchor cable and constant resistance device.* USA.

He, M. C., Tao, Z. G., & Zhang, B. (2014c). *Constant-resistance and large deformation anchor cable and constant resistance device.* Japan.

He, M. C., Tao, Z. G., & Zhang, B. (2014d). *Constant-resistance and large deformation anchor cable and constant resistance device.* Spain.

He., M. C., & Feng, J. L. (2010). *Constant resistance large deformation anchor.* China.

Heal, D., & Potvin, Y. (2007). In-situ dynamic testing of ground support using simulated ROCKBURST. *Proceeding of 4th International Seminar on Deep and High Stress Mining* (pp. 373-394). Perth: Australian Centre for Geomechanics.

Heal, D., Hudyma, M., Langille, C., Potvin, Y., Butcher, R., Ball, R., & Hartmann, B. (2005). In-situ testing of ground support performance under strong dynamic loading. *Proceedings of the 6th international symposium on rockbursts and seismicity in mines* (pp. 85-94). Perth: Australian Centre for Geomechanics.

Helte, A., Lundgren, J., Örnhed, H., & Norrefeldt, M. (2006). *Prestandabestämning av svensk sprängdeg m/46, rapport nr FOI-R-2051-SE.* Stockholm: FOI, ISSN 1650-1942.

Hoek, E. (1994). Strength of rock and rock masses. *ISRM News Journal*, 4-16.

Hoek, E., & Brown, E. T. (1997). Practical estimates of rock mass strength. *International Journal of Rock Mechanics and Mining Sciences*, 1165-1186.

Hoek, E., Kaiser, P. K., & Bawden, W. F. (1995). *Support of underground excavations in hard rock.* Rotterdam: Balkema.

Hyett, A. J., Bawden, W. F., Hedrick, N., & Blackall, J. (1996). A laboratory evaluation of the 25 mm Garford bulb anchor for cable bolt reinforcement. *International Journal of Rock Mechanics and Mining Sciences & Geomechanics Abstracts*, 172.

ITASCA Consulting Group. (2023). *3DEC Manual.*

ITASCA Consulting Group. (2023). *UDEC Manual.*

Jager, A. J. (1992). Two new support units for the control of rockburst damage. *Rock Support in Mining and Underground Construction. International Symposium on Rock Support*, (pp. 621-631). Sudbury.

Jing, L. (2003). A review of techniques, advance and outstanding issues in numerical modelling for rock mechanics and rock engineering. *International Journal of Rock Mechanics & Mining Sciences*, 283-353.

Kabwe, E. (2023). Performance of dynamic reinforcements to restrain remote triggered strainburst associated failure. *Tunnelling and Underground Space Technology incorporating Trenchless Technology Research*.

Kaiser, P. K., McCreath, D. R., & Tannant, D. D. (1996). *Canadian rockburst support handbook.* Geomechanics Research Centre.

Lak, M., Marji, M. F., Bafghl, A. R., & Abdollahipour, A. (2019). Discrete element modeling of explosion-induced fracture extension in jointed rock masses. *Journal of Mining and Environment*, 125-138.

Larsson, K. (2004). *Mining Induced Seismicity in Sweden.* Luleå: Luleå University of Technology.

Lee, E. L., Horning, H. C., & Kury, J. W. (1968). *A dilabatic expansion of high explosives detonation products.* Lawrence Livermore National Laboratory, University of California, Livermore, TID4500-UCRL 50422.

Li, C. C. (2010). A new energy-absorbing bolt for rock support in high stress rock masses. *International Journal of Rock Mechanics & Mining Sciences*, 396-404.

Li, C. C. (2012). Performance of D-bolts under static loading. *Rock Mechanics & Rock Engineering*, 183-192.

Li, C. C. (2017). *ROCKBOLTING Principles and Applications.* Butterworth-Heinemann.

Li, C. C., & Håkansson, U. (1999). Performance of the Swellex bolt in hard and soft rocks. *Proceedings of the international symposium on ground support*, (pp. 103-108). Kalgoorlie.

Li, C. C., & Marklund, P. I. (2004). Field tests of the cone bolts in the Boliden mines. *Fjellsprengninsteknikk/ Bergmekanikk/ Geoteknikk* (p. 12). NORSK JORD- OG FJELLTEKNISK FORBUND.

Li, C. C., Stjern, G., & Myrvang, A. (2014). A review on the performance of conventional and energy-absorbing rockbolts. *Journal of Rock Mechanics and Geotechnical Engineering*.

Li., C. C. (2011). Dynamic test of a high energy-absorbing rock bolt. *12th ISRM International Congress on Rock Mechanics - Harmonising Rock Engineering and the Environment.* Beijing.

Ma, G., & An, X. (2008). Numerical simulation of blasting-induced rock fractures. *International Journal of Rock Mechanics and Mining Sciences*, 966-975.

Malmgren, L. (2005). *Interaction between shotcrete and rock - experiment and numerical study, PhD Thesis.* Luleå University of Technology.

Malmgren, L. (2007). Strength, ductility and stiffness of fibre-reinforced shotcrete. *Magazine of Concrete Research*, 59(4): 287-296.

Malmgren, L., & Sjöberg, J. (2006). *Bergmekaniska analyser för ny huvudnivå KUJ (avv 1365).* LKAB: 06-797.

Malmgren, L., Sjöberg, J., & Krekula, H. (2008). *Brytning mot och under KUJ 1045 - Bergmekaniska rekommendationer.* LKAB: 08-711.

Mccreath, D. R., & Kaiser, P. K. (1995). *Current support practices in burst-prone ground,.* Mining Research Directorate. In Canadian Rock burst Research Project (1990–95). GRC, Laurentian University.

Mitelman, A., & Elmo, D. (2014). Modelling of blast-induced damage in tunnels using a hybrid finite-discrete numerical approach. *Journal of Rock Mechanics and Geotechnical Engineering*, 565-573.

Ning, Y., Yang, J., An, X., & G., M. (2011). Modelling rock fracturing and blast-induced rock mass failure via advanced discretisation within the discontinuous deformation analysis framework. *Computers and Geotechnics*, 40-49.

Olsson, M., Markström, I., Pettersson, A., & Sträng, M. (2009). *Examination of the Excavation Damaged Zone in the TASS tunnel, Äspö HRL. R-09-39.* Stockholm: Svensk Kärnbränslehantering AB.

Onederra, I. A., Furtney, J. K., Sellers, E., & Iverson, S. (2012). Modelling blast induced damage from a fully coupled explosive charge. *International Journal of Rock Mechanics and Mining Sciences*, 73-84.

Ortlepp, W. D. (1969). An empirical determination of the effectiveness of rock bolt support under impulse loading. *Proceedings of the International Symposium on Large Permanent Underground Openings* (pp. 197-205). Australian Center for Geomechanics.

Ortlepp, W. D. (1992). Design of Support for the Containment of Rockburst Damage in Tunnels—An Engineering Approach. *Proceedings of the international symposium on rock support*, (pp. 593-609). Sudbury, Ontario, Canada.

Ortlepp, W. D. (1994). Grouted rock-studs as rockburst support: A simple design approach and an effective test procedure. *Journal of the Southern African Institute of Mining and Metallurgy*, 47-53.

Ortlepp, W. D., & Stacey, T. R. (1998). Performance of tunnel support under large deformation static and dynamic loading. *Tunnelling and Underground Space Technology*, 15-21.

Ouchterlony, F. (1997). Prediction of crack lengths in rock after cautious blasting with zero inter-hole delay. *Fragblast - International Journal for Blasting and Fragmentation*, 417-444.

Ouchterlony, F., Olsson, M., & Bergqvist, I. (2002). Towards New Swedish Recommendations for Cautious Perimeter Blasting. *Fragblast - International Journal for Blasting and Fragmentation*, 169-181.

Ozbay, U., & Neugebauer, E. (2009). In-situ pull testing of a yieldable rock bolt, roofex. *International Symposium on Rockburst and Seismicity in Mines Proceedings: Controlling Seismic Hazard and Sustainable Development of Deep Mines (Volume 2).* Dalian: Rinton Press.

Palmström, A., & Stille, H. (2007). Ground behaviour and rock engineering tools for underground excavations. *Tunnelling and Underground Space Technology*, 363-376.

Park, B., & Jeon, S. (2005). Characteristics of blast-induced fracturing for the determination of optimal spacing in contour blasting using bonded particle model. *Geosystem Engineering*.

Potvin, Y., Wesseloo, J., & Heal, D. (2010). An interpretation of ground support capacity submitted to dynamic loading. *Proceedings of the 5th international*

seminar on deep and high stress mining (pp. 251-272). Australian Center for Geomechanics.

Priest, S. D. (1993). *Discontinuity Analysis for Rock Engineering.* Lodon: CHAPMAN & HALL.

Riedel, W., Thoma, K., Hiermaier, S., & Schmolinske, E. (1999). Penetration of reinforced concrete by BETA-B-500, numerical analysis using a new macroscopic concrete model for hydrocodes. *Proceedings of the 9th International Symposium on Interaction of the Effects of Munitions with Structures.* Berlin.

Saiang, D. (2008). *Behaviour of blast-induced damaged zone around underground excavations in hardrock mass.* Luleå: Luleå University of Technology.

Saiang, D., Malmgren, L., & Nordlund, E. (2005). Laboratory tests on shotcrete-rock joints in direct shear, tension and compression. *Rock Mechanics and Rock Engineering*, 38(4): 275-297.

Sandström, D. (2003). *Analysis of the Virgin State of Stress at the Kiirunavaara Mine.* Luleå: Luleå Univerisity of Technology, Licentiate Thesis.

Shirzadegan, S. (2020). *Development of a Methodology for Dynamic Testing of Rock Support.* Luleå University of Technology.

Shirzadegan, S., Nordlund, E., & Zhang, P. (2016a). Large scale dynamic testing of rock support system at Kiirunavaara underground mine. *Rock Mechanics and Rock Engineering*, 49(7): 2770-2794.

Shirzadegan, S., Nordlund, E., & Zhang, P. (2016b). Large scale dynamic testing of rock support at Kiirunavaara – Improved test design. *Tunneling and Underground Space Technology*, 59: 183-198.

Simser, B. (2002). *Modified cone bolt static and dynamic tests.* Quebec: Noranta Technology Centre Internal Report.

Simser, B., Parrott, T., Turcotte, P., Mercier-Langevin, F., & Andrieux, P. (2006). Field behaviour and failure modes of modified conebolts at the Craig, LaRonde and Brunswick Mines in Canada. *Deep and High Stress Mining*, (p. 2006).

Skrzypkowski, K., Korzeniowski, W., Zagórski, K., & Zagórska, A. (2020a). Adjustment of the yielding system of mechanical rock bolts for room and pillar mining method in stratified rock mass. *Energies*, 2082.

Skrzypkowski, K., Korzeniowski, W., Zagórski, K., & Zagórska, A. (2020b). Modified rock bolt support for mining method with controlled roof bending. *Energies*, 1868.

Stacey, T. (2012). A philosophical view on the testing of rock support for rockburst conditions. *Journal of the Southern African Institute of Mining and Metallurgy ISSN 2411-9717*, 703-710.

Sui, Q., He, M., He, P., Xia, M., & Tao, Z. (2022). State of the art review of the large deformation rock bolts. *Underground Space*, 465-482.

Tannant, D. D., Brummer, R. K., & Yi, X. (1995). Rockbolt behaviour under dynamic loading: field tests and modelling. *International Journal of Rock Mechanics and Mining Sciences & Geomechanics Abstracts*, 537-550.

Tannant, D. D., McDowell, G. W., & McCreath, D. R. (1994). Shotcrete performance during simulated rocksbursts. *Workshop on applied rockburst research (eds) IVth south american congress on rock mechanics*, (pp. 241-248). Santiago.

Torbica, S., & Lapčević, V. (2015). Estimating extent and properties of blastdamaged zone around underground excavations. *Rem Revista Escola de Minas*, 441-453.

Vakili, A., Penney, A., & Woo, S. (2014). *Understanding critical parameters in stochastic Discrete Fracture Network.* Vancouver: DFNE conference.

Varden, R. P. (2009). Implementation of the garford dynamic bolt at kanowna belle mine. *International Symposium on Rockburst and Seismicity in Mines - Controlling Seismic Hazard and Sustainable Development of Deep Mines.* Dalian.

Varden, R., Lachenicht, R., Player, J., Thompson, A., & Villaescusa, E. (2008). Development and implementation of the Garford Dynamic Bolt at the Kanowna Belle Mine. *Tenth Underground Operators' Conference*, (pp. 95-102). Launceston.

Wang, J., Yin, Y., & Esmaieli, K. (2018a). Numerical simulations of rock blasting damage based on laboratory-scale experiments. *Journal of Geophysics and Engineering*, 2399-2417.

Wang, Y., Wang, S., Zhao, Y., Guo, P., Liu, Y., & Cao, P. (2018b). Blast Induced Crack Propagation and Damage Accumulation in Rock Mass Containing Initial Damage. *Shock and Vibration*.

Wang, Z., Konietzky, H., & Shen, R. (2009). Coupled finite element and discrete element method for underground blast in faulted rock masses. *Soil Dynamics and Earthquake Engineering*, 29(6): 939-945.

Warema, S., Shirzadegan, S., Nordlund, E., Yi, C. P., & Lanaro, F. (2023). Numerical Analysis of the Sensitivity of Joint Parameters to the Cross-cut in Response of Dynamic Loading. *Proceedings of the NROCK 2023: The IV Nordic Symposium on Rock Mechanics and Rock Engineering*.

Yoon, J., & Jeon, S. (2009). Use of a modified particle-based method in simulating blast-induced rock fracture. *Proc. of the 9th Int. Symp. on Rock Fragmentation by Blasting—FRAGBLAST9.*

Yu, C., & Li, C. C. (2015). Performance of fully encapsulated rebar bolts and D-Bolts under combined pull-and-shear loading. *Tunnelling and Underground Space Technology*, 99–106.

Zhang, P., Yi, C., Nordlund, E., Shirzadegan, S., Nyberg, U., Malmgren, L., & Nordqvist, A. (2013). Numerical back analysis of simulated rockburst field tests by using coupled numerical technique support in mining and underground construction. *Proceeding of seventh international symposium on ground* (pp. 562-585). Perth: Australian centre for Geomechanics.

BeFo

Box 5501
SE-114 85 Stockholm

info@befoonline.org • www.befoonline.org
Visiting address: Storgatan 19, Stockholm

ISSN 1104-1773